Catalytic Properties of Palladium Nanoclusters Synthesized within Microphase-Separated Diblock Copolymers

by

Jane Farrol Ciebien

Bachelor of Science, Engineering Chemistry
Queen's University, Kingston, Ontario, Canada, 1992

Master of Science of Chemical Engineering Practice
Massachusetts Institute of Technology, Cambridge, Massachusetts, 1994

Submitted to the Department of Chemical Engineering
in partial fulfillment of the requirements for the degree of

DOCTOR OF PHILOSOPHY IN CHEMICAL ENGINEERING
AT THE
MASSACHUSETTS INSTITUTE OF TECHNOLOGY

JUNE 1997

Signature of Author:_____
Department of Chemical Engineering
April 29, 1997

Certified by:_____
Robert E. Cohen
Professor of Chemical Engineering
Thesis Supervisor

Accepted by:_____
Robert E. Cohen
St.Laurent Professor of Chemical Engineering
Chairman, Committee for Graduate Students

Catalytic Properties of Palladium Nanoclusters Synthesized within Microphase-Separated Diblock Copolymers

by

Jane Farrol Ciebien

Submitted to the Department of Chemical Engineering on April 29, 1997,
in partial fulfillment of the requirements for the degree of
Doctor of Philosophy in Chemical Engineering

ABSTRACT

Palladium nanoclusters, 14-35 Å in diameter, were synthesized within microphase-separated diblock copolymer films by reduction of organometallic repeat units comprising one of the blocks. TEM analysis showed that the clusters were roughly spherical, had a narrow size distribution, and were located predominantly within the original organometallic domains.

Gas phase experiments demonstrated that the nanocomposite materials were active catalysts for hydrogenation of ethylene, propylene, and 1,3-butadiene despite the fact that the clusters are completely embedded within a non-porous polymer matrix. The activity of the nanocomposites for hydrogenation generally increased in the order: propylene < ethylene < 1,3-butadiene. The nanocomposites also showed good selectivity for butenes in the hydrogenation of 1,3-butadiene and the selectivity for 1-butene in particular could be improved by lowering the reaction temperature or hydrogen partial pressure. Exposure of the nanocomposites to C_4 gases resulted in plasticization of the polymer matrix, opening of 15-60 μm diameter voids in the matrix, and reduction of mass transfer resistance within the films, leading to an increase in activity.

A permeation study was conducted on a polyMTD sample at room temperature. These experiments revealed that while the diffusion coefficients of ethylene, propylene, and 1,3-butadiene in polyMTD are similar, the solubility coefficient increases by an order of magnitude with increasing penetrant molecular weight. Therefore, the permeability increases by nearly an order of magnitude from ethylene to 1,3-butadiene.

Thesis Supervisor: Robert E. Cohen
Title: Professor of Chemical Engineering

Acknowledgments

When I was not quite five years old, my mother took me to school for my first day of kindergarten. Standing at the foot of what appeared to be an impossibly long path leading to the classroom door, my mother claims that I tugged on her hand and said that I wasn't sure I wanted to go to school. I know that this is true because I still recall my feeling of dread. So who would have believed that, nearly 24 *years* later, I am just now finishing school?!?

I guess I discovered that I liked school after all. But it's not only that. If not for the unbounded love and affection that my parents have always shown me, and their unfaltering support in every challenge and adventure I have undertaken, I wouldn't be where I am - or who I am - today. I thank them for everything they have done for me. They really are the best parents a person could ask for.

I also want to thank my sister, not only for her love and support, but also for her ability to put any situation into perspective. Who else could have told me to quit whining when I was worried about passing the core courses because, even if I failed, surely the world would not come to an end! She is also responsible for assuring me that being a geek is okay, because geek's make a lot of money. (I hope.)

I want to thank my advisor, Bob Cohen, whose ever-present smile sets the tone for the group, and whose positive attitude was of great help to me, especially when my experiments weren't going as well as I would have liked. I am fortunate to have had the opportunity to work with Bob; he is largely responsible for the fact that my time at MIT has been so rewarding and enjoyable.

MIT is a special place, but it is the people here who make it great. The opportunity to meet people from all over the world is one of the best things about this school. Many of my closest friends here are from distant countries I may never get the chance to visit (although I will certainly try!), and I am fortunate to have been able to learn not only about their culture, but also about my own as seen through their eyes. In particular, I want to thank Jyotsna for helping me get through the core courses and Practice School without an irreversible loss of sanity; Colleen and BH who each graciously withstood months of questions from me about everything and anything in the lab; and all the Cohengroup members who have been such a great source of advice, entertainment, and friendship over the years. I must also thank Alejandra who arrived at just the right moment to provide her skills as an analytical chemist and her support as a friend. She shared many of the most exciting moments of this research with me, and I don't know how I would have been able to get things together without her help.

I am grateful to my thesis committee members, Profs. Maria Flytzani-Stephanopoulos, Paula Hammond, Paul Laibinis, and Edward Merrill, for their thoughtful

guidance. I also want to thank Liz, Janet, and Elaine for their help with a thousand little things, all of them important in the process of completing a degree.

I don't think that I have ever come up with an elegant conclusion to anything that I have written, and nothing special comes to mind right now. So I think I'll just end by quoting two fortune cookie messages I have been carrying around with me since I first came to MIT. I think that they are appropriate here.

"Your path is arduous but will be amply rewarding."

"There are no simple solutions - only intelligent choices."

Table of Contents

List of Figures

List of Tables

1. Introduction

1.1 Motivation

Nanoclusters and nanostructured materials are presently the subject of research and product development because they may possess interesting and useful catalytic,[1-3] magnetic,[4-6] optical,[7-11] semiconductor,[12] or other properties. These materials, with characteristic length scales on the order of nanometers, often display properties intermediate between the bulk and the atom, arising from quantum size effects[13,14] or the large surface area-to-volume ratio[15] of such small particles.

For most practical applications, nanoclusters must be compressed into a nanostructured material or supported by a stabilizing matrix that can easily be processed in subsequent fabrication steps. Polymers make attractive support materials for a number of reasons. Polymers are able to effectively stabilize clusters against agglomeration and most commercial polymers can be processed with relative ease, either in solution or in the melt. Further, with the variety of polymers available, a material with particularly favorable physical properties for a given application can be identified.

Research in the Cohen group has focused on producing nanoclusters *in situ* within microphase-separated diblock copolymer films. Clusters synthesized using this technique are generally roughly spherical with a narrow size distribution, and are homogeneously distributed within the polymer matrix. These characteristics are important for applications such as UV absorbing coatings where the nanocluster properties are strongly dependent on size[10] and where a homogeneous distribution of clusters is essential for the material to be effective.

The polymers used in this work were synthesized by "living" ring opening metathesis polymerization (ROMP).[16,17] This technique was made possible by the development of organometallic polymerization initiators by Prof. Schrock's group[18,19] at MIT, and Prof. Grubbs' group[20,21] at CalTech. The unique features of these initiators are that they are selective towards strained cyclic alkenes and tolerant of a variety of functional groups. Because ROMP polymerizations are "living" and initiation is much faster than propagation, low polydispersity block copolymers can be synthesized.

The monomer, polymer, and cluster synthetic techniques used in this work have been published previously.[22] The objectives of this project were to reproduce each of these syntheses, to characterize the resulting materials, and to study the catalytic activity and selectivity of diblock copolymer/palladium nanocluster composite materials. Gas phase alkene and diene hydrogenation reactions were studied because the activity and selectivity of bare palladium metal for these reactions is well known and alumina- or silica-supported palladium catalysts are used industrially for these reactions. Our aim was to investigate the extent to which palladium nanoclusters retain their catalytic activity and selectivity when they are completely covered by a polymer and not directly in contact with the gas phase, as are supported or wire gauze catalysts.

1.2 Nanoclusters

Nanoclusters, nanostructured materials, and the so-called nanocomposite materials into which they may be incorporated have been the subject of growing interest over the past several years. Nanoclusters are small particles of metals, metal oxides, or semiconductor materials; the particle size range of interest is usually 10-500 Å in

diameter. Nanostructured materials are bulk materials with grain sizes on the order of nanometers. Nanocomposite materials are composites in which one or more of the phases has a characteristic length scale on the order of nanometers.

Nanoclusters are of practical engineering interest because of the unique properties they may possess, arising from quantum size effects[13,14] or the very large surface area-to-volume ratio[15] of these materials. Nanoclusters of nickel and palladium are highly active catalysts for hydrogenation reactions[23] and may be deposited on porous alumina or silica supports for use as heterogeneous catalysts. Nanoclusters may also have useful optical properties which can be tuned by changing the size of the clusters. For example, suspensions of ZnO nanoclusters in 2-propanol absorb light in the UV region.[10] The absorption edge can be altered by changing the size of the clusters: the onset absorption was 306 nm for particles less than 5 Å in diameter, and shifted steadily with increasing cluster size to 365 nm for 50 Å clusters. One possible application of UV absorbing clusters is to incorporate them into a polymer matrix, such as polycarbonate, for use as visually transparent protective coatings. Nanocomposite materials may also be useful in capacitors; the interaction of electrically conductive nanoclusters with a nonconductive matrix can result in a material with a high dielectric constant.[24] Nanocomposite materials containing γ-Fe_2O_3 clusters have also been synthesized and the materials were found to exhibit superparamagnetic behavior.[4] Magnetic properties could make these materials useful for information storage applications and magnetic refrigeration. For all of these applications, the cluster properties vary greatly with size and the clusters must be

stabilized against agglomeration and growth to maintain the performance of the material within engineering specifications.

A variety of nanocluster synthetic methods have been developed. A more detailed description of these techniques is given in Section 3.1. A common method to produce relatively large quantities of clusters is condensation of metal vapors[25] with or without solvent. A number of solution-based techniques have also been reported. These generally involve the reduction of a metal salt in aqueous or ethanol solution in the presence of a stabilizing polymer or surfactant.[26,27] Nanoclusters have been synthesized within reverse micelles[28] and diblock copolymer micelles.[29] Electrochemical reduction[30] and sol-gel techniques[31] have also been used to synthesize clusters in solution.

Comparatively few techniques have been developed to synthesize bulk quantities of nanoclusters within a polymer matrix. One reported method involves the condensation of metal vapors into a liquid monomer which is later polymerized.[32] Another interesting technique uses supercritical carbon dioxide to load bulk polymer films with metal salts, and to convert these salts to metal nanoclusters by chemical post-treatment.[33] This method could have great practical importance if it is found to be applicable to a range of commercially available polymers. Nanocomposite materials are made in the Cohen group using microphase-separated diblock copolymers. Two methods have been developed. The first method, used in this work, involves the reduction of organometallic repeat units comprising one block of a diblock copolymer. The second method uses diblock copolymers where one block is composed of a dicarboxylic acid functionalized norbornene monomer that acts as an ion-exchange site.[34] Ions of various metals can be

loaded from aqueous solution using either the -COOH or -COONa form of the functionalized norbornene block.

1.3 Polymer Blends and Block Copolymers

For a given pair of homopolymers poly(A) and poly(B), there is usually only a narrow range of miscibility. The reason for this can be understood by examining the thermodynamics of mixing for a macromolecular system. As in the case of small molecules, ΔG_{mix} must be negative for two polymers to be miscible. That is:

$$\Delta G_{mix} < 0 \qquad (1\text{-}1)$$

and, $$\Delta G_{mix} = \Delta H_{mix} - T\Delta S_{mix} \qquad (1\text{-}2)$$

From the Flory-Huggins theory,[35] ΔH_{mix} can be expressed as:

$$\Delta H_{mix} = \chi_{AB}\, n_A\, \phi_B\, k\, T \qquad (1\text{-}3)$$

where $$\chi_{AB} = \frac{z\, \Delta w_{AB}\, x_A}{k\, T} \qquad (1\text{-}4)$$

and χ_{AB} = Flory-Huggins interaction parameter

n_i = number of molecules of polymer *i*

ϕ_i = volume fraction of polymer *i*

k = Boltzmann's constant

T = temperature

z = number of contacts between a repeat unit and its neighbors

Δw_{AB} = change in energy for formation of an AB contact pair

x_i = number of repeat units in polymer *i*

Therefore, ΔH_{mix} values for macromolecules will be similar to values for small molecules because the large value of x_A is canceled by the small value of n_A. ΔH_{mix} will be small

and positive in the absence of specific, favorable interactions such as hydrogen bonding. In contrast, ΔS_{mix} for polymers is small because of its dependence on n_A and n_B:

$$\Delta S_{mix} = k\,T\,(n_A\,ln\phi_A - n_B\,ln\phi_B) \qquad (1\text{-}5)$$

That is, the entropy of the system increases very little when polymers are mixed because so few molecules are present in the system. The value of ΔS_{mix} is usually too small to overcome ΔH_{mix} at room temperature.

Block copolymers can be thought of as two (or more) chemically distinct homopolymers which have been joined by covalent bonds. As in the case of blends of homopolymers described above, the blocks of a diblock copolymer are usually immiscible. However, the macroscopic phase separation observed for homopolymer blends is not possible for diblock copolymers because the two blocks are linked together. Instead, the phenomenon usually referred to as "microphase separation" occurs, resulting in formation of distinct domains of A and B. Microphase separation is more appropriately referred to as an order-disorder transition because there is actually only one phase present in the system and the characteristic length scale of the A and B domains is on the order of nanometers.

A number of microphase-separated morphologies have been predicted theoretically[36-38] and observed experimentally.[39,40] Examples are illustrated in Figure 1-1. Which of these morphologies will be observed depends on the molecular weight of the polymer, the volume fraction of each block, the temperature of the system, and the specific chemical structure of each block. The most commonly observed diblock copolymer morphologies are alternating lamellae of A and B, and cylinders or spheres of

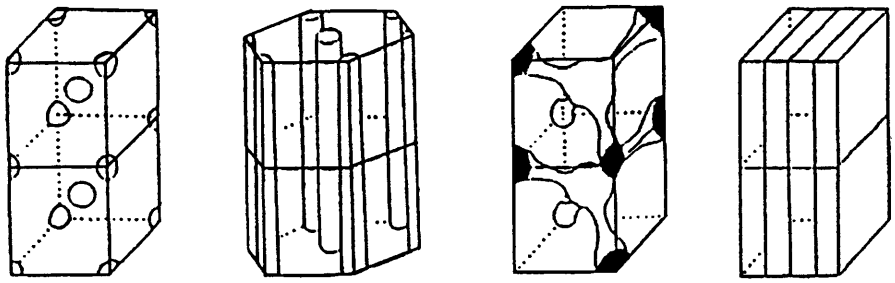

Figure 1-1: Commonly observed diblock copolymer morphologies - spherical, cylindrical, OBDD, and lamellar.

A within a continuous matrix of B. Various bicontinuous morphologies,[39,41] such as the ordered bicontinuous double diamond (OBDD), have been reported.

Microphase-separated block copolymers are of practical engineering interest because they may exhibit useful mechanical, chemical, or other properties. For example, materials with a lamellar or cylindrical morphology may have anisotropic gas transport properties making them useful as gas separation or barrier materials.[42] Thermoplastic elastomers, a class of materials with great commercial value, also take advantage of microphase separation.[43] These triblock (or multiblock) copolymers contain two short "hard" end blocks and a central "soft" amorphous block with a low T_g. The end blocks may be glassy or crystalline at ambient conditions. When these materials microphase separate, the "hard" domains act as physical cross-links in a rubbery matrix. Thermoplastic elastomers are valuable because they have mechanical properties similar to conventional chemically cross-linked polymers, but the physical cross-links are reversible and can be removed by heating the material above its order-disorder transition temperature, where it behaves like a linear polymer. Therefore, thermoplastic elastomers

are easily processed and reprocessed, opening up possibilities for recycling. An example of this class of materials is Kraton®, a polystyrene-*b*-polybutadiene-*b*-polystyrene (SBS) triblock copolymer used for running shoe soles and hot melt adhesives.

Using methods developed by the Cohen and Schrock groups at MIT,[22,44,45] microphase-separated diblock copolymer systems can be used as micro-reactors, within which a variety of chemical reactions can be conducted. Specifically, metal,[22,46-48] metal oxide,[4] and metal sulfide[46,49-51] nanoclusters have been synthesized within the domains of microphase-separated diblock copolymers, taking advantage of the small domain size and the presence of microdomain interfaces to synthesize clusters with a narrow size distribution, homogeneously distributed throughout the polymer matrix. The cluster synthesis can be performed in one of two ways. In the first method, metal atoms are introduced into the material by incorporation of an organometallic block. The second method utilizes a dicarboxylic acid functionalized norbornene block as an ion exchange site, and metal atoms are loaded from aqueous solution. In both cases, the diblock copolymer film requires chemical post-treatment to convert the complexed metal ions to the corresponding metal, metal oxide, or metal sulfide.

1.4 Nanocomposite Materials

The term "nanocomposite" describes a material in which one or more phases has a characteristic length scale on the order of nanometers. In this work, a continuous microphase-separated diblock copolymer phase acts as a physical support for metal nanoclusters, and the catalytic properties of the materials were studied. In this section, general aspects of polymer/cluster nanocomposite materials are discussed.

There are several reasons why polymers are an attractive matrix material for nanocomposites. First is the diversity of materials available. A particular polymer can be chosen for a specific application based on its physical properties. For example, a transparent, glassy material such as PMMA or polycarbonate can be used for optical or non-linear optical applications, non-conductive polymers can be chosen for use in dielectric devices, and a porous or gas-permeable polymer support can be chosen for gas- or liquid-phase heterogeneous catalysis. Second, polymers can effectively stabilize nanoclusters against agglomeration. Agglomeration is highly undesirable because the valuable properties of clusters arise from their diminutive size or large surface area. Finally, most commercially available polymers have good processing characteristics. They may be dissolved and cast into films or spin-coated onto a substrate, or they may be melted and extruded into pellets or sheets.

There are also challenges to using polymers in nanocomposite materials. Polymers are subject to temperature limitations which may be a constraint in certain applications. A specific polymer may be undesirable if it undergoes a glass transition within the temperature range required for an application. At higher temperatures, polymers will degrade. Temperature limitations are of particular concern for catalytic applications because most industrial catalytic reactions are run at elevated temperatures. A second major challenge is to achieve a uniform distribution of nanoclusters within the polymer matrix. This is not a trivial task because of the difficulty of mixing small particles with high viscosity polymer melts or concentrated polymer solutions. Achieving a uniform cluster distribution can be very important for coating or dielectric

applications, and it is in this respect that the *in situ* synthesis of nanoclusters within microphase-separated diblock copolymers gains an advantage over other techniques.

Work done in the Cohen group has shown that it is possible to produce nearly monodisperse nanoclusters, homogeneously distributed within a polymer matrix by synthesizing clusters *in situ*, within microphase-separated diblock copolymer films. Three factors contribute to the well controlled formation of these materials. First, the metal ions are initially homogeneously distributed within the organometallic or ion-exchange domain of the microphase-separated diblock copolymer. Second, the presence of the microdomain interfaces helps to control cluster nucleation and growth. Third, the well-defined, thermodynamically controlled polymer morphology leads to a uniform distribution of clusters throughout the matrix, at least when length scales greater than the d-spacing of the domains are considered. The morphology is easily varied by changing the molecular weight, block length, or temperature, offering another degree of control over the system.

Polymer-based nanocomposite materials may be useful as heterogeneous catalysts for gas or liquid phase reactions because of the large surface area-to-volume ratio of the clusters and the ability of the polymer to stabilize the clusters against agglomeration and subsequent loss of catalytically active surface sites. The materials are interesting because they are processable: they can be cast into various shapes or coated onto a substrate. It is also possible that the polymer matrix could act as a permselective membrane and used to separate products from reactants or byproducts in a membrane reactor (see Section 6.2.1). However, there are at least two major impediments to using polymer-based

nanocomposites for catalysis. First, temperature limitations on the stability of the polymer matrix restrict the applicability of the materials to industrial catalytic reactions performed at relatively low temperatures. Using high temperature stable polymers would help to address this problem. Second, the clusters are completely embedded within the polymer matrix and many catalytically active sites will be covered by adsorbed polymer. Therefore, not only will catalytic reactions be severely mass transfer limited, but the nature of the interaction between the reactant and the palladium surface may be altered by the presence of the polymer chains.

1.5 Ring Opening Metathesis Polymerization

Ring opening metathesis polymerization takes place when cyclic alkenes undergo olefin metathesis, the switching of ligands between two alkene molecules.[52] An example of olefin metathesis is the reaction of 2-butene with perdeuterated 2-butene illustrated in Figure 1-2. The two molecules come together to form a cyclic transition state, then the molecules switch ligands to form two partially deuterated 2-butene molecules. When olefin metathesis occurs between two cyclic alkenes, a polymer is formed as the switching of ligands results in linkage of the two molecules. This reaction is known as metathesis polymerization. Figure 1-3 illustrates the metathesis polymerization of cyclooctene as an example. Polymerization occurs as the cyclooctene molecules become linked by $-C_6H_{12}-$ chains. A major drawback of metathesis polymerization is that the carbon-carbon double bonds remaining in the polymer backbone are also reactive, leading to chain scission and formation of cyclic oligomers. Therefore, the resulting polymer has a large polydispersity index.

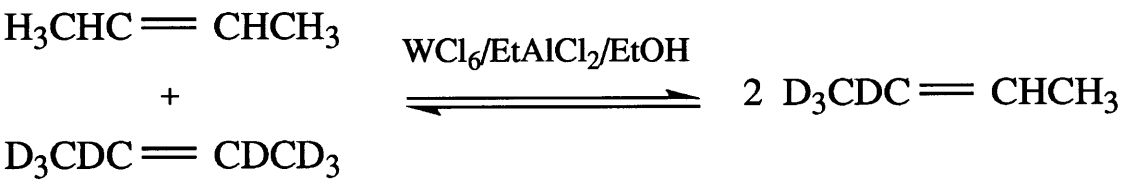

Figure 1-2: Olefin metathesis reaction between 2-butene and perdeuterated 2-butene.

The polydispersity problems associated with metathesis polymerization have been overcome by the development of new polymerization initiators by Schrock[18,19] and Grubbs[20,21] and their respective research groups. The Schrock initiators, two examples of which are shown in Figure 1-4, have either a tungsten or molybdenum alkylidene active center and the alkoxide ligands can be changed to tune the reactivity. The initiators react only with strained cyclic alkenes and are sterically prevented from reacting with carbon-carbon double bonds in the polymer backbone. This feature, combined with the fact that initiation is fast compared to propagation, allows low polydispersity polymers to be synthesized using ring opening techniques. The initiators are tolerant of a variety of

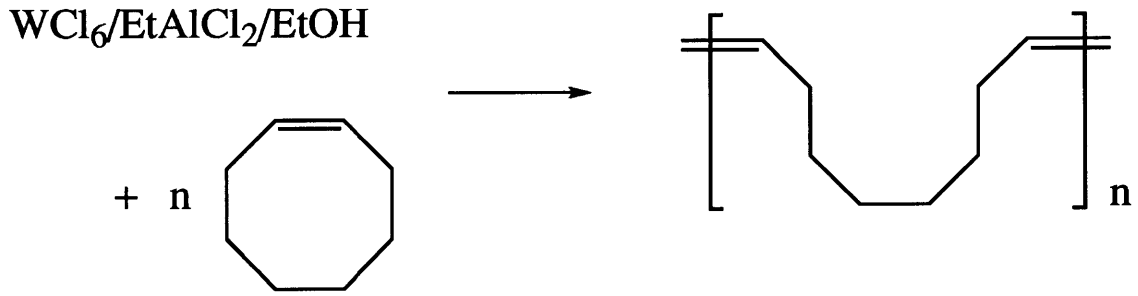

Figure 1-3: Metathesis polymerization of cyclooctene.

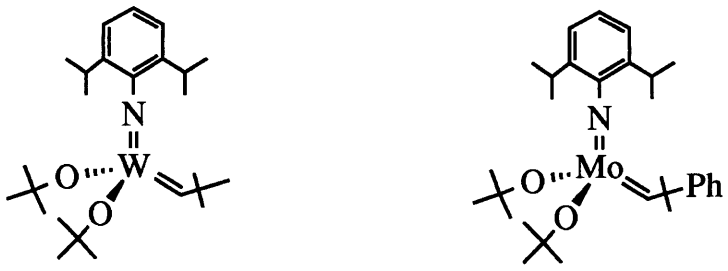

Figure 1-4: Schrock polymerization initiators - tungsten- and molybdenum-based initiators.

functional groups and, because the initiator remains active until it is cleaved from the polymer chain by addition of a capping agent, low polydispersity block copolymers can also by synthesized. Several ROMP monomers are shown in Figure 1-5.

Figure 1-6 illustrates the ROMP mechanism. In this example, the carbon-carbon double bond of the MTD molecule forms a cyclic transition state with the metal-carbon double bond of the initiator. Metathesis occurs, opening the MTD cyclopentene ring and regenerating the active site for further polymerization via insertion reactions. After the mixture has been given ample time for reaction, a second monomer is added to give a diblock copolymer. Finally, benzaldehyde is injected into the reaction solution to cleave the initiator from the polymer and terminate the polymerization.

There are a number of drawbacks to the ROMP technique. Only a few monomers and initiators are available commercially and they are very expensive because of their complex synthesis. The initiators and some of the monomers are sensitive to water and oxygen, so polymerizations must be performed inside a glove box or by using

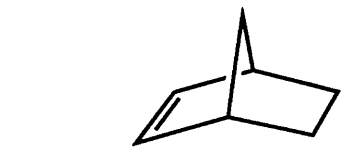

Norbornene

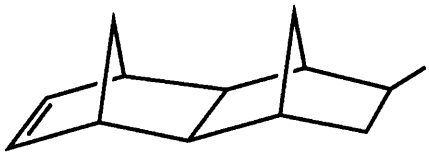

MTD

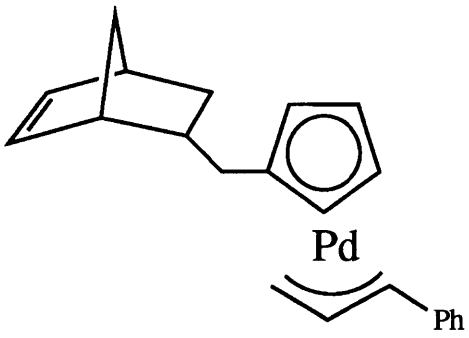

"[Pd]"

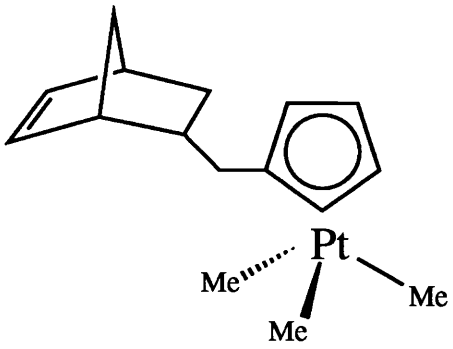

"[Pt]"

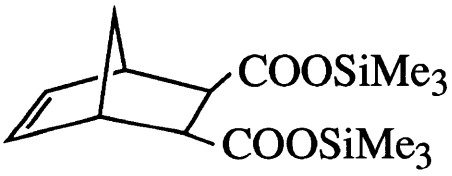

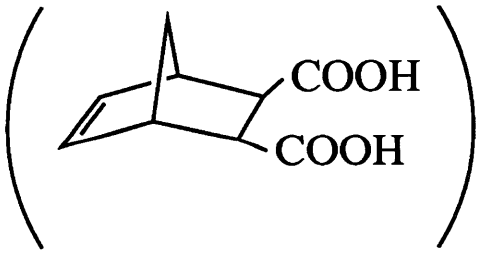

NORCOOH

Figure 1-5: ROMP monomers.

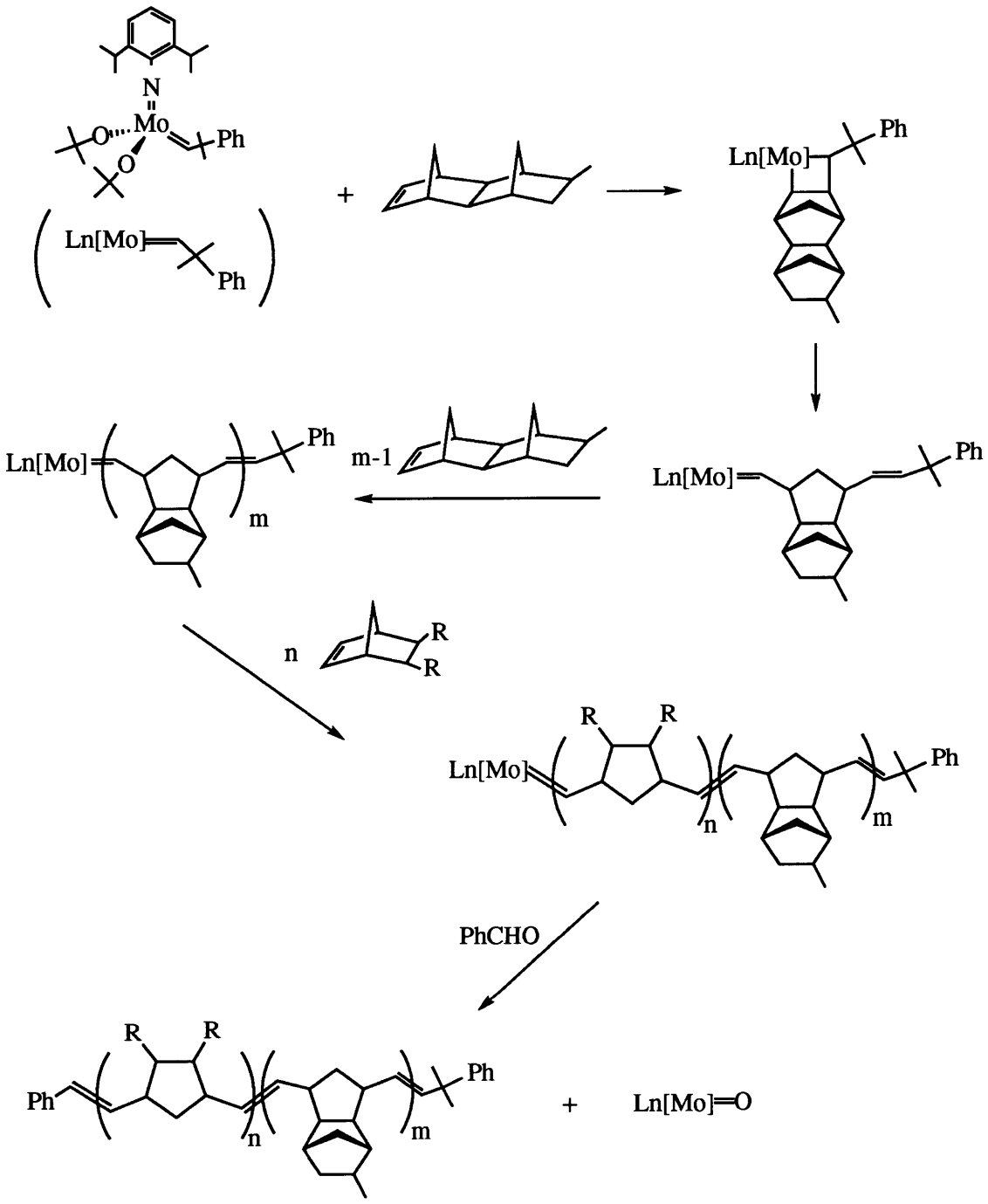

Figure 1-6: ROMP mechanism for diblock copolymer polymerization using a Schrock initiator.

Schlenk line techniques, although this is being addressed by the development of initiators tolerant of water and oxygen.[21] The limited choice of available organometallic monomers restricts the type of clusters that can be studied, since a new organometallic monomer must be synthesized for each metal of interest. This problem is being overcome by the development of the universal cluster synthesis using ion-exchange methods described previously.[34] Finally, these polymers are not mechanically stable at high temperatures. Polynorbornene and polyMTD have a T_g of 35°C and roughly 200°C, respectively.[22]

1.6 Heterogeneous Catalysis

The following brief introduction to heterogeneous catalysis explains the terms catalyst, activity, selectivity, and deactivation.[23] This discussion refers to heterogeneous catalysts, which usually consist of metal or alloy nanoclusters deposited on a support such as alumina or activated carbon. A major advantage of heterogeneous catalysis over homogeneous catalysis is the ease with which the catalyst can be separated from the products and reactants. In practice, this represents a substantial cost savings and heterogeneous catalysis is used industrially whenever possible.

A catalyst is a substance that increases the rate of a reaction towards equilibrium. The catalyst cannot alter the equilibrium state of the system, only speed the rate at which the system approaches that equilibrium. Strictly speaking, the catalyst should not be consumed in the course of the reaction.

The catalyst activity is the rate at which a reaction will proceed towards equilibrium in the presence of the catalyst. This rate may be expressed in a number of

different ways and will depend on reaction conditions, so the temperature, pressure, and reactant concentrations used should also be reported. A popular way of expressing the rate of a heterogeneous reaction is:

$$\text{rate} = \frac{\text{molecules reacted}}{\text{time} * \text{area}} \qquad (1\text{-}6)$$

In this work, the rate, or activity, is expressed in a modified form. The number of molecules reacted is expressed in moles and the units of time are seconds. Further, the activity is expressed per mole of palladium rather than per unit area because the nanocluster surface area could not be measured by chemisorption since the clusters are completely embedded within a dense polymer matrix and gas molecules adsorbed on the cluster surface cannot be distinguished from those sorbed by the polymer matrix. This substitution is acceptable from an engineering point of view because of the high cost of palladium.

When more than one product is possible in a chemical reaction, the selectivity of the catalyst is of prime importance. The catalyst selectivity is expressed as the ratio of the moles of the desired product produced to the moles of reactant consumed. The desired product is usually an intermediate, rather than the species produced by allowing the reaction to proceed to the lowest free energy state. The catalyst selectivity will also depend on the reaction temperature, pressure, composition, and conversion; therefore, the selectivity can be improved by running the reaction at conditions that favor the desired product thermodynamically.

Catalyst deactivation refers to the loss of activity or selectivity and may have one or more causes. A catalyst can be poisoned by an impurity in the feed stream that adsorbs to the surface, blocking active sites. Poisoning may be reversible if the impurity does not adsorb strongly. Fouling is caused by the formation of carbonaceous deposits on the metal surface, and may be controlled by increasing the hydrogen partial pressure in the feed stream. The loss of active sites by sintering or migration of metal clusters is a serious problem for supported metal catalysts, particularly when reactions are run at high temperatures.

Supported palladium catalysts are used industrially for a number of reactions including hydrogenation, oxidation, and acid catalysis. Palladium supported on carbon is used to hydrogenate fine organic chemicals. Alumina supported catalysts are used to hydrogenate benzene to cyclohexane and in the partial hydrogenation of acetylene present as an impurity in ethylene streams from thermal cracking processes. Palladium is also used to oxidize carbon monoxide, hydrocarbons, and NO_x present in automobile exhaust and other industrial emissions. Monolith supports are used for these applications because of their low pressure drop. Vinyl acetate is synthesized from acetic acid by reaction with ethylene and oxygen over a palladium catalyst on an acid-resistant support, and palladium deposited on zeolites is used for hydrocracking, i.e. catalytic cracking of hydrocarbons with hydrogenation.

1.7 References

(1) Pocard, N. L.; Alsmeyer, D. C.; McCreery, R. L.; Neenan, T. X.; Callstrom, M. R. *J. Am. Chem. Soc.* **1992**, *114*, 769.

(2) Klabunde, K. J.; Li, Y. X.; Tan, B. J. *Chem. Mater.* **1991**, *3*, 30.

(3) Davis, S. C.; Klabunde, K. J. *Chem. Rev.* **1982**, *82*, 153.

(4) Sohn, B. H.; Cohen, R. E. *Chem. Mater.* **1997**, *9*, 264.

(5) Ichiyanagi, Y.; Kimishima, Y. *Jpn. J. Appl. Phys.* **1996**, *35*, 2140.

(6) Lesliepelecky, D. L; Rieke, R. D. *Chem. Mater.* **1996**, *8*, 1770.

(7) Gao, M.; Yang, Y.; Yang, B.; Shen, J. *J. Chem. Soc. Faraday Trans.* **1995**, *91*, 4121.

(8) Magruder III, R. H.; Weeks, R. A.; Morgan, S. H.; Pan, Z.; Henderson, D. O.; Zuhr, R. A. *J. Non-Crystall. Solids* **1995**, *193*, 546.

(9) Puech, K.; Henari, F.; Blau, W.; Duff, D.; Schmid, G. *Europhys. Lett.* **1995**, *32*, 119.

(10) Bahnemann, D. W. *Israel J. Chem.* **1993**, *33*, 115.

(11) Perrin, J.; Despax, B.; Kay, E. *Phys. Rev. B* **1985**, *32*, 719.

(12) Henglein, A. *Chem. Rev.* **1989**, *89*, 1861.

(13) Stucky, G. D.; MacDougall, J. E. *Science* **1990**, *247*, 669.

(14) Halperin, W. P. *Rev. Mod. Phys.* **1986**, *58*, 533.

(15) Bond, G. C. *Surf. Sci.* **1985**, *156*, 966.

(16) Schrock, R. R. *Acc. Chem. Res.* **1990**, *23*, 158.

(17) Grubbs, R. H.; Tumas, W. *Science* **1989**, *243*, 907.

(18) Schrock, R. R.; DePue, R. T.; Feldman, J.; Yap, K. B.; Yang, D. C.; Davis, W. M.; Park, L.; DiMare, M.; Schofield, M.; Anhaus, J.; Walborsky, E.; Evitt, E.; Krüger, C; Betz, P. *Organometallics* **1990**, *9*, 2262.

(19) Schrock, R. R.; Murdzek, J. S.; Bazan, G. C.; Robbins, J.; DiMare, M.; O'Reagan, M. *J. Am. Chem. Soc.* **1990**, *112*, 3875.

(20) Schwab, P.; Grubbs, R. H.; Ziller, J. W. *J. Am. Chem. Soc.* **1996**, *118*, 100.

(21) Lynn, D. M.; Kanaoka, S.; Grubbs, R. H. *J. Am. Chem. Soc.* **1996**, *118*, 784.

(22) Ng Cheong Chan, Y.; Craig, G. S. W.; Schrock, R. R.; Cohen, R. E. *Chem. Mater.* **1992**, *4*, 885.

(23) Satterfield, C. N. *Heterogeneous Catalysis in Industrial Practice*; Second Edition; McGraw-Hill, Inc.: New York, 1991, pp. 6-18.

(24) Sohn, B. H.; Cohen, R. E. *Acta Polymerica* **1996**, *47*, 340.

(25) Bradley, J. S.; Hill, E.; Leonowicz, M. E.; Witzke, H. *J. Mol. Catal.* **1987**, *41*, 59.

(26) Toshima, N.; Takahashi, T. *Bull. Chem. Soc. Jpn.* **1992**, *65*, 400.

(27) Hirai, H.; Chawanya, H.; Toshima, N. *Bull. Chem. Soc. Jpn.* **1985**, *58*, 682.

(28) Petit, C.; Lixon P.; Pileni, M. P. *J. Phys. Chem.* **1993**, *97*, 12974.

(29) Roescher, A.; Moller, M. *Adv. Mater.* **1996**, *8*, 337.

(30) Reetz, M. T.; Helbig, W.; Quaiser, S. A.; Stimming, U.; Breuer, N.; Vogel, R. *Science* **1995**, *267*, 367.

(31) Breitscheidel, B.; Zieder, J.; Schubert, U. *Chem. Mater.* **1991**, *3*, 559.

(32) El-Shall, M. S.; Slack, W. *Macromolecules* **1995**, *28*, 8456.

(33) Watkins, J. J.; McCarthy, T. J. *Chem. Mater.* **1995**, *7*, 1991.

(34) Clay, R.; Cohen, R. E. *Supramolecular Science* **1995**, *2*, 183.

(35) Flory, P. J. *Principles of Polymer Chemistry*; Cornell University Press: Ithaca, NY, 1953, pp. 507-511.

(36) Bates, F. S.; Fredrickson, G. H. *Annu. Rev. Phys. Chem.* **1990**, *41*, 525.

(37) Hashimoto, T.; Tanaka, H.; Hasegawa, H. *Macromolecules* **1985**, *18*, 1864.

(38) Liebler, L. *Macromolecules* **1980**, *13*, 1602.

(39) Hasegawa, H.; Tanaka, H.; Yamasaki, K.; Hashimoto, T. *Macromolecules* **1987**, *20*, 1651.

(40) Argon, A. S.; Cohen, R. E.; Jang, B. Z.; Vander Sande, J. B. *Polym. Sci. Polym. Phys. Ed.* **1981**, *19*, 253.

(41) Thomas, E. L.; Alward, D. B.; Kinning, D. J.; Martin, D. C.; Handlin, D. L.; Fetters, L. J. *Macromolecules* **1986**, *19*, 2197.

(42) Kofinas, P.; Cohen, R. E. *Macromolecules* **1995**, *28*, 336.

(43) Sperling, L.H. *Introduction to Physical Polymer Science*; Wiley-Interscience: New York, NY, 1986, pp. 346-349.

(44) Sankaran, V.; Cohen, R. E.; Cummins, C. C.; Schrock, R. R. *Macromolecules* **1991**, *24*, 6664.

(45) Cummins, C. C.; Beachy, M. D.; Schrock, R. R.; Vale, M. G.; Sankaran, V.; Cohen, R. E. *Chem. Mater.* **1991**, *3*, 1153.

(46) Sankaran, V.; Yue, J.; Cohen, R. E.; Schrock, R. R.; Silbey, R. J. *Chem. Mater.* **1993**, *5*, 1133.

(47) Ng Cheong Chan, Y.; Schrock, R. R.; Cohen, R. E. *Chem. Mater.* **1992**, *4*, 24.

(48) Ng Cheong Chan, Y.; Schrock, R. R.; Cohen, R. E. *J. Am. Chem. Soc.* **1992**, *114*, 7295.

(49) Yue, J.; Sankaran, V.; Cohen, R. E.; Schrock, R. R. *J. Am. Chem. Soc.* **1993**, *115*, 4409.

(50) Cummins, C. C.; Schrock, R. R.; Cohen, R. E. *Chem. Mater.* **1992**, *4*, 27.

(51) Sankaran, V.; Cummins, C. C.; Schrock, R. R.; Cohen, R. E.; Silbey, R. J. *J. Am. Chem. Soc.* **1990**, *112*, 6858.

(52) Rempp, P.; Merrill, E. W. *Polymer Synthesis*; Second Edition; Hüthig and Wepf: Basel, Switzerland, 1991, pp. 195-197.

2. Synthetic Techniques

2.1 Introduction

This chapter describes the techniques used to synthesize the organometallic, derivatized norbornene monomer $Pd(Cp^N)PA$. The synthetic route to $LiCp^N$ was developed by C. C. Cummins, and further information can be found in his thesis,[1] as well as those of R. Saunders[2] and V. Sankaran.[3] A description of the final step to synthesize $Pd(Cp^N)PA$ from $LiCp^N$ and $[Pd(PA)Cl]_2$ is given in G. S. W. Craig's thesis.[4] The following complete description of the $Pd(Cp^N)PA$ synthesis includes information taken from all of these sources.

Sections 2.3, 2.4, and 2.5 describe, respectively, the synthesis of diblock copolymers, static casting of the precursor microphase-separated diblock copolymer films, and formation of palladium nanoclusters within these films. All of these techniques have been used by previous members of the Cohen group.[2-5]

2.2 Palladium Monomer Synthesis

The synthetic scheme for the monomer is represented in Figure 2-1. A Diels-Alder reaction between cyclopentadiene and methyl acrylate to form *endo*-2-(carbomethoxy)norborn-5-ene is followed by reduction to *endo*-2-(hydroxymethyl)norborn-5-ene with $LiAlH_4$, tosylation, then reaction with NaCp to give HCp^N. $Li(Cp^N)$ is obtained by the reaction of HCp^N with *n*-butyl lithium, then reacted with $[Pd(PA)Cl]_2$ in the final step to give $Pd(Cp^N)PA$. This reaction path gives the *endo* product almost exclusively, simplifying the NMR analysis. An alternative is to purchase

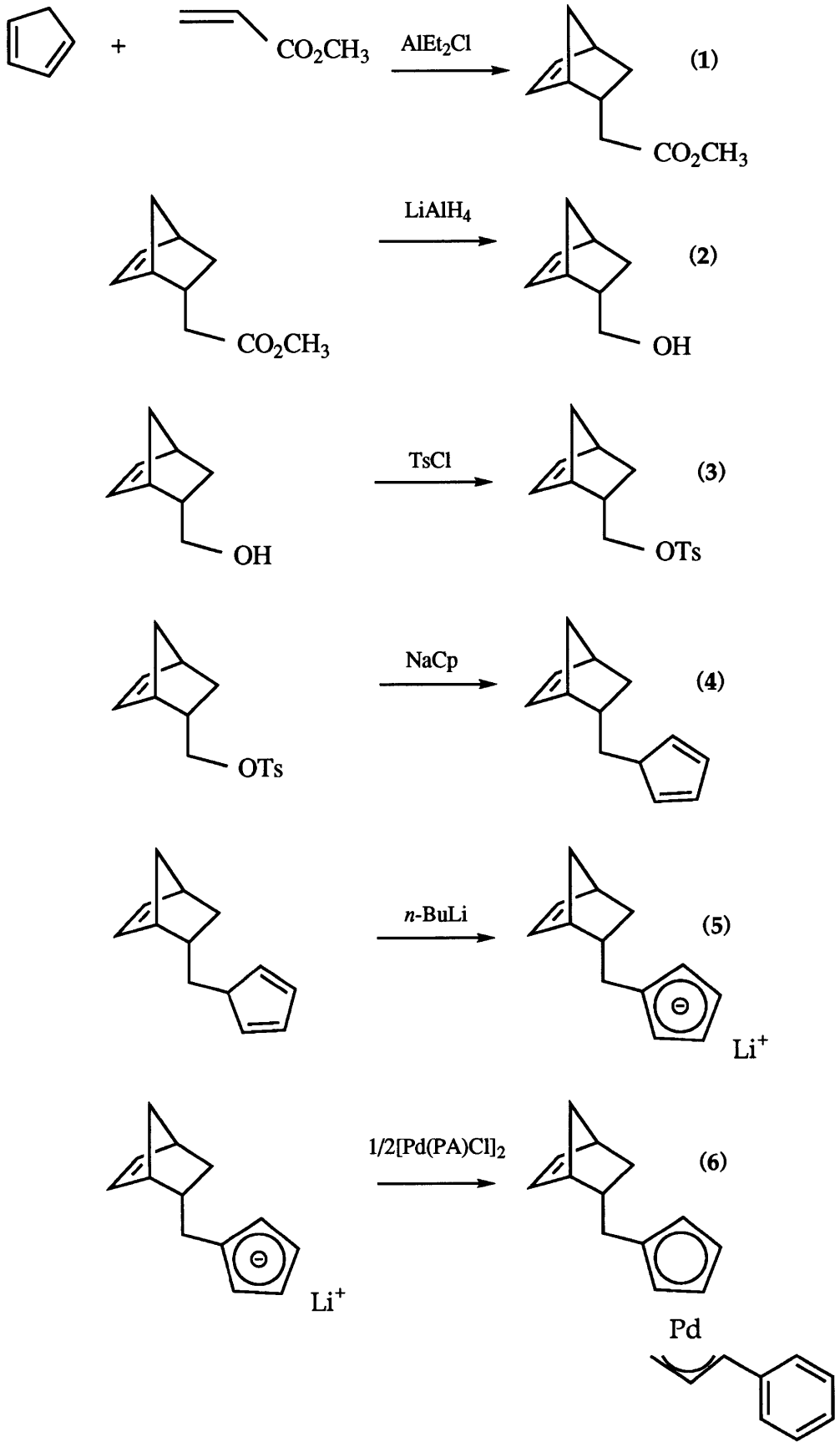

Figure 2.1: Synthetic Route to Pd(Cp^N)PA.

an *endo/exo* mixture of the hydroxymethyl derivative **2** from Aldrich, or another supplier, and continue with steps three through six.

2.2.1 General

All syntheses were conducted under a nitrogen atmosphere in a Vacuum Atmospheres glove box, or by using standard Shlenck and vacuum line techniques. Dichloromethane, THF, pentane, and benzene for the monomer synthesis were dried over sodium hydride and vacuum distilled prior to use. Diethyl ether and pyridine were used from freshly opened containers.

2.2.2 *endo*-2-(carbomethoxy)norborn-5-ene (1) Synthesis

Diethylaluminum chloride (Et_2AlCl, 21.0 g, 174.2 mmol) was weighed inside the glove box and dissolved in dichloromethane (CH_2Cl_2, 250 mL) in a 500 mL two-necked flask. The flask was fitted with a gas-adapter and a rubber septum, removed from the glove box, and placed under a nitrogen atmosphere. The contents of the flask were then cooled to -78°C in a dry ice/isopropanol bath. Methyl acrylate (15.0 g, 174.2 mmol) was added to the stirred solution using a gas-tight syringe to give a pale yellow solution. The solution was stirred for 15 minutes before freshly cracked cyclopentadiene (11.5 g, 174.2 mmol) was added via gas-tight syringe. The reaction mixture was slowly warmed to room temperature over a period of 2-3 hours, and stirred overnight.

The reaction was quenched by slowly transferring portions of the solution into a 0°C solution of ammonium chloride (NH_4Cl, 45 g, 0.84 mol) in distilled water (500 mL) via cannula using a modest back pressure of nitrogen. CAUTION: UNREACTED Et_2AlCl REACTS VIOLENTLY WITH THE SALT SOLUTION. THE CANNULA

OUTLET SHOULD BE KEPT SUBMERGED IN THE SALT SOLUTION AT ALL TIMES. Swirl the NH_4Cl solution while quenching, and stop the transfer briefly if there is too much frothing. There will be a strong smell.

The quenched reaction solution was transferred to a separatory funnel and the organic layer (bottom) was removed. The organic layer was washed with water (250 mL), dried over magnesium sulfate ($MgSO_4$) for one hour, and filtered. The volatiles were then removed in vacuo to yield the product - a colorless, viscous liquid [22.7 g, 149.1 mmol, 85.7% yield].

2.2.3 *endo*-2-(hydroxymethyl)norborn-5-ene (2) Synthesis

A 500 mL three-necked flask was fitted with a reflux condenser, a dropping funnel (center neck), and a gas adapter. The flask was flushed with nitrogen and filled with diethyl ether (250 mL) from a freshly opened container. Lithium aluminum hydride ($LiAlH_4$, 5.7 g, 149 mmol) was weighed out in the fume hood, and transferred to the flask using a plastic funnel. The dropping funnel was charged with a solution of **1** (22.7 g, 149 mmol) in diethyl ether (60 mL). The flask was placed under a nitrogen blanket, and the ester solution was allowed to drip slowly into the $LiAlH_4$ suspension (rate $\approx$ 1 drop/s). Stirring was continued overnight.

The reaction slurry was chilled to 0°C and carefully quenched under a nitrogen purge by dropwise addition of water (4 mL), a 15% sodium hydroxide solution (4 mL), and water (12 mL) with vigorous stirring. The resulting fine, white precipitate was filtered through a glass frit and washed with diethyl ether (4 x 100 mL). The filtrate was

dried over sodium sulfate (Na_2SO_4) for about one hour, filtered, and the volatiles were removed in vacuo leaving a colorless, viscous liquid product [18.4 g, 148 mmol, 99.5% yield].

2.2.4 *endo*-2-(tosylatomethyl)norborn-5-ene (3) Synthesis

A solution of **2** (18.4 g, 148 mmol) in pyridine (100 mL) was placed in a 250 mL round bottom flask. The solution was cooled to 0°C with stirring. Toluene-4-sulfonyl chloride (36.8 g, 193 mmol) was added to the flask in portions over 45 minutes, then the reaction solution was stirred for another 24 hours. Initially, the solution was yellow, then pink Py*HCl began to precipitate.

To quench the reaction, the contents of the flask were poured into a stirred flask of distilled water (300 mL) cooled to 0°C. The mixture was extracted with anhydrous diethyl ether (175 mL), and the extraction was repeated on the resulting aqueous layer (4 x 150 mL). The combined organic extracts were washed with chilled hydrochloric acid (2 N, 200 mL), then distilled water (2 x 250 mL). The organic solution was pale yellow. NOTE: IF THE SOLUTION IS STILL PINKISH, REPEAT THE HCl EXTRACTION. The ether solution was dried over anhydrous sodium sulfate (Na_2SO_4) for one hour, filtered, and the volatiles were removed in vacuo leaving a white, waxy, crystalline solid [29.4 g, 106 mmol, 71.4% yield].

2.2.5 HCp^N (or *endo*-NbeCp) (4) Synthesis

A solution of sodium cyclopentadienylide (NaCp) in THF (2 M, 100 mL, 0.2 mol) was transferred to a 250 mL three-necked flask inside the glove box. The flask was fitted with a gas adapter, an addition funnel (center neck), and a glass stopper. **3** (12 g,

43.1 mmol) was dissolved in THF (20 mL) and the solution was poured into the addition funnel. The flask was then sealed completely, removed from the glove box, and placed under an argon blanket. The NaCp solution was chilled to 0°C, and the tosylate solution was added dropwise (rate ≈ 1 drop/s) with stirring. The ice bath was removed after complete addition of the tosylate solution and the reaction was continued for another 24 hours at room temperature, resulting in a cloudy, pink solution.

The reaction mixture was poured into an Erlenmeyer flask containing ammonium chloride (NH_4Cl, 10 g) dissolved in distilled water (500 mL) and stirred for 15 minutes. The organic layer was removed with a separatory funnel and washed with petroleum ether (hexanes, 3 x 200 mL). The organic layers were collected and dried over anhydrous magnesium sulfate ($MgSO_4$) for one hour, filtered, and the volatiles were removed in vacuo. The crude product, still containing **3** as an impurity, was an amber colored liquid. The purified product is obtained as a clear, colorless liquid using a short path distillation column under vacuum. Keeping the pot at 90-95°C, the overhead product is collected at 42-45°C. NOTE: USE AIR TO COOL THE CONDENSER, NOT WATER.

Important: This step should be completed quickly because HCp^N will undergo a Diels-Alder reaction if kept too long at elevated temperatures. The next synthetic step should be done soon after purification of **4**.

2.2.6 $LiCp^N$ (or *endo*-NbeCpLi) (5) Synthesis

Freshly prepared HCp^N (mass unknown) was dissolved in pentane (100 mL) in a round bottom flask and the solution was chilled to -40°C in a dry box freezer. A solution

of *n*-butyl lithium (2.5 M in hexanes, 13 mL, 32.5 mmol, large excess) was added via syringe. The mixture was allowed to warm to room temperature, and stirred for another 2.5 hours. A white product began to precipitate. The mixture was then chilled to -40°C for six hours, after which the excess solvent was removed with a Pasteur pipette. The product was washed five times with pentane in the reaction flask, removing the solvent with a pipette after each washing. Finally, the product was dried using a Rotovap inside the dry box.

2.2.7 Pd(Cp^N)PA Synthesis

$[Pd(PA)Cl]_2$ (780 mg, 1.51 mmol) was added to a THF/benzene mixed solvent (THF:benzene = 1:1 by volume, 20 mL) in a small round bottom flask inside the dry box. $LiCp^N$ (536 mg, 2.99 mmol) was dissolved in THF, chilled to -40°C, then added dropwise to the stirred $[Pd(PA)Cl]_2$ suspension over 15 minutes. The reaction mixture was warmed to room temperature, and left to stir for another five hours. The solvent was then removed in vacuo, and the residue was extracted with pentane (20 mL) to remove LiCl. The purple, crystalline product was collected by cooling the pentane extract to -40°C, removing the excess solvent with a Pasteur pipette, and drying the remaining crystals in vacuo. The recovery process was repeated three times.

2.2.8 NMR Analysis of Pd(Cp^N)PA

A comparison of the NMR spectrum of the final reaction product to that previously reported for the palladium monomer[6] (see Table 2.1) proved that the monomer synthesis was successful. Table 2.1 lists chemical shifts in ppm down field of TMS, the

$\delta_{observed}$	$\delta_{expected}$[6]	Peak Type	Peak Assignment[6]
8.65-8.42	8.68-8.40	m	phenyl
7.48	7.48	m	olefin
7.33	7.32	m	olefin
7.16	7.15	br s	Cp
7.07	7.06	m	Cp
6.84	6.83	br m	Cp
6.66	6.65	m	allyl
5.24	5.24	dd	allyl
4.81	4.80	d	allyl
4.11	4.11	br s	bridgehead
4.06	4.06	br s	bridgehead
3.68	3.67	d	allyl
3.46	3.46	m	*exo*-methine
3.20-3.10	3.23-3.08	m	1-*exo*-CH_2, 2 Cp H_2
2.87	2.87	dm	C(7) H_2
2.52	2.51	d	C(7) H_2
1.96	1.96	ddd	*endo* CH_2

Table 2.1: Comparison of NMR spectra of Pd(Cp^N)PA with previous results.

type of peak observed, and the peak assignments.[6] NMR spectra were recorded at 300 MHz on a Varian XL-300 spectrometer.

2.3 Polymer Synthesis

2.3.1 Synthesis of $[MTD]_{113}[Pd(Cp^N)PA]_{50}$

Diblock copolymers with the nominal formula $[MTD]_{113}[Pd(Cp^N)PA]_{50}$ containing 50 wt% of each block were synthesized as in previous work[4, 6] via ring opening metathesis polymerization. A typical synthesis is described here. A solution of $Mo(CHCMe_2Ph)(NAr)(O\text{-}t\text{-}Bu)_2$ (4.17 mg, $7.59x10^{-3}$ mmol in toluene) was injected with a micropipette into a rapidly stirred solution of MTD (0.15 g, 0.86 mmol) in toluene (3.75 mL). After 15 minutes, 1.25 mL of the reaction solution was removed and quenched with

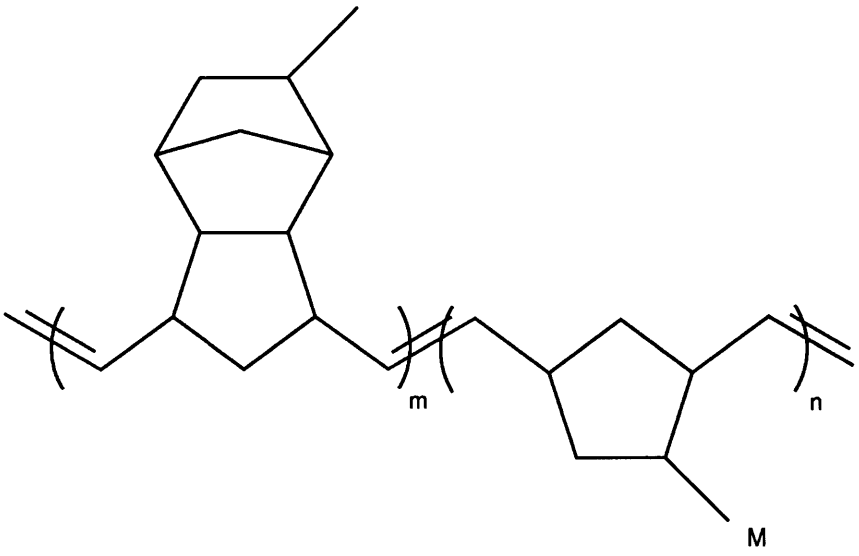

Figure 2-2: Chemical structure of $[MTD]_m[Pd(Cp^N)PA]_n$ diblock copolymer. M = $CH_2CpPd(PA)$.

10 μL of benzaldehyde. A solution of $Pd(Cp^N)PA$ (0.10 g, 0.25 mmol, in 2.5 mL toluene) was added to the original reaction mixture, allowed to react for a further 15 minutes, then quenched with 10 μL of benzaldehyde. A portion of each solution was reserved for GPC analysis. The chemical structure of the diblock copolymer is shown in Figure 2-2.

2.3.2 GPC Analysis of Polymers

The molecular weight distribution of both the $[MTD]_{113}$ homopolymer and the $[MTD]_{113}[Pd(Cp^N)PA]_{50}$ diblock copolymer were analyzed by gel permeation chromatography using Waters Ultrastyrogel columns connected to a differential refractometer. GPC was conducted in toluene (flow rate = 1 mL/min) at room temperature, and the polymer solutions were passed through Millex-SR 0.5 μm filters

Polymerization Run	$[MTD]_{113}$		$[MTD]_{113}[Pd(Cp^N)PA]_{50}$	
	PD	MW (g/mol)	PD	MW (g/mol)
1	1.12	25,000	n/a	n/a
2	1.08	26,000	1.05	41,000
3	1.10	19,000	1.10	31,000
4	1.11	24,000	1.27	37,000
6	1.11	25,000	1.09	40,000

Table 2.2: Polydispersity and polystyrene-equivalent molecular weight for $[MTD]_{113}$ and $[MTD]_{113}[Pd(Cp^N)PA]_{50}$.

prior to analysis to remove particulates. The GPC columns were calibrated using polystyrene standards, and molecular weights are reported as the polystyrene equivalent. Sample chromatograms are shown in Figures 2-3 and 2-4 for $[MTD]_{113}$, and $[MTD]_{113}[Pd(Cp^N)PA]_{50}$, respectively. The appearance of a shoulder on the main peak, as well as the presence of some high molecular weight polymer, can be avoided for the most part by using anhydrous toluene for polymer syntheses. The toluene should be stirred over sodium for a few days and filtered just prior to use. Table 2.2 gives the polydispersity index and the location of the peak maximum for each polymer sample.

2.4 Film Casting

Polymer films were formed by static casting. A 3-5 wt% solution of the diblock copolymer in toluene was placed in a casting boat constructed from Teflon-coated aluminum foil pressed to a glass microscope slide. The casting boat was then placed inside a jar, loosely covered, and the solvent was allowed to evaporate slowly over 3-5 days either in the glove box or in a fume hood. Traces of solvent were removed from the films by storing them in a vacuum oven at least overnight. The morphology of these

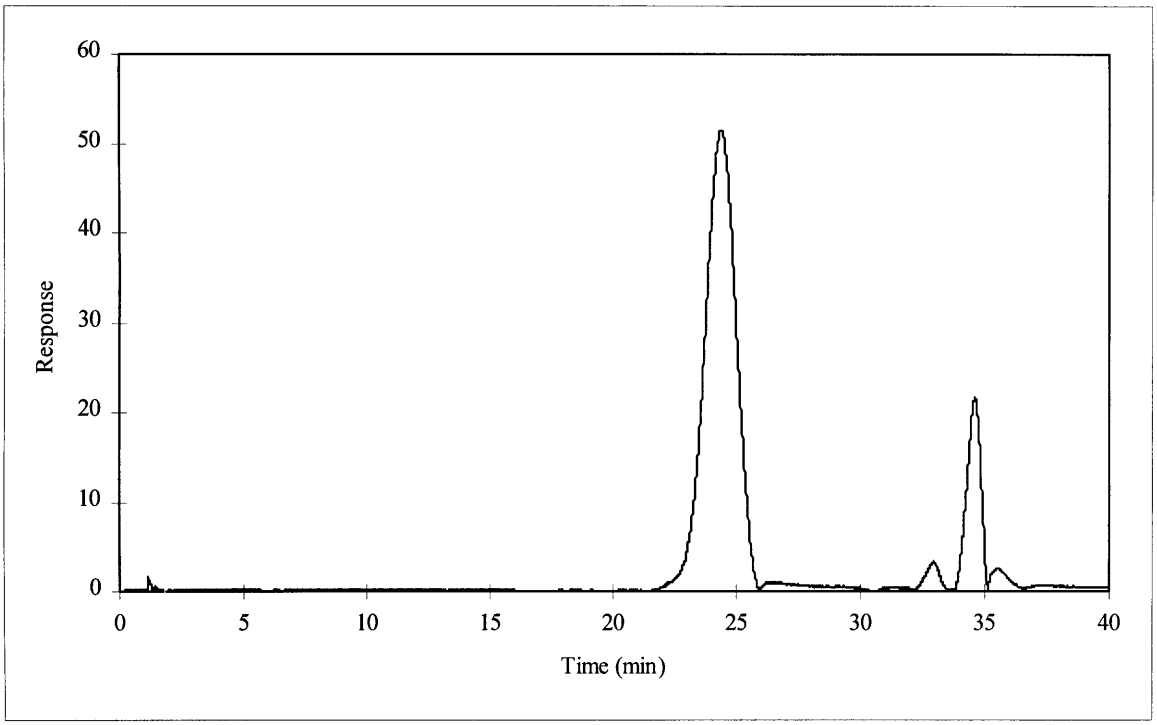

Figure 2-3: Gel permeation chromatogram of $[MTD]_{113}$.

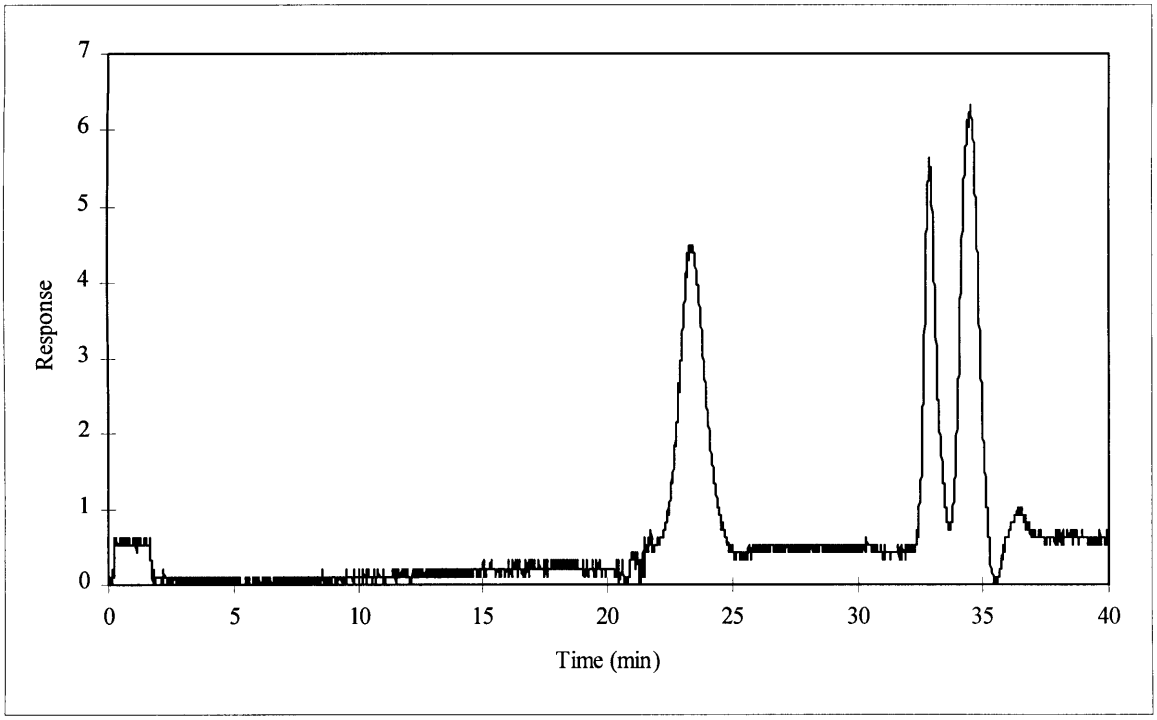

Figure 2-4: Gel permeation chromatogram of $[MTD]_{113}[Pd(Cp^{N})PA]_{50}$.

precursor films was studied by TEM and SAXS. Further details of these analysis techniques are given in Sections 3.2.5 and 3.2.6; results are presented in Sections 3.3.1 and 3.3.2.

2.5 Cluster Formation

Clusters were formed *in situ* by reduction of the palladium complex attached to each Pd(Cp^N)PA repeat unit. The reduction was accomplished by placing the polymer films inside a Fischer-Porter bottle and exposing them to hydrogen at 30 psi_g and 100°C for three days. NOTE THAT TO REDUCE THE RISK OF FIRE OR EXPLOSION, THE FISCHER-PORTER BOTTLE WAS PURGED WITH ARGON OR NITROGEN BEFORE TRANSFERRING THE HYDROGEN GAS. The cluster size and distribution within the polymer matrix were studied by TEM and SAXS. Results of these studies for various films are presented in Sections 3.3.1, 3.3.2, and 4.3.1.

2.6 References

(1) Cummins, C. C. Doctoral Thesis, Massachusetts Institute of Technology, Department of Chemistry **1993**.

(2) Saunders, R. S. Doctoral Thesis, Massachusetts Institute of Technology, Department of Chemical Engineering **1992**.

(3) Sankaran, V. Doctoral Thesis, Massachusetts Institute of Technology, Department of Chemical Engineering **1993**.

(4) Craig, G. S. W. Doctoral Thesis, Massachusetts Institute of Technology, Department of Chemical Engineering **1993**.

(5) Sohn, B. H. Doctoral Thesis, Massachusetts Institute of Technology, Department of Mechanical Engineering **1996**.

(6) Ng Cheong Chan, Y.; Craig, G. S. W.; Schrock, R. R.; Cohen, R. E. *Chem. Mater.* **1992**, *4*, 885-894.

3. Ethylene Hydrogenation

3.1 Introduction

There has been growing interest during recent years in materials with characteristic length scales on the order of nanometers. Nanoclusters and the nanocomposite materials into which they may be incorporated are they may possess potentially useful catalytic,[1] magnetic,[2] dielectric,[3] or other properties.

An array of nanocluster synthetic techniques have been developed. Many of these involve the reduction of metal salts in solution with a stabilizing polymer or surfactant.[4,5] In some cases, protected nanoclusters have been immobilized on crosslinked polymer gels[6] or porous alumina particles[7] for use as heterogeneous catalysts. Other solution-based techniques use reverse micelles[8,9] or diblock copolymer micelles.[10,11] Nanoclusters have been formed on the surface of functionalized polymer spheres capable of binding metal atoms in solution.[12] Nanoclusters may be synthesized via sol-gel[13,14] or electrochemical[15-17] techniques. Other synthetic methods include direct reduction of metal salts without solvent or stabilizer,[18,19] condensation of metal vapor into a cold solution of a stabilizing polymer,[20] and pyrolysis of organometallic reagents by injection into a hot coordinating solvent.[21,22]

Relatively few techniques have been developed to produce bulk polymer-based nanocomposite materials, despite the many interesting potential applications of such materials. One novel method involves reduction of metal complexes in solution where the solvent acts as both a ligand and as a monomer which can later be polymerized.[23] Metal vapors may also be condensed into a liquid monomer which is subsequently

polymerized.[24,25] Bulk nanocomposite materials have been produced by loading and reduction of metal salts via supercritical CO_2 solution.[26] Nanoclusters may be synthesized within bulk microphase-separated diblock copolymers, either by reduction of organometallic repeat units comprising one of the blocks[27] or by loading of metal ions from solution via complexation to dicarboxylate functional groups.[28]

As mentioned above, nanoclusters and nanocomposite materials may display interesting catalytic properties. These materials should be active catalysts because of their large surface area-to-volume ratio; they may also be selective catalysts in reactions where more than one product is possible. Most studies of the catalytic activity of polymer-stabilized nanoclusters have been conducted in solution as essentially homogeneous reactions. Toshima and coworkers have done extensive work on evaluating the catalytic activity of Pt,[5,6] Pd,[4,5] Rh,[29] and bimetallic clusters[30-32] stabilized in solution by water-soluble polymers. The nanoclusters displayed good catalytic activity under mild conditions for the hydrogenation of a number of substrates including cyclohexene, cyclooctadiene, and fatty acids, and for light-induced evolution of hydrogen from water. Recently, the Toshima group has demonstrated the ability of polymer-immobilized neodymium ions to act as promoters, increasing the activity of polymer-stabilized palladium clusters for the liquid phase hydrogenation of 1-hexene and acrylic acid.[33]

Tamai *et al.*[12] deposited Pt, Pd, and Rh nanoclusters on fine polymer spheres and used these composites to hydrogenate 1-hexene in *n*-heptane solution at room temperature. Biffis *et al.*[34] deposited Pd nanoclusters on a microporous, cross-linked

polymer support and investigated the effect of metal content and degree of cross-linking on their catalytic activity for the hydrogenation of cyclohexene in methanol. One disadvantage of this method is that the palladium was prone to leaching from the polymer support. Pt, Pd, Rh, and bimetallic clusters have also been deposited electrochemically within polymer films coated on carbon electrodes[17] and used for the electrocatalytic hydrogenation of limonene and carronene.

A comparatively small number of studies have been undertaken to examine the catalytic activity of free-standing polymer-based nanocomposite materials in the presence of gaseous reagents. The catalytic activity of nanoclusters completely embedded within bulk, non-porous polymeric materials could be assumed to be entirely blocked by polymer segments adsorbed to the cluster surface. On the contrary, Shim and coworkers have found that Rh,[35] Pd,[36] and Ru[37] nanoclusters formed within cellulose acetate films are active for a number of gas phase reactions including ethylene hydrogenation, CO oxidation, the water-gas shift reaction, and Fischer-Tropsch type reactions. Further, Gao *et al.*[38] report that nanocomposite films formed from solutions of polymer-stabilized Pd clusters are active for the gas phase hydrogenation of isoprene and cyclopentadiene. A different system was studied by Touroude *et al.*,[7] who deposited surfactant-stabilized Pt/Pd alloy clusters within the pores of an alumina support and found these materials to be active for a number of hydrogenolysis and isomerization reactions. In all cases, the role of the protective polymer is to stabilize the clusters against agglomeration and subsequent loss of catalytically active surface sites.

The nanocomposite synthetic method used in this work is unusual in that the nanoclusters are formed *in situ* by reduction of organometallic repeat units in a diblock copolymer film. In contrast to many of the methods described above, this material initially has an homogeneous concentration of palladium ions within the organometallic domains of the copolymer film. This enables production of bulk nanocomposite materials consisting of metal clusters with a narrow size distribution, homogeneously distributed within a stabilizing polymer matrix. The polymer not only stabilizes the clusters, but also provides a structural support that can be cast into a variety of shapes that can in turn be incorporated into magnetic, electro-optic, or other devices. In this case, the nanocomposite films are used as heterogeneous catalysts and their activity for ethylene hydrogenation is studied as a function of cluster size. The ability to cast free-standing or surface-conforming films allows the possibility of incorporating these nanocomposites into catalytic membrane reactors, where catalysis and product separation occur in a single unit operation. The nanocomposite could act as both the catalyst and the permselective membrane. This application is described in more detail in Section 6.2.1.

3.2 Experimental

3.2.1 General

All syntheses were conducted under a nitrogen atmosphere in a Vacuum Atmospheres glove box or by using standard Shlenck and vacuum line techniques. Dichloromethane, THF, pentane, and benzene for the monomer synthesis were dried over sodium hydride and vacuum distilled prior to use. Diethyl ether and pyridine were used from freshly opened containers. Anhydrous toluene was purchased from Aldrich and

stirred over sodium, then filtered through a glass frit before being used for polymerization reactions.

3.2.2 Organometallic Monomer Synthesis

HCp^N was synthesized as previously reported[27] at low temperature by the $AlEt_2Cl$ catalyzed Diels-Alder reaction of cyclopentadiene with methyl acrylate, followed by reduction to *endo*-2-(hydroxymethyl)norborn-5-ene by $LiAlH_4$, tosylation, and treatment with NaCp. HCp^N was reacted with *n*-BuLi in pentane to give $Li(Cp^N)$ which was subsequently reacted with $[Pd(PA)Cl]_2$ to produce the palladium-containing monomer, $Pd(Cp^N)PA$.

3.2.3 Polymer Synthesis

A diblock copolymer with the nominal formula $[MTD]_{113}[Pd(Cp^N)PA]_{50}$ containing 50 wt% of each block was synthesized as in previous work[27] via ring opening metathesis polymerization. A typical synthesis is described in Section 2.3.1. GPC analysis showed that the homopolymer and diblock copolymer had polystyrene-equivalent molecular weights of 19,000 g/mol (calculated value = 20,000 g/mol) and 31,000 g/mol (calculated value = 40,000 g/mol), respectively. The polydispersity index was 1.10 in both cases. The chemical structure of the diblock copolymer is shown in Figure 2-2.

3.2.4 Polymer Film Formation and Cluster Synthesis

Microphase-separated copolymer films, *ca.* 200 μm thick, were static cast directly from the polymerization solution which was diluted with GPC grade toluene to *ca.* 4 wt% polymer. Films were cast in Teflon-lined boats in air. The solvent was allowed to

evaporate slowly over 3-5 days. The resulting dark purple films were then placed under vacuum for two days before further analysis. Palladium nanoclusters were formed by exposing the films to hydrogen at 30 psi_g and 100°C for 3-4 days inside a Fischer-Porter bottle.

3.2.5 Morphological Characterization

TEM was performed on a JEOL 200 CX at 200 kV. Samples 100-150 nm thick were microtomed at room temperature using a Sorval MT 5000 Ultra Microtome and collected on gold grids.

SAXS was performed on bulk samples using a Rigaku rotating Cu anode X-ray source (λ = 1.54 Å). The Cu K_α line generated at 40 kV and 30 mA was focused and aligned with a Charles Supper double-mirror system. In some cases, a 1 mm diameter beam collimator was also used. Scattering intensities were measured on a Nicolet two-dimensional area detector. The sample-to-detector distance was either 130 or 182 cm, and a helium-filled beam-line tube was used to reduce random atmospheric scattering. Two sets of data were collected for each sample and averaged. A set of scattering data collected with no sample present was subtracted from the raw, averaged data to correct for sample absorption, background scattering, and detector inhomogeneities. The computer program PDH[39] was used to process the SAXS data.

3.2.6 Morphological Modeling of SAXS Data

The radial-averaged X-ray scattering patterns of cluster-containing samples were modeled as in previous studies of organic and organometallic block copolymers[27,40,41] assuming a random distribution of spheres in the polymer matrix. Both interparticle

interference and intraparticle scattering mechanisms were included in the model.[42] The Percus-Yevick correlation function[43-45] was used to model the interparticle interference, while the intraparticle scattering was modeled by the single-particle form factor described by the Bessel function $J_{3/2}$.

3.2.7 Ethylene Hydrogenation Experiments

Ethylene hydrogenation experiments were run as batch reactions in a Fischer-Porter bottle equipped with a magnetic stirrer and a gas sampling port. The nanocomposite films (4-6 mg, 15 wt% palladium) were placed in a stainless steel sample holder and positioned roughly in the center of the reactor. The films, *ca.* 200 μm thick, were cut into one or two pieces. The reactor was alternately evacuated and purged with argon three times to remove air from the system. The reactor was then evacuated, filled with ethylene, and heated to the reaction temperature of 120°C. The system was allowed to stabilize for 20 minutes before the hydrogen gas was transferred. A hydrogen:ethylene molar ratio of 2:1 was used and initial reaction pressures were typically 34 psi_g. The reactor temperature was controlled with a Cole-Parmer Digi-Sense temperature controller (model 2186-10A) and reactor pressure was measured with a PSI-TRONIX electronic pressure gauge (model 68920-38).

3.2.8 Gas Chromatography

Gas chromatography was performed on a Hewlett-Packard HP 6890 GC equipped with a split/splitless injection port, an HP-PLOT/Al_2O_3 "S" column (50 m x 530 μm x 15 μm), and a flame ionization detector. Gas samples (150 μL) were injected manually with a gas-tight syringe using a split ratio of 70. The column flow rate was 7.0 mL/min, and

the oven temperature was constant at 60°C. Helium was used as both the carrier gas and FID make up gas. Gas samples were withdrawn from the reactor at approximately five minute intervals. The reactor pressure was recorded before and after sample withdrawal so that corrections could be made in calculating the catalytic activity of the polymer film.

3.3 Results and Discussion

3.3.1 Morphology of Precursor Polymer

Figure 3-1 shows the transmission electron micrograph of the microphase-separated polymer film before cluster formation. The organometallic domains are distinguishable as the darker regions in the micrograph. The interdomain spacing, d, as measured from the micrograph is *ca.* 180 Å. The micrograph reveals a non-equilibrium cylindrical morphology in contrast to previously reported results[27] where a diblock copolymer of the same composition exhibited a well-ordered lamellar morphology. This can be explained by differences in the rate of toluene evaporation from the polymer solution. In this case, the films were cast in air and the solvent was completely evaporated in less than five days, whereas in the previous study the films were cast inside a glove box and evaporation took place over 5-8 days.

Figure 3-2 is the radial-averaged SAXS profile of the precursor polymer. Intensity is plotted as a function of $Q = (4\pi/\lambda)\sin\theta$, where λ is the wavelength of the X-rays, and θ is the scattering angle. A single peak is observed in the pattern, in agreement with the lack of long-range order observed by TEM. The maximum in the intensity *versus* Q plot is located at 0.192 nm^{-1}, corresponding to a d-spacing of 330 Å according to the relation $d = 2\pi/Q$. The large discrepancy between d-spacings determined by TEM

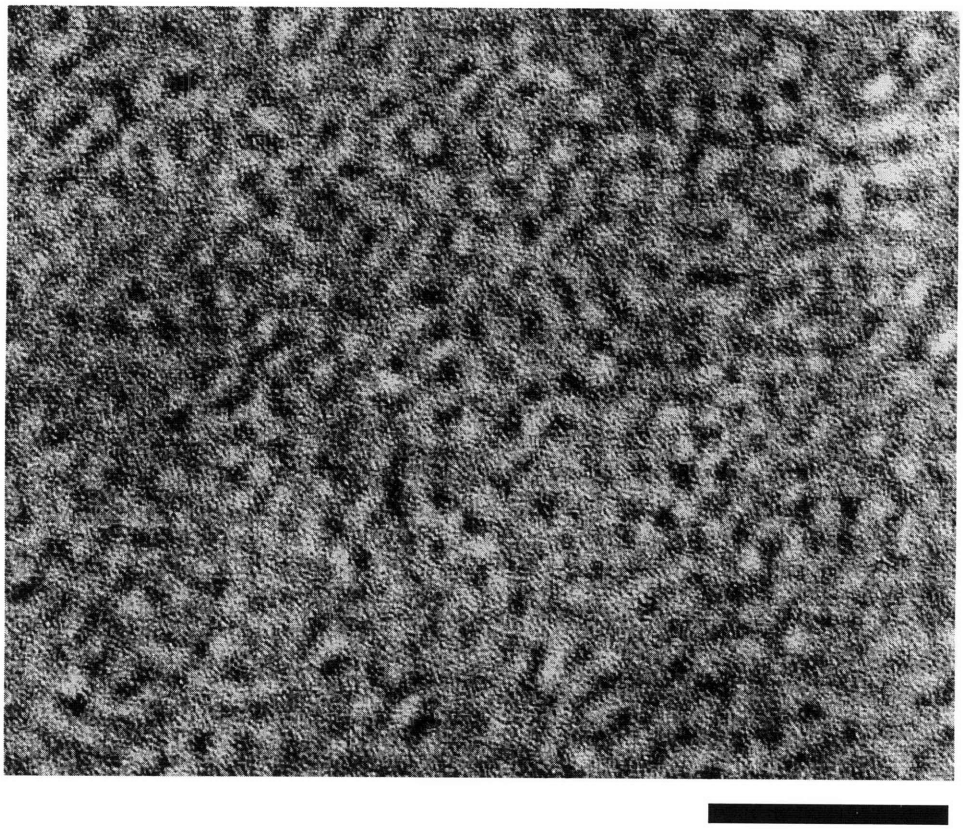

Figure 3-1: Electron micrograph of diblock copolymer film before cluster formation. (bar = 1000 Å)

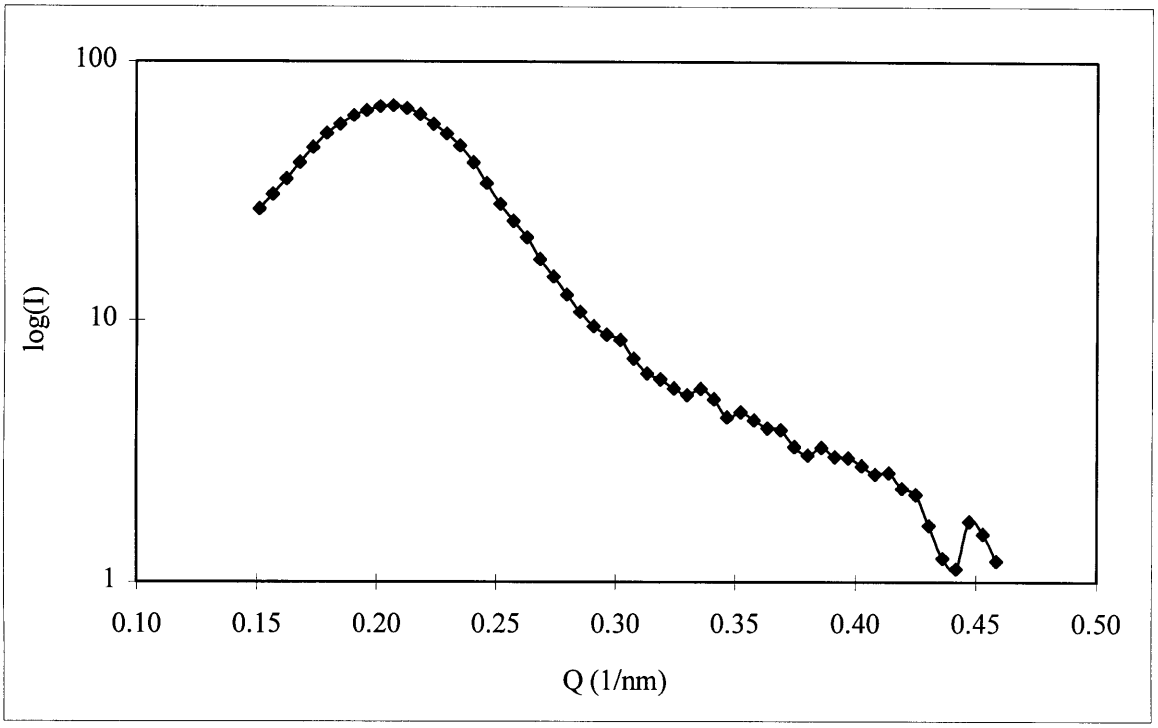

Figure 3-2: Radial-averaged SAXS pattern of diblock copolymer film before cluster formation.

and SAXS is discussed below.

3.3.2 Cluster Morphology Before and After Hydrogenation Reactions

Two polymer films were cast by dividing the polymer solution between two casting boats. The films were reduced separately in hydrogen and different cluster size distributions resulted. The films will be referred to as catalyst 1 and 2. In both cases, TEM showed that the clusters were roughly spherical with a narrow size distribution. The micrographs are shown in Figures 3-3 and 3-4, clearly demonstrating the difference in cluster size. The clusters in catalyst 1 had an average diameter of 30 Å, and seemed to have formed preferentially within the original, cylindrical organometallic domains.

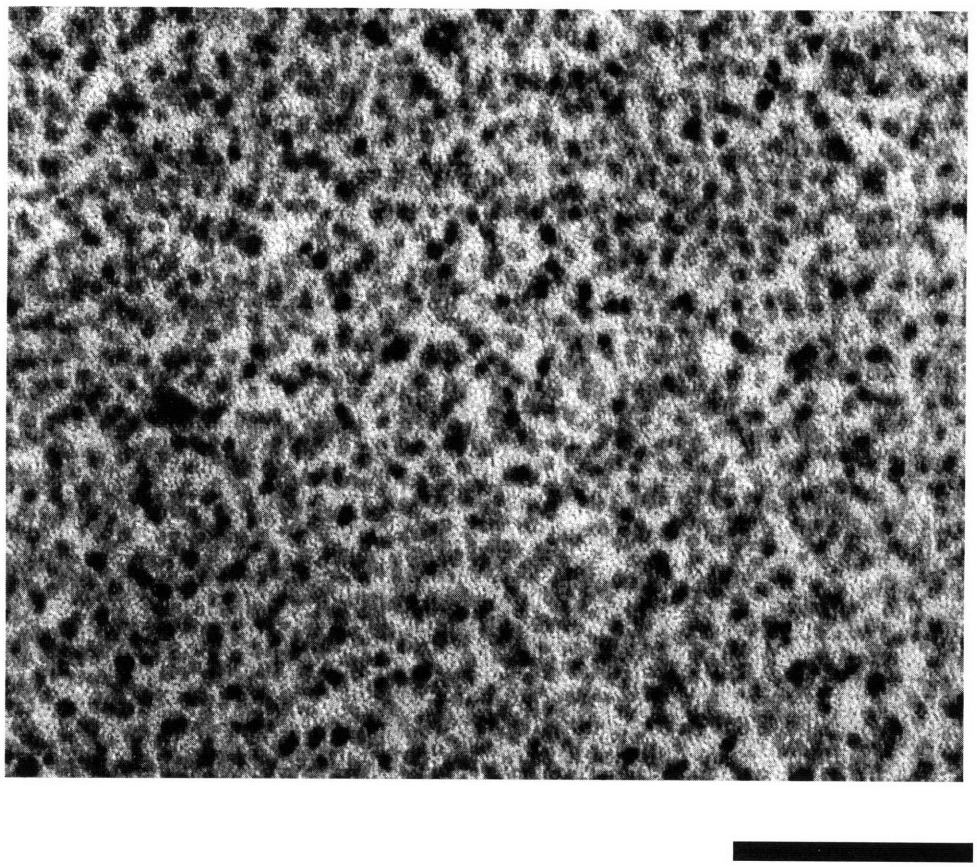

Figure 3-3: Electron micrograph of catalyst 1 before ethylene hydrogenation reactions. (bar = 500 Å)

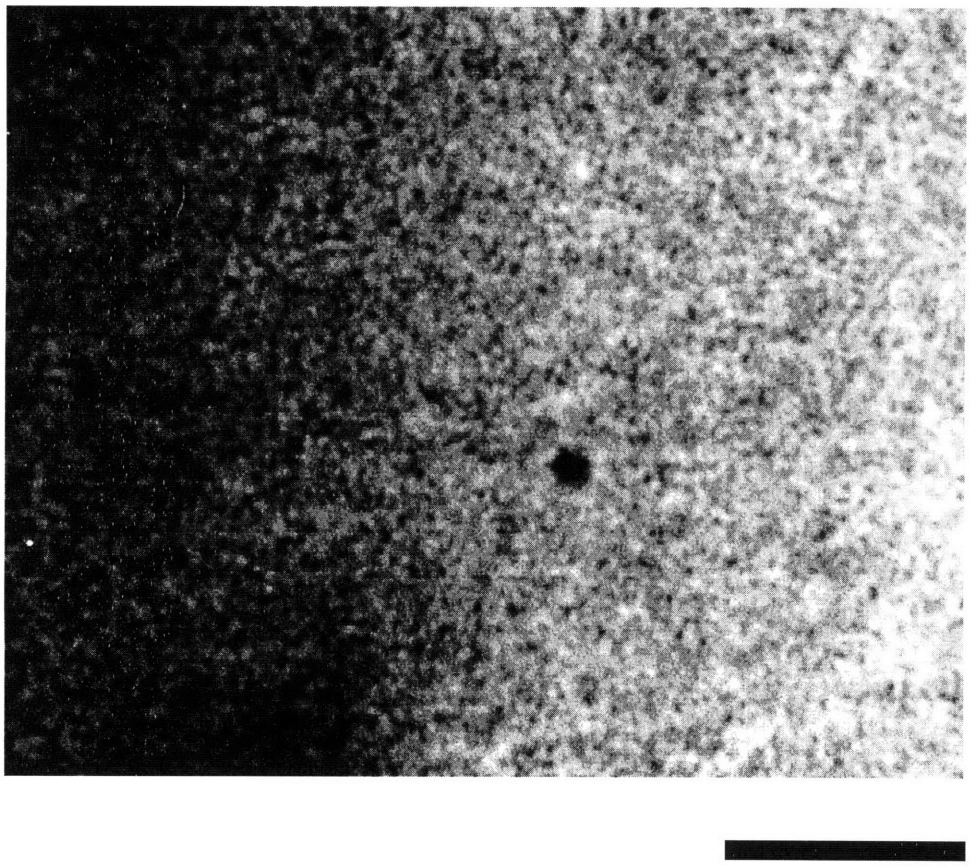

Figure 3-4: Electron micrograph of catalyst 2 before ethylene hydrogenation reactions. (bar = 500 Å)

Catalyst 2 contained clusters of *ca.* 14 Å diameter, but their spatial arrangement withinthe polymer matrix followed no discernible pattern.

Catalyst 1 and 2 were again examined by TEM after being used for ethylene hydrogenation reactions. Micrographs are shown in Figures 3-5 and 3-6. The average cluster diameter for catalyst 1 after ten ethylene hydrogenation experiments was unchanged at 30 Å, indicating that the polymer matrix was effective in stabilizing the clusters against agglomeration. In contrast, TEM showed that the average cluster diameter in catalyst 2 increased 36%, from 14 to 19 Å, after eight experimental runs. These results are summarized in Table 3.1.

Mean Cluster Diameter	Catalyst 1	Catalyst 2
Before Hydrogenation	30 Å	14 Å
After Hydrogenation	30 Å	19 Å
Percent Increase	n/a	36 %

Table 3.1: Average cluster size by TEM before and after ethylene hydrogenation.

The catalysts were also studied by small angle X-ray scattering. The average cluster diameter was determined by fitting the Percus-Yevick/Bessel function model to the SAXS data. This model has three adjustable parameters: the cluster radius, R_b; the hard sphere radius of the clusters, R_{hs}; and the volume fraction of hard spheres, η. R_{hs} is equal to one-half the mean center-to-center distance between clusters. By choosing appropriate values for R_b, R_{hs}, and η, the model can be fit to the SAXS data and the average cluster radius determined. The fitted parameters can also be used to estimate the percent conversion of the pendant organometallic complexes to Pd clusters. The model is

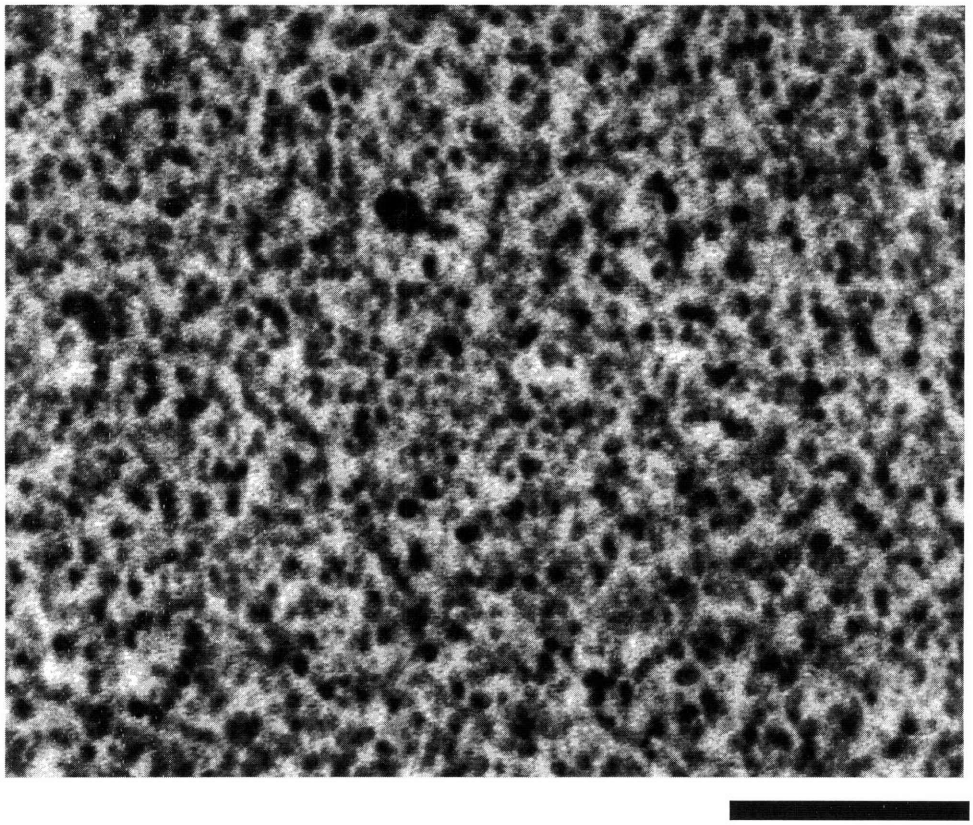

Figure 3-5: Electron micrograph of catalyst 1 after ten ethylene hydrogenation reactions. (bar = 500 Å)

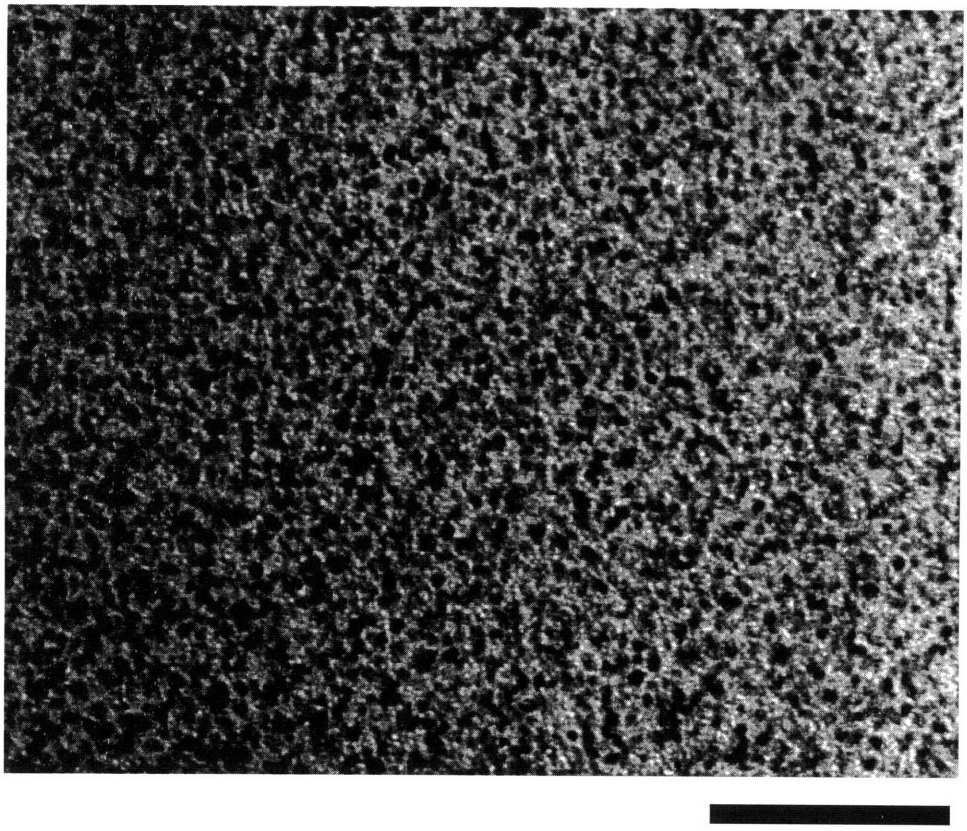

Figure 3-6: Electron micrograph of catalyst 2 after eight ethylene hydrogenation reactions. (bar = 500 Å)

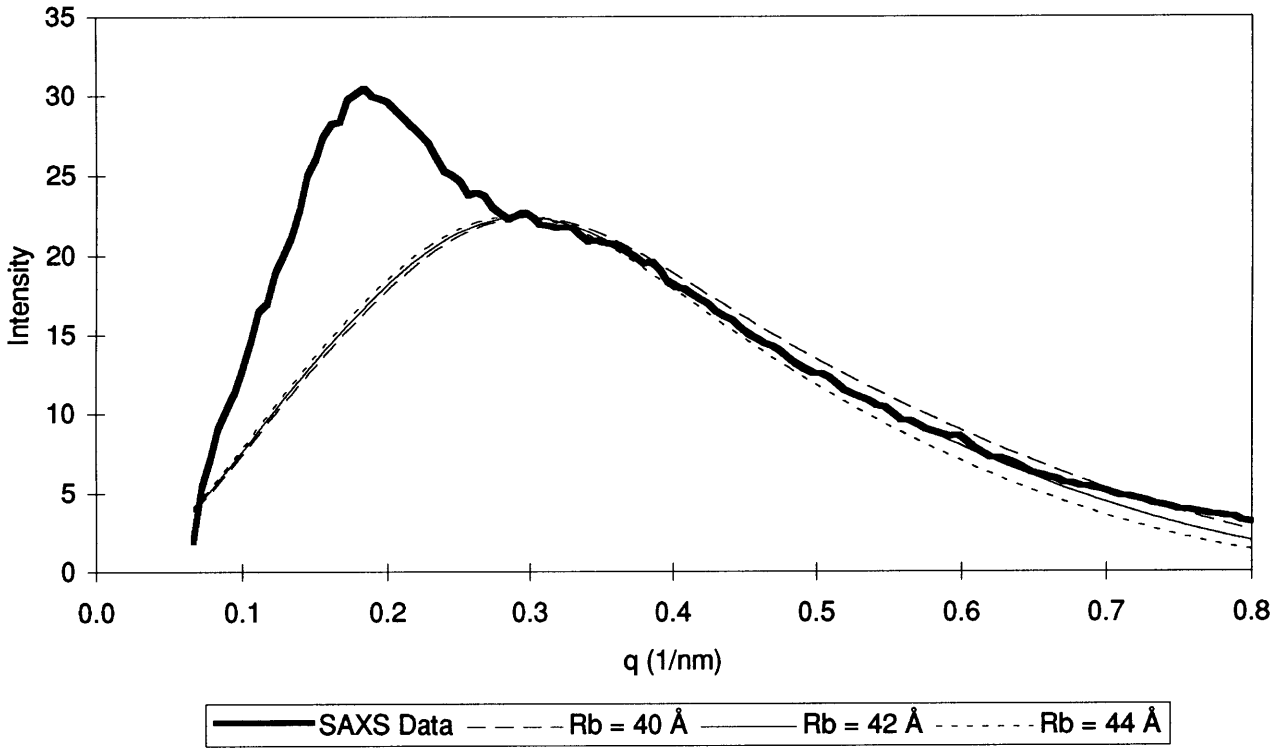

Figure 3-7: Radial-averaged SAXS pattern of catalyst 1 before ethylene hydrogenation reactions. Fits of Percus-Yevick/Bessel function model of scattering shown as dashed lines.

	Catalyst 1 Before Reaction	Catalyst 1 After Reaction	Catalyst 2 After Reaction
R_b (Å)	42	33	37
R_{hs} (Å)	106	83	99
η	0.27	0.27	0.27
% Conversion	131	135	112

Table 3.2: Summary of Percus-Yevick/Bessel Function modeling of SAXS data.

very sensitive to the value of R_b, as shown in Figure 3-7. The results of the SAXS data analysis are summarized in Table 3.2.

In contrast to the TEM results which showed that the average cluster size in catalyst 1 was unchanged after the hydrogenation reactions, the SAXS modeling results indicate a decrease in average cluster size. SAXS data are indicative of an average cluster size;[40] therefore, the results imply that new palladium nanoclusters are being nucleated during the hydrogenation reaction runs, but that these clusters do not grow beyond a very small size. This explanation is supported by the decrease in R_{hs}. That is, because the number of clusters per unit volume of polymer has increased, the average separation among clusters has decreased.

Although no absolute conclusions can be drawn from the conversion data, we can compare the relative degree of conversion among the nanocomposites. There was little change in the percent conversion for catalyst 1 after the hydrogenation reactions, implying that relatively few new clusters were nucleated. The conversion value calculated for catalyst 2 after ethylene hydrogenation was lower than those for catalyst 1, implying that the clusters in catalyst 2 are smaller because fewer palladium atoms were available for cluster growth. These clusters continued to grow during the hydrogenation reactions as unreacted organometallic complexes were reduced by excess hydrogen in the reactor, making palladium atoms available for cluster growth.

There were large discrepancies between TEM and SAXS measurements of both the precursor polymer d-spacing and the average nanocluster diameter. These results are summarized in Table 3.3. Similar discrepancies have been observed in previous work,[44] although the d_{TEM}/d_{SAXS} ratio was smaller, in the range 0.69-0.84. The differences

	TEM	SAXS	d_{TEM}/d_{SAXS}
Precursor Polymer d-Spacing	180 Å	330 Å	0.55
Catalyst 1 Before Reaction	30 Å	84 Å	0.36
Catalyst 1 After Reaction	30 Å	66 Å	0.45
Catalyst 2 Before Reaction	14 Å	-	-
Catalyst 2 After Reaction	19 Å	74 Å	0.26

Table 3.3: Summary of cluster size as determined by TEM and SAXS.

between the TEM and SAXS length scales may be due to truncation or deformation of the microphase-separated domains and clusters during the microtoming process.

3.3.3 Ethylene Hydrogenation

The catalytic activity of nanocomposites for ethylene hydrogenation was studied as a function of palladium cluster size. The hydrogenation reactions were run as batch reactions and gas chromatography was used to monitor the progress of the reaction. The activity of the membrane was calculated as the moles of ethylene consumed per mole palladium per second. Because of the difficulty in sampling reproducible volumes of gas manually, an absolute calibration curve for the GC could not be constructed. Instead, the ethane:ethylene molar ratio was measured and the absolute amount of ethylene in the reactor was calculated based on the amount initially charged to the reactor. Pressure measurements were taken before and after sample withdrawal to correct for the loss of material from the reactor.

3.3.4 Activity as a Function of Cluster Size

To study the catalyst activity as a function of cluster size, ethylene hydrogenation reactions were run at 120°C, P_{H2} = 30 psi_a, and P_{C2H4} = 15 psi_a for both catalyst 1 and 2. Plots of mole percent ethylene as a function of time are shown for both catalysts in Figure

3-8. The activity of each catalyst was calculated as the moles of ethylene reacted per mole palladium in the catalyst per second. The maximum activity for each run, as calculated from pairs of consecutive data points, is reported in Table 3.4. The results are reported in chronological order.

Run Number	Maximum Activity (mol/mol•s)	
	Catalyst 1	Catalyst 2
1	2.0×10^{-2}	2.0×10^{-2}
2	6.9×10^{-3}	1.3×10^{-2}
3	9.8×10^{-3}	1.6×10^{-2}
4	1.3×10^{-2}	2.5×10^{-2}
5	1.3×10^{-2}	2.7×10^{-2}
6	1.1×10^{-2}	2.5×10^{-2}
7		1.6×10^{-2}
8		2.3×10^{-2}
Average	**1.2×10^{-2}**	**2.1×10^{-2}**
Standard Deviation	4×10^{-3}	5×10^{-3}

Table 3.4: Maximum activity for ethylene hydrogenation for catalyst 1 and 2 at 120°C, $P_{H2} = 30$ psi_a, and $P_{C2H4} = 15$ psi_a.

The average catalytic activity for ethylene hydrogenation was 0.012 ± 0.004 mol/mol•s for catalyst 1, and 0.021 ± 0.005 mol/mol•s for catalyst 2. There is no trend toward loss of catalytic activity with repeated use of the nanocomposites. Catalyst 2 is 1.8 times more active for ethylene hydrogenation, on average, than catalyst 1. This difference in reactivity can be explained in terms of the difference in total palladium surface area between the two catalysts. Both catalysts contain the same weight fraction palladium; therefore, the ratio of the total palladium surface area in each catalyst can be estimated

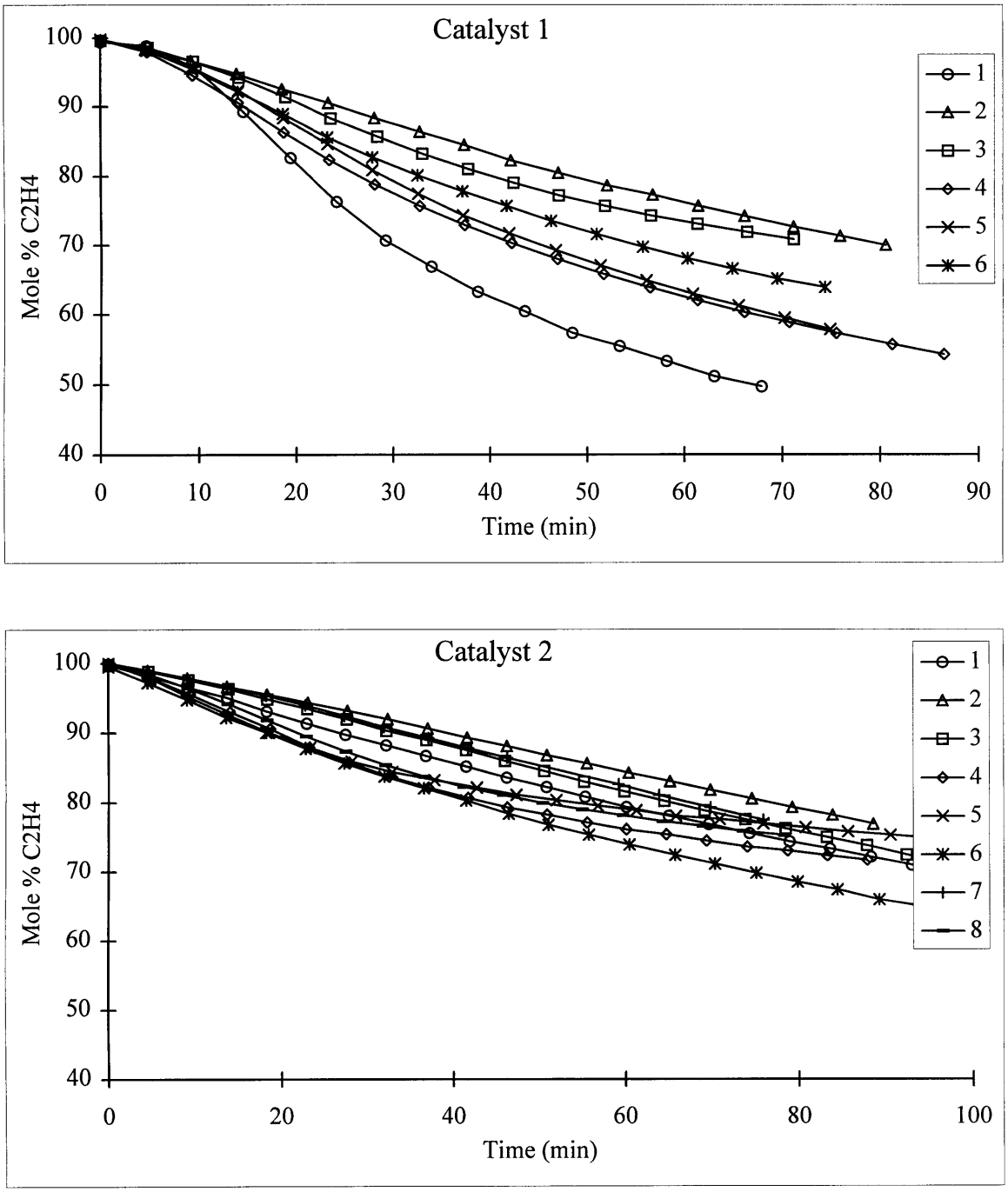

Figure 3-8: Mole percent ethylene as a function of time for hydrogenation runs on catalyst 1 and 2.

from the average cluster diameter, assuming that the clusters are spherical, monodisperse, and that the palladium complexes have been reduced to the same extent. Using TEM cluster diameter measurements made before and after the hydrogenation experiments, catalyst 2 is expected to be 1.6 - 2.2 times more active than catalyst 1, based solely on the difference in total palladium surface area. This result is in agreement with the experimental observations.

3.3.5 Ethylene Hydrogenation after Exposure to Butenes

In a separate study, the nanocomposites were used to catalyze 1,3-butadiene hydrogenation(see Chapter 4). It was found that butadiene, and the butenes and butane produced in this reaction plasticize the polymer matrix. The films were initially non-porous with smooth surfaces, but after exposure to the C_4 mixture, the surface of each film became rough as internal void spaces were formed. These void spaces, 15-60 μm in diameter, were clearly visible when microtomed sections were examined with a light microscope. Moreover, the films showed signs of deformation after being heated to the reaction temperature, indicating that the glass transition temperature had been lowered by the plasticizing effect of the C_4 gas mixture.

The ethylene hydrogenation experiments were repeated using the same nanocomposite catalysts after they had been exposed to the C_4 gas mixture. It was expected that the presence of macroscopic voids would improve mass transport within the films, enhancing catalytic activity. The results of these experiments, given in Table 3.5, show that the catalytic activity of catalyst 1 and 2 more that doubled after exposure to the C_4 gas mixture.

Run Number	Maximum Activity (mol/mol • s)	
	Catalyst 1	Catalyst 2
1	4.4×10^{-2}	5.5×10^{-2}
2	2.6×10^{-2}	4.9×10^{-2}
3	2.2×10^{-2}	
4	2.0×10^{-2}	
Average	$\mathbf{2.8 \times 10^{-2}}$	$\mathbf{5.2 \times 10^{-2}}$
Standard Deviation	9×10^{-3}	

Table 3.5: Maximum activity of catalyst 1 and 2 for ethylene hydrogenation at 120°C, $P_{H2} = 30$ psi_a, and $P_{C2H4} = 15$ psi_a after exposure to C_4 gases.

3.4 Summary

This study has shown that bulk, non-porous diblock copolymer films containing palladium nanoclusters are effective catalysts for the gas phase hydrogenation of ethylene, and that the catalytic activity is stable after repeated use of the material. The catalytic activity of the membranes was found to scale with the total palladium surface area. Although the polymer matrix impedes mass transport to the catalytically active sites, mass transfer can be improved by opening voids within the matrix, decreasing the permeation length scale and increasing mass transfer rates.

3.5 References

(1) Lewis, L. N. *Chem. Rev.* **1993**, *93*, 2693.

(2) Sohn, B. H.; Cohen, R. E. *Chem. Mater.* **1997**, *9*, 264.

(3) Sohn, B. H.; Cohen, R. E. *Acta Polymerica* **1996**, *47*, 340.

(4) Hirai, H.; Chawanya, H.; Toshima, N. *Bull. Chem. Soc. Jpn.* **1985**, *58*, 682.

(5) Toshima, N.; Takahashi, T. *Bull. Chem. Soc. Jpn.* **1992**, *65*, 400.

(6) Ohtaki, M.; Toshima, N.; Komiyama, M.; Hirai, H. *Bull. Chem. Soc. Jpn.* **1990**, *63*, 1433.

(7) Touroude, R.; Girard, P.; Maire, G.; Kizling, J.; Boutonnet-Kizling, M.; Stenius, P. *Colloids and Surfaces* **1992**, *67*, 9.

(8) Petit C.; Lixon, P.; Pileni, M. P. *J. Phys. Chem.* **1993**, *97*, 12974.

(9) Eastoe, J.; Cox, A. R. *Colloids and Surfaces, A* **1995**, *101*, 63.

(10) Roescher, A.; Moller, M. *Advanced Materials* **1996**, *8*, 337.

(11) Bronstein, L.; Seregina, M. *Advanced Materials* **1995**, *7*, 1000.

(12) Tamai, H.; Sakurai, H.; Hirota, Y.; Nishiyama, F.; Yasuda, H. *J. Appl. Polym. Sci.* **1995**, *56*, 441.

(13) Tour, J. M.; Pendalwar, S. L.; Cooper, J. P. *Chem. Mater.* **1990**, *2*, 647.

(14) Lukehart, C. M.; Milne, S. B.; Stock, S. R.; Shull, R. D.; Wittig, J. E. *Mater. Sci. Eng.* **1995**, *A204*, 176.

(15) Reetz, M. T.; Helbig, W. *J. Am. Chem. Soc.* **1994**, *116*, 7401.

(16) Reetz, M. T.; Helbig, W.; Quaiser, S. A.; Stimming, U.; Breuer, N.; Vogel, R. *Science* **1995**, *267*, 367.

(17) Moutet, J. C.; Ouennoughi, Y.; Ourari, A.; Hamar-Thibault, S. *Electrochimica Acta* **1995**, *40*, 1827.

(18) Lewis, L. N.; Lewis, N. *Chem. Mater.* **1989**, *1*, 106.

(19) Duan, Z.; Hampden-Smith, M. J.; Datye, A.; Nigrey, P.; Quintana, C.; Sylwester, A. P. *J. Catalysis* **1993**, *139*, 504.

(20) Bradley, J. S.; Hill, E.; Leonowicz, M. E.; Witzke, H. *J. Mol. Catal.* **1987**, *41*, 59.

(21) Murray, C. B.; Norris, D. J.; Bawendi, M. G. *J. Am. Chem. Soc.* **1993**, *115*, 8706.

(22) Danek, M.; Jensen, K. F.; Murray, C. B.; Bawendi, M. G. *Chem. Mater.* **1996**, *8*, 173.

(23) Golden, J. H.; Deng, H.; DiSalvo, F. J.; Frechet, J. M. J.; Thompson, P. M. *Science* **1995**, *268*, 1463.

(24) Klabunde, K. J., Habdas, J.; Cadenas-Trivino G. *Chem. Mater.* **1989**, *1*, 481.

(25) El-Shall, M. S.; Slack, W. *Macromolecules* **1995**, *28*, 8456.

(26) Watkins, J. J.; McCarthy, T. J. *Chem. Mater.* **1995**, *7*, 1991.

(27) Ng Cheong Chan, Y; Craig, G. S. W.; Schrock, R. R.; Cohen, R. E. *Chem. Mater.* **1992**, 4, 885.

(28) Clay, R.; Cohen, R. E. *Supramolecular Science* **1995**, *2*, 183.

(29) Ohtaki, M.; Komiyama, M.; Hirai, H.; Toshima, N. *Macromolecules* **1991**, *24*, 5567.

(30) Toshima, N.; Yonezawa, T. *Makromol. Chem., Macromol. Symp.* **1992**, *59*, 281.

(31) Toshima, N.; Harada, M.; Yamazaki, Y.; Asakura, K. *J. Phys. Chem.* **1992**, *96*, 9927.

(32) Harada, M.; Asakura, K.; Toshima, N. *J. Phys. Chem.* **1993**, *97*, 5103.

(33) Teranishi, T.; Nakata, K.; Miyake, M.; Toshima, N. *Chem. Lett.* **1996**, *4*, 277.

(34) Biffis, A.; Corain, B.; Cvengrosova, Z.; Hronec, M.; Jerabek, K.; Kralik, M. *Appl. Catal. A: General* **1995**, *124*, 355.

(35) Park, K. M.; Shim, I. W. *J. Appl. Polym. Sci.* **1991**, *42*, 1361.

(36) Hwang, S. T.; Shim, I. W. *J. Appl. Polym. Sci.* **1992**, *46*, 603.

(37) Chu. J. W.; Shim, I. W. *J. Molecular Catalysis* **1993**, *78*, 189.

(38) Gao, H.; Xu, Y.; Liao, S.; Liu, R.; Yu, D. *J. Appl. Polym. Sci.* **1993**, *50*, 1035.

(39) Program PDH (PC - SAXS version 2.1); © 1990 Ergo Computing, Inc.

(40) Sankaran, V.; Cohen, R. E.; Cummins, C. C.; Schrock, R. R. *Macromolecules* **1991**, *24*, 6664.

(41) Berney, C. V.; Cheng, P. L.; Cohen, R. E. *Macromolecules* **1988**, *17*, 2235.

(42) Kinning, J. K.; Thomas, E. L. *Macromolecules* **1984**, *17*, 1712.

(43) Percus, J. K.; Yevick, G. J. *Phys. Rev.* **1958**, *110*, 1.

(44) Wertheim, M. S. *Phys. Rev. Lett.* **1963**, *10*, 321.

(45) Thiele, E. J. *Chem. Phys.* **1963**, *39*, 474.

(46) Berney, C. V.; Cohen, R. E.; Bates, F. S. *Polymer* **1982**, *23*, 1222.

(47) Ponec, V.; Bond, G. C. *Catalysis by Metals and Alloys*; Elsevier: Amsterdam, The Netherlands, 1995, pp. 468-488.

4. 1,3-Butadiene Hydrogenation

4.1 Introduction

The selective hydrogenation of 1,3-butadiene to butenes is of great importance in the petrochemical industry.[1,2] C_4 alkene feed streams produced by steam cracking of naphtha or catalytic cracking of heavier hydrocarbons contain 1,3-butadiene as an impurity which must be removed selectively with minimal loss of butenes to saturation or isomerization reactions. 1-butene is used as a comonomer in LLDPE production and 2-butenes are valuable for methyl ethyl ketone (MEK) production and alkylation reactions.

The selectivity of a catalyst is more important than its activity in industrial selective hydrogenation processes. Supported palladium catalysts have exceptionally good activity for 1,3-butadiene hydrogenation and butene selectivities close to 100% can be achieved. The relative amount of 1-butene, *cis*-2-butene, and *trans*-2-butene varies with reaction conditions.[2]

The activity of pure palladium crystals is reported to be 2.5×10^{-9} mol/cm^2 • s and 1.2×10^{-8} mol/cm^2 • s on the (111) and (110) face, respectively, with butene selectivities of 100% at 27°C, 5.1 kPa total pressure, and a hydrogen:butadiene ratio of 10.[3] The selective hydrogenation of 1,3-butadiene over supported palladium catalysts has been studied extensively. Ohnishi *et al.*[4] studied this reaction over 5 wt% palladium on alumina at -38 to -28°C, a total reactor pressure of 33 kPa, and a hydrogen:butadiene ratio of 2:1. They found that the selectivity for butenes was 100% up to approximately 90% butadiene conversion with 1-butene as the major product (79%). Furlong *et al.*[5] studied the selective hydrogenation of 1,3-butadiene in the presence of a 10:1 excess of 1-butene

over 0.42 wt% palladium on alumina at 15-40°C and ambient pressure. They found that a 99% selectivity for butenes could be achieved for conversions up to 40%. 1-Butene was the major product and the selectivity could be maintained up to higher conversions by lowering the reaction temperature. Palladium particles deposited on amorphous carbon or graphite by evaporation have also been studied as model catalysts.[6] Hydrogenation reactions were run at room temperature with a five-fold excess of hydrogen, and selectivities approaching 100% were maintained up to high 1,3-butadiene conversions (*ca.* 85%). Lun *et al.*[7] studied the selectivity of similar catalysts as a function of temperature and found that 100% selectivity for butenes could be maintained up to a reaction temperature of 127°C. The performance of palladium catalysts can be improved by alloying, and recent work has been done on alloys of palladium with cobalt,[1] nickel,[3] thallium,[4] copper,[5] and niobium.[8]

In the partial hydrogenation of alkynes or dienes to the desired product is an intermediate, not the thermodynamically most stable product, and selectivity can arise by two different mechanisms.[2] If the desired alkene is able to desorb from the catalyst surface before further hydrogenation can take place, then the selectivity is said to be mechanistically controlled. On the other hand, if the catalyst is selective because the alkyne or diene adsorbs much more strongly than the alkene, then the selectivity is thermodynamically controlled. It is generally true that alkynes and dienes adsorb to metal surfaces much more strongly than alkenes, so excellent selectivities are often possible in partial hydrogenation reactions.

A more quantitative analysis of the basis for palladium catalyst selectivity can be performed by considering the "rake" scheme of 1,3-butadiene hydrogenation, illustrated in Figure 4-1, which has been shown to adequately describe this reaction.[3]

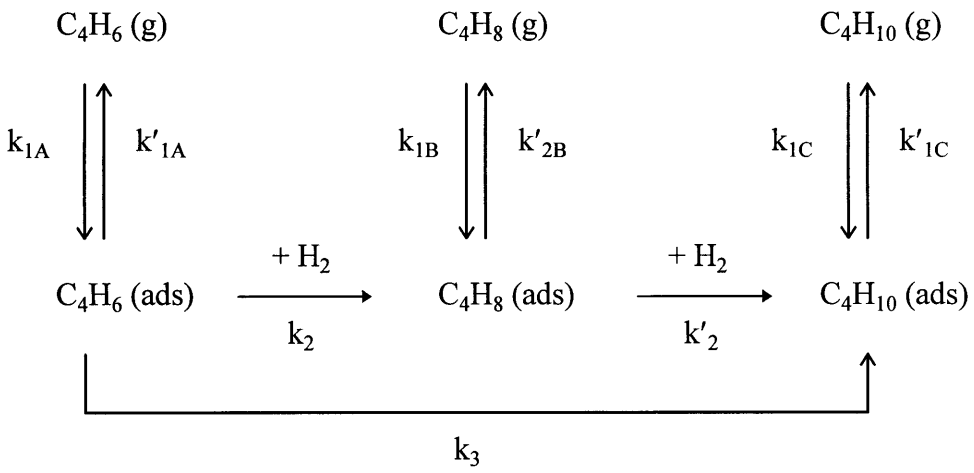

Figure 4-1: "Rake" scheme of 1,3-butadiene hydrogenation.

k_{1A} (k'_{1A}), k_{1B} (k'_{2B}), and k_{1C} (k'_{1C}) are the adsorption (desorption) constants for 1,3-butadiene, butenes, and butane, respectively. k_2 and k'_2 are the rate constants for hydrogenation of butadiene and butene, respectively. k_3 is the rate constant for hydrogenation of butadiene directly to butane, without desorption and readsorption of the butene intermediate. On a palladium catalyst $k_{1C} \approx 0$ and hydrogenation of 1,3-butadiene directly to butane is negligible (i.e. $k_3 \approx 0$). Miegge *et al.*[3] found that k_2 and k'_2 are of the same order of magnitude; therefore, the excellent selectivity of the palladium catalyst must be because $(k_{1A} / k'_{1A}) >> (k_{1B} / k'_{2B})$, i.e. 1,3-butadiene adsorption is much more favorable than butene adsorption. 1,3-butadiene is approximately twice as strongly

adsorbed on palladium than are butenes because 1,3-butadiene adsorbs via both carbon-carbon double bonds, while butenes have only one double bond available.

Another study undertaken by Ouchaib *et al.*[9] reinforces the conclusion that selectivity in this reaction is thermodynamically controlled. 1,3-butadiene reactions were performed over both palladium and platinum catalysts. The ratio of the butadiene and butene hydrogenation rate constants (k_2 / k'_2) was found to be larger on platinum (0.8) than on palladium (0.33). Therefore, if selectivity is mechanistically controlled, platinum should be the more selective catalyst. However, this was not the case; a Pd/SiO_2 catalyst had a butene selectivity of 90%, while that of a similar Pt/SiO_2 catalyst was only 60%. When the ratio of the adsorption constants of 1,3-butadiene and 1-butene on each metal were compared, k_{1A} / k_{1B} was 12 times larger on palladium than on platinum, clearly demonstrating that the selectivity of the palladium catalyst arises from its capacity to adsorb the diene much more strongly than butene molecules.

The catalytic activity and selectivity of palladium nanoclusters within bulk diblock copolymer films for 1,3-butadiene hydrogenation was studied as a function of reactant concentration, reaction temperature, and cluster size. Our aim was to study the catalytic properties of these nanoclusters when they are completely embedded within a polymer matrix with many active sites covered by adsorbed polymer repeat units.

4.2 Experimental

4.2.1 1,3-Butadiene Hydrogenation Experiments

1,3-butadiene hydrogenation experiments were run as batch reactions in a Fischer-Porter bottle equipped with a magnetic stirrer and a gas sampling port. The

nanocomposite films (4-6 mg, 15 wt% palladium) were placed in a stainless steel sample holder and positioned roughly in the center of the reactor. The films, *ca.* 200 μm thick, were cut into one or two pieces. The reactor was alternately evacuated and purged with argon three times to remove air from the system. The reactor was then evacuated and filled with 1,3-butadiene. Reactions were run either at room temperature or at 120°C. In the later case, the reactor was heated to 120°C after transfer of the 1,3-butadiene and allowed to stabilize for 20 minutes before the hydrogen gas was transferred. Hydrogen:butadiene molar ratios of 4:1, 1:1, and 1:2 were used, and initial reaction pressures were 15 or 35 psi_g. The reactor temperature was controlled with a Cole-Parmer Digi-Sense temperature controller (model 2186-10A) and reactor pressure was measured with a PSI-TRONIX electronic pressure gauge (model 68920-38).

4.2.2 Gas Chromatography

Gas chromatography was performed on a Hewlett-Packard HP 6890 GC equipped with a split/splitless injection port, an HP-PLOT/Al_2O_3 "S" column (50 m x 530 μm x 15 μm), and a flame ionization detector (FID). Samples (150 μL) were injected manually with a gas-tight syringe using a split ratio of 40; the column flow rate was 5.0 mL/min. The oven temperature was held constant at 110°C for the first four minutes of the chromatographic run, then increased to 160°C at a rate of 15°C/min, and finally held at 160°C for one minute. Helium was used as both the carrier gas and FID make up gas. Samples were withdrawn from the reactor at approximately ten minute intervals. The reactor pressure was recorded before and after sample withdrawal to account for loss of material from the reactor in activity calculations.

4.3 Results and Discussion

4.3.1 Nanocomposite Morphology Before and After Hydrogenation Reactions

Two nanocomposite films containing an equal weight percent palladium were used in 1,3-butadiene hydrogenation experiments; the films will be referred to as catalyst 1 and 2. The only difference between the catalysts was the size of the palladium clusters. Both catalysts had been used previously for ethylene hydrogenation experiments, after which the clusters in catalyst 1 had a mean diameter from TEM analysis of 30 Å (see Figure 3-5), while those of catalyst 2 averaged 19 Å in diameter (see Figure 3-6).

The TEM analysis was repeated after the 1,3-butadiene hydrogenation experiments to assess the ability of the polymer matrix to stabilize the clusters against agglomeration. Micrographs of catalyst 1 and 2 are shown in Figures 4-2 and 4-3, respectively. The mean cluster diameter of catalyst 1 increased 17% to 35 Å after a total of 27 hydrogenation runs, while that of catalyst 2 increased 68% to 32 Å after 32 hydrogenation runs.

Exposure to the C_4 gas mixture resulted in plasticization of the polymer matrix. Before exposure, the films were flat and had smooth, shiny surfaces. After only one 1,3-butadiene hydrogenation run, the surface of each film became rough as it appeared that macroscopic void spaces had opened within the polymer matrix. This was confirmed when examination of microtomed sections with a light microscope revealed 15-60 μm diameter holes in the sections. Further evidence of the depression of T_g below 120°C was that the initially flat films softened during the reaction and curled around the stainless

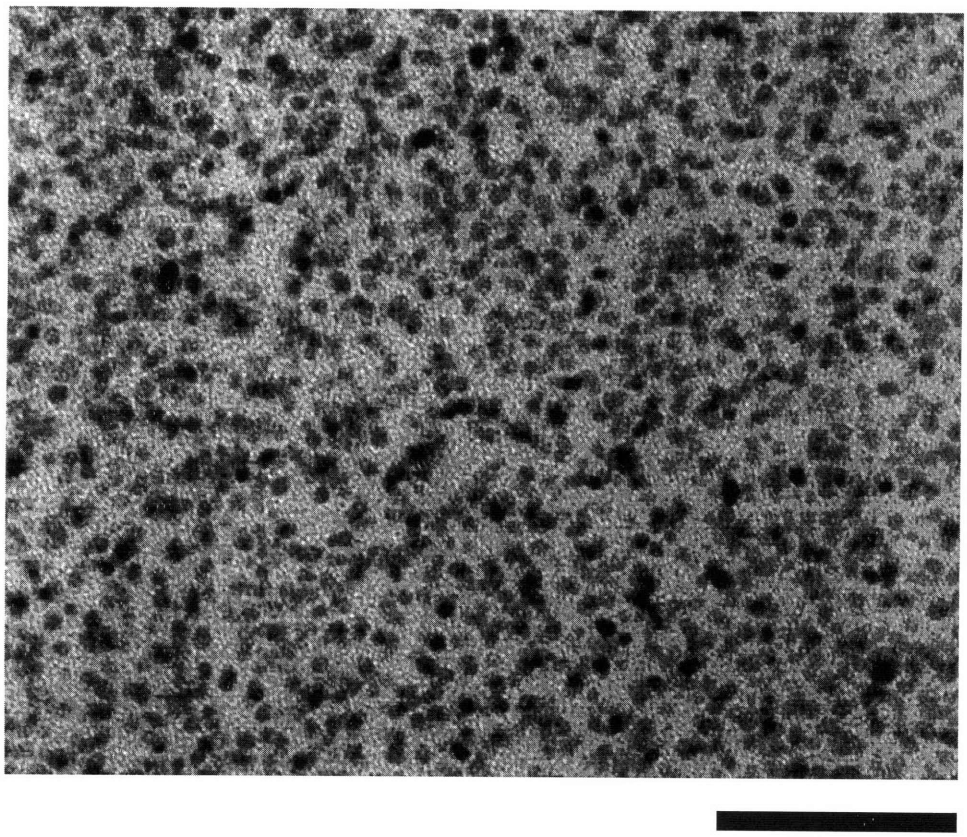

Figure 4-2: Transmission electron micrograph of catalyst 1 after 27 hydrogenation reactions. (bar = 500 Å)

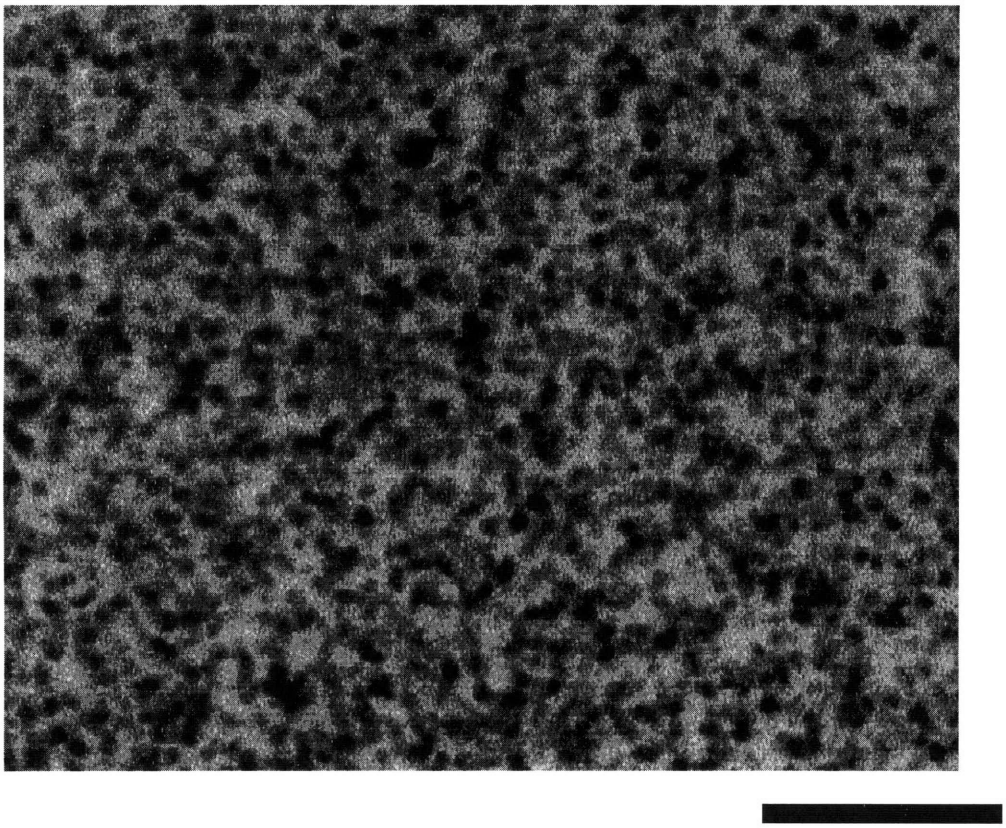

Figure 4-3: Transmission electron micrograph of catalyst 2 after 32 hydrogenation reactions. (bar = 500 Å)

steel sample holder. Visual inspection of the catalysts indicated that the plasticization effect was augmented by repeated exposure to C_4's. It was thought that the plasticized films would have enhanced catalytic activity because mass transfer resistance would be reduced by the presence of the macroscopic voids. In fact, ethylene hydrogenation reactions repeated using these catalysts after exposure to C_4's showed that the activity of each catalyst had more than doubled (see Section 3.3.5), presumably due to decreased mass transfer resistance within the polymer matrix.

4.3.2 1,3-Butadiene Hydrogenation Reactions

The catalytic activity and selectivity of palladium cluster-containing nanocomposites for 1,3-butadiene hydrogenation was studied as a function of reactant partial pressure, temperature, and cluster size. The hydrogenation reactions were run as batch reactions and gas chromatography was used to measure the relative concentration of 1,3-butadiene, 1-butene, *cis*-2-butene, *trans*-2-butene, and *n*-butane in the reaction mixture. The activity of the membrane was calculated as the moles of 1,3-butadiene consumed per mole palladium per second. Because of the difficulty in sampling reproducible volumes of gas manually, an absolute calibration curve for the GC could not be constructed. Instead, the moles of 1,3-butadiene in the reactor were calculated from the amount initially charged and the relative molar concentration as measured by GC. Pressure measurements were taken before and after sample withdrawal to correct for loss of material from the reactor. The selectivity of the membranes for butenes (1-butene, *cis*-2-butene, and *trans*-2-butene) over *n*-butane is expressed as the number of moles of

butenes produced per mole of 1,3-butadiene reacted. That is, a selectivity of 1.00 indicates 100% selectivity for butenes.

4.3.3 Catalytic Activity and Selectivity as a Function of Reactant Partial Pressure

To study the effect of reactant partial pressure on the catalytic activity and selectivity of the nanocomposite material, hydrogenation reactions were conducted using catalyst 1 at hydrogen:butadiene ratios of 4:1, 1:1, and 1:2. All experiments were run at 120°C and each set of reaction conditions was repeated at least three times. The maximum activity and butene selectivity for each experimental run are reported for each set of reaction conditions in Table 4.1. Reaction conditions and average maximum activities and selectivities are summarized in Table 4.2.

The data clearly show that the selectivity of the nanocomposite for butenes over *n*-butane increases as the partial pressure of hydrogen decreases. However, decreasing the hydrogen partial pressure to low values (i.e. $P_{H2} = 10$ psi_a) results in a marked decrease in catalytic activity.

The rate of 1,3-butadiene hydrogenation is reported[2] to be first order in the hydrogen partial pressure, and zero order in butadiene partial pressure. The activity data do not follow this trend. This discrepancy may be due to two effects. First, it is unlikely that the Henry's Law coefficient of hydrogen is equal to one in this polymer. Therefore, changes in the hydrogen partial pressure will not necessarily accurately reflect changes in the concentration of hydrogen in the polymer matrix. Second, as was discussed in Section 4.3.1, the C_4 gas mixture was found to plasticize the polymer matrix, opening

void spaces inside the polymer which were visible in a light microscope. This plasticization effect improved the mass transport properties of the polymer film and was

Run Number	Maximum Activity (mol/mol Pd*s)	Maximum Selectivity (mol/mol)
	P_{H2}:P_{C4H6} = 4:1	
1	5.5×10^{-2}	0.67
2	2.2×10^{-2}	0.57
3	9.3×10^{-2}	0.55
4	8.6×10^{-2}	0.60
5	1.2×10^{-1}	0.70
Average	**7.5×10^{-2}**	**0.62**
Std. Dev.	3.4×10^{-2}	0.06
	P_{H2}:P_{C4H6} = 1:1	
6	9.7×10^{-2}	0.81
7	1.3×10^{-1}	0.88
8	8.7×10^{-2}	0.85
Average	**1.0×10^{-1}**	**0.85**
Std. Dev.	2×10^{-2}	0.03
	P_{H2}:P_{C4H6} = 1:2	
9	2.9×10^{-2}	0.99
10	2.6×10^{-2}	0.96
11	2.4×10^{-2}	0.96
12	2.5×10^{-2}	0.92
Average	**2.6×10^{-2}**	**0.96**
Std. Dev.	2×10^{-3}	0.02

Table 4.1: Maximum activity and selectivity of catalyst 1 for 1,3-butadiene hydrogenation reactions at 120°C, and P_{H2} : P_{C4H6} = 4:1, 1:1, or 1:2.

P_{H2} (psi_a)	P_{C4H6} (psi_a)	Average Maximum Activity (mol/mol Pd*s)	Average Maximum Selectivity (mol/mol)
40	10	7.5×10^{-2}	0.62
15	15	1.0×10^{-1}	0.85
10	20	2.6×10^{-2}	0.96

Table 4.2: Summary of reactant partial pressures and average maximum activity and selectivity of catalyst 1 for 1,3-butadiene hydrogenation at 120°C.

augmented with repeated exposure of the film to the C_4 gas mixture. Therefore, it is not possible to make unqualified comparisons among the data sets, because the experiments were not conducted in random order. Note that the variation in both the maximum activity and selectivity tends to decrease with repeated exposure of the catalyst to C_4's, indicating that the degree to which mass transport can be improved by this method reaches a plateau after 5-10 experimental runs.

The product distribution data, summarized in Table 4.3, show that the *trans*-2-butene and *cis*-2-butene selectivities change little with changing reactant concentration, but that the selectivity for 1-butene increases with decreasing hydrogen partial pressure. Therefore, the overall loss of selectivity for butenes with increasing P_{H2} can be attributed to an increase in the rate of hydrogenation of 1-butene to *n*-butane.

P_{H2} (psi_a)	P_{C4H6} (psi_a)	1-Butene	*trans*-2-Butene	*cis*-2-Butene	Butane
40	10	20%	30%	11%	39%
15	15	27%	39%	18%	16%
10	20	45%	35%	16%	4%

Table 4.3: Summary of reactant partial pressures and average maximum selectivity for butenes at 120°C.

4.3.4 Catalytic Activity and Selectivity as a Function of Cluster Size and Reaction Temperature

To study the effect of cluster size on the catalytic activity and selectivity of the nanocomposites, butadiene hydrogenations were performed on both catalysts at room temperature and a hydrogen:butadiene of 1:1, with $P_{H2} = P_{C4H6} = 15$ psi_a. The data are summarized in Table 4.4. The experimental run numbers are given in parentheses.

Room Temperature

	Maximum Activity (mol/mol Pd*s)		Maximum Selectivity (mol/mol)	
	Catalyst 1	**Catalyst 2**	**Catalyst 1**	**Catalyst 2**
	1.7×10^{-2} (13)	1.0×10^{-2} (1)	0.77	0.96
	1.9×10^{-2} (14)	1.1×10^{-2} (2)	0.78	0.92
	2.7×10^{-2} (15)	9.1×10^{-3} (3)	0.76	0.92
	2.9×10^{-2} (16)	1.2×10^{-2} (4)	0.79	0.94
	-	1.2×10^{-2} (5)	-	0.94
Average	$\mathbf{2.3 \times 10^{-2}}$	$\mathbf{1.1 \times 10^{-2}}$	**0.78**	**0.94**
Std. Dev.	5×10^{-3}	1×10^{-3}	0.01	0.01

Table 4.4: Maximum activity and selectivity of catalyst 1 and 2 for 1,3-butadiene hydrogenation at room temperature and $P_{H2} = P_{C4H6} = 15$ psi_a. The experimental run numbers are given in parentheses.

The average maximum activity of catalyst 1 is 2.3×10^{-2} mol/mol Pd*s, while that of catalyst 2 is only 1.1×10^{-2} mol/mol Pd*s at these conditions. That is, catalyst 2 is only 47% as active as catalyst 1 for 1,3-butadiene hydrogenation at room temperature. This result is surprising because catalyst 2, with its smaller clusters and greater palladium surface area, was found in previous work to be 1.8 times more active than catalyst 1 for ethylene hydrogenation at 120°C (see Section 3.3.4). That variation in activity was explained by the difference in cluster size between the two catalysts, which resulted in a larger total palladium surface area for catalyst 2. Based on this same type of surface area calculation, it is expected that catalyst 2 should be 1.1 to 1.6 times more active for butadiene hydrogenation than catalyst 1. However, as was discussed in section 4.3.1, the C_4 gas mixture plasticizes the polymer matrix, opening void spaces, and improving mass transport within the polymer. This effect appears to be cumulative; therefore, the hydrogenation rate will depend on the degree to which the catalyst has been exposed to

and plasticized by the C_4 gas mixture. Because catalyst 1 had been used in ten butadiene hydrogenation runs at 120°C before the room temperature experiments were performed, while catalyst 2 was used without prior exposure to C_4 gases, it may be assumed that the mass transport properties of catalyst 1 were much more favorable when these experiments were performed and a direct comparison of catalytic activities of the catalysts may not be possible.

1,3-Butadiene hydrogenation reactions were also conducted at 120°C and $P_{H2} = P_{C4H6} = 15$ psi_a (see Table 4.5). In this case, catalyst 1 and 2 had received similar exposure to the C_4 mixture, so their mass transfer characteristics were similar. Therefore, the higher activity of catalyst 2 can be attributed to the greater palladium surface area available for reaction. A comparison of the data obtained at 120°C to that obtained at room temperature indicates that raising the reaction temperature by roughly 100°C increases the catalyst activity by one order of magnitude.

T = 120°C

	Maximum Activity (mol/mol Pd·s)		**Maximum Selectivity** (mol/mol)	
	Catalyst 1	**Catalyst 2**	**Catalyst 1**	**Catalyst 2**
	9.7×10^{-2} (6)	2.7×10^{-1} (6)	0.81	0.90
	1.3×10^{-1} (7)	8.5×10^{-2} (7)	0.88	0.75
	8.7×10^{-2} (8)	8.9×10^{-2} (8)	0.85	0.88
	-	3.1×10^{-1} (9)	-	0.92
Average	**1.0×10^{-1}**	**1.9×10^{-1}**	**0.85**	**0.86**
Std. Dev.	2×10^{-2}	1.0×10^{-1}	0.03	0.07

Table 4.5: Maximum activity and selectivity of catalyst 1 and 2 for 1,3-butadiene hydrogenation at 120°C and $P_{H2} = P_{C4H6} = 15$ psi_a. The experimental run numbers are given in parentheses.

Table 4.6 summarizes the average selectivities for 1-butene, *trans*-2-butene, and *cis*-2-butene for both catalysts at room temperature and 120°C. The *cis*-2-butene and *trans*-2-butene selectivities vary little with reaction temperature or cluster size. However, the data show that the selectivity for 1-butene increases significantly as the reaction temperature is lowered from 120°C to room temperature. Catalyst 2 also appears to have better selectivity for 1-butene than catalyst 1. The consistently high *trans/cis* ratio for 2-butene production is typical for palladium catalysts.[2]

	1-Butene	***trans*-2-Butene**	***cis*-2-Butene**	**Butane**
	Room Temperature			
Catalyst 1	37%	30%	10%	23%
Catalyst 2	47%	34%	13%	6%
	120°C			
Catalyst 1	27%	39%	18%	16%
Catalyst 2	36%	35%	16%	13%

Table 4.6: Average maximum selectivity for each butene isomer at room temperature or 120°C, and $P_{H2} = P_{C4H6} = 15$ psi_a.

4.4 Summary

This study has shown that palladium nanoclusters synthesized within diblock copolymer films are active and selective catalysts for 1,3-butadiene hydrogenation in the gas phase. The polymer matrix was able to stabilize the clusters against aggregation, but could not prevent an increase in the cluster diameter. The C_4 gas mixture plasticized the polymer matrix, opening macroscopic voids, and improving mass transport within the film.

Raising the reaction temperature by *ca.* 100°C increased the catalyst activity by one order of magnitude. The variation of rate with reactant partial pressure was not the same as that reported in the literature, but lowering P_{H2} to ≤ 10 psi_a significantly lowered the reaction rate. Study of the catalytic activity as a function of cluster size was complicated by the cumulative effect of C_4 plasticization.

The overall selectivity for butenes, and particularly the selectivity for 1-butene, increased with decreasing hydrogen partial pressure. The loss of selectivity with increasing P_{H2} was due to an increase in the rate of hydrogenation of 1-butene to *n*-butane. The 1-butene selectivity was also improved by lowering the reaction temperature.

4.5 References

(1) Sarkany, A.; Zsoldos, Z.; Stefler, Gy.; Hightower, J. W.; Guczi, L. *J. Catal.* **1995**, *157*, 179.

(2) Ponec, V.; Bond, G. C. *Catalysis by Metals and Alloys*; Elsevier, Amsterdam, The Netherlands, 1995, pp. 227-279, 477, 482, 491, 500-504.

(3) Miegge, P.; Rousset, J. L.; Tardy, B.; Massardier, J.; Bertolini, J. C. *J. Catal.* **1994**, *149*, 404.

(4) Ohnishi, R.; Suzuki, H.; Ichikawa, M. *Catal. Lett.* **1995**, *33*, 341.

(5) Furlong, B. K.; Hightower, J. W.; Chan, T. Y. L.; Sarkany, A.; Guczi, L. *Appl. Catal. A: General* **1994**, *117*, 41.

(6) Tardy, B.; Noupa, C.; Leclercq, C.; Bertolini, J. C.; Hoareau, A.; Treilleux, M.; Faure, J. P.; Nihoul, G. *J. Catal.* **1991**, *129*, 1.

(7) Yeung, K. L.; Lee, K. H.; Wolf, E. E. *J. Catal.* **1995**, *156*, 120.

(8) Sarkany, A.; Schay, Z.; Stefler, Gy.; Borko, L.; Hightower, J. W.; Guczi, L. *Appl. Catal. A: Gen.* **1995**, *124*, L181.

(9) Ouchaib, T.; Massardier, J.; Renouprez, A. *J. Catal.* **1989**, *119*, 517.

5. Hydrogenation of Ethylene/Propylene Mixtures

5.1 Introduction

5.1.1 Shape Selective Hydrogenation Reactions

The selective hydrogenation of a single chemical species, usually a minor component, in a mixed product stream is an important process in the petrochemical industry. For example, ethylene feed stocks for polymerization produced by steam cracking of natural gas contain small amounts of acetylene and butadiene as impurities.[1,2] Although the acetylene and butadiene concentrations are low, typically *ca.* 3500 ppm and 6500 ppm, respectively, their total annual production makes recovery or conversion economically attractive. Acetylene must be removed because it poses a potential explosion hazard in downstream cryogenic distillation processes. Partial hydrogenation of acetylene to ethylene and recovery of butadiene are both desirable because the unsaturated species are more valuable than the corresponding saturated hydrocarbons.

Zeolite catalysts have been applied to the selective hydrogenation of particular species in a mixture.[1] Zeolites are highly crystalline hydrated aluminosilicates with a uniform pore structure. They have high activity and selectivity for acid-catalyzed reactions, but may also be loaded with transition metals and used for hydrogenation or other reactions. The unusual selectivity of zeolites arises from the extremely fine pore structure of these materials; minimum channel diameters are typically in the range of 3 to 10 Å. Therefore, only reactants and products below a certain maximum size can penetrate into or escape out of the zeolite crystals. This is the basis of shape selective catalysis.

Shape selectivity in zeolites depends on the pore size and shape and may arise by one of three different mechanisms. When only the smaller molecules in a mixture are able to penetrate the zeolite pore structure and react, the phenomenon is called "reactant selectivity". Similarly, when only small molecules formed within the zeolite pores are able to diffuse out, one has "product selectivity". Finally, "spaciospecific selectivity" results when certain products cannot form because required transition states are unattainable due to spatial restrictions within the zeolite pore structure. The shape selectivity of zeolites make them ideal catalysts for reforming and alkylation processes.

In one study, the selectivity of a rhodium/zeolite catalyst for hydrogenation of alkenes was compared to that of rhodium deposited on carbon.[3] Reactions were carried out in hexane at 50°C under hydrogen at atmospheric pressure. The relative activity of the zeolite catalyst for hydrogenation of alkenes correlated with the size of the reactants: 1-hexene ≈ 1-octene ≈ cyclohexene > cyclooctene >> cyclododecene. The shape selectivity of the Rh/zeolite for the hydrogenation of mixtures was also studied and compared to that of the commercial Rh/carbon catalyst. The zeolite performed significantly better than the commercial catalyst in all reactions. For example, in mixtures of cyclohexene and cyclooctene, both substrates were hydrogenated at the same rate by the Rh/carbon catalyst, but the rate of cyclohexene hydrogenation was five times faster than that of cyclooctene on the zeolite.

Corbin *et al.*[2] studied the purification of ethylene feed stocks described at the beginning of this chapter. Their objective was to selectively hydrogenate acetylene to ethylene, while minimizing the saturation of ethylene and butadiene. The gas phase

reactions were carried out at atmospheric pressure using a nickel/zeolite catalyst. The reactant mixture was formulated to mimic industrial processes, with 28% hydrogen, 32% ethylene, 0.35% acetylene, 0.65% butadiene, and the balance helium. Because of the hazards associated with acetylene in ethylene feed streams, catalyst selectivities were reported at or near the acetylene break through point (i.e. 99-100% acetylene hydrogenation). By selectively poisoning the non-shape selective zeolite surface sites, complete hydrogenation of acetylene with only 10-20% hydrogenation of butadiene and virtually no hydrogenation of ethylene could be achieved. The zeolite catalyst performed much better than the commercial $Ni/SiO_2/Al_2O_3$ catalyst, where 100% conversion of acetylene was accompanied by hydrogenation of 60% of the butadiene.

Transition metal functionalized clays have also been investigated as shape selective catalysts.[4,5] By changing the interlayer distance of the clays, it should be possible to alter the selectivity of the catalyst. In one study, the shape selectivity of two ruthenium/hectorite catalysts with different interlayer distances, d_{001} = 12.4 Å and d_{001} = 13.6 Å, was compared to that of a commercial Ru/SiO_2 catalyst.[4] Reactions were carried out at 120°C and $P_{H2} = P_{alkene}$ = 200 Torr. In all three cases, the hydrogenation activity of the catalyst decreased in the order: ethylene > propylene > 1-butene > *iso*-butene > 1-pentene > cyclohexene. The commercial catalyst had the highest absolute activity for all substrates, followed by the d_{001} = 13.6 Å, and d_{001} = 12.4 Å clays. The shape selectivity differed among the samples. The activity of the Ru/SiO_2 catalyst decreased gradually with increasing alkene size from ethylene through to cyclohexene. In contrast, there was a large drop in the activity of the d_{001} = 13.6 Å clay catalyst from ethylene to *iso*-butene,

and only a moderate decrease in activity from *iso*-butene to cyclohexene. For the d_{001} = 12.4 Å clay, the biggest drop in the hydrogenation rate was between ethylene and propylene, and the rate decreased gradually from propylene to cyclohexene. This study demonstrates that changing the interlayer distance results in changes in the shape selectivity of the catalyst.

In a similar study, montmorillonite functionalized palladium (II) complexes were found to exhibit shape selectivity in alkyne hydrogenations, consistent with the degree of steric bulkiness surrounding the carbon-carbon triple bond.[5] Reactions were carried out in THF solution at room temperature under hydrogen at atmospheric pressure. The relative hydrogenation rates of the alkynes decreased in the order: phenylacetylene > 1-phenyl-1-propyne ≈ methylphenylpropiolate > diphenylacetylene.

In this work, the possibility of using polymer/nanocluster composite materials as shape selective catalysts for hydrogenation of ethylene-propylene mixtures was explored. Assuming that the rate limiting step is transport of reactant gases through the polymer matrix, our hypothesis was that differences in the permeability of the reactant gases in the polymer matrix should result in different rates of hydrogenation. That is, the reactant in the mixture with the highest permeability in the diblock copolymer matrix should have the highest rate of hydrogenation.

A permeation study was conducted on a polyMTD sample to complement the hydrogenation rate experiments. The diffusion and solubility coefficients of ethylene, propylene, and 1,3-butadiene in polyMTD at room temperature were calculated from

interval desorption data. Further details of the theory of gas transport in polymers, and the permeation experiments are given in Sections 5.1.2 and 5.2, respectively.

5.1.2 Gas Transport Phenomena in Polymers

The diffusion of small molecules in polymers has been studied extensively because polymers have increasingly found application as gas separation media and as barrier materials for the packaging industry.[6,7] The aim of this work was to measure the permeability of the reactant gases - ethylene, propylene, and 1,3-butadiene - in polyMTD to assess the potential of the polymer matrix to act as a permselective membrane and selectively hydrogenate a particular species in a gas mixture.

Imagine that a penetrant pressure drop is applied across a polymer membrane. Transport of the penetrant molecule from the upstream to the downstream side of the membrane can be broken down into three processes.[8] First, the penetrant dissolves in the polymer at the upstream interface. Second, the absorbed gas diffuses through the membrane driven by the local concentration gradient. Third, the penetrant gas is released into the gas phase on the downstream side of the membrane. The first process, sorption of the gas at the membrane surface, can be described by Henry's Law:

$$c = Sp \qquad (5\text{-}1)$$

where c is the penetrant concentration in the polymer (g/cm^3), S is the Henry's Law solubility coefficient ($g/cm^3 \cdot psi$), and p is the penetrant partial pressure in the gas phase (psi). Diffusion of the penetrant through the polymer is proportional to the local concentration gradient and is described by Fick's Law:

$$J = D\nabla c \qquad (5\text{-}2)$$

where J is the penetrant flux (g/cm • s) and D is the diffusion coefficient (cm^2/s). Assuming that the penetrant concentration varies only in the x-direction (normal to the plane of the membrane), then equation (5-2) becomes:

$$J = - D(\partial c/\partial x) \qquad (5\text{-}3)$$

Assuming that the solubility and diffusion coefficients are independent of penetrant concentration, Henry's Law applies and equation (5-1) can be substituted into equation (5-3). Therefore:

$$J = - DS(\partial p/\partial x) \qquad (5\text{-}4)$$

$$= - \frac{DS(p_2 - p_1)}{(x_2 - x_1)}$$

$$= \frac{DS\Delta p}{h}$$

where h is the membrane thickness.

The permeability, P, is the product of the diffusion and solubility coefficients. The diffusion coefficient represents the kinetic contribution to permeation, while the solubility coefficient represents the thermodynamic contribution. If the components of a gas mixture do not interact with each other and do not appreciably solvate the polymer (causing plasticization and changing the polymer properties), then the permeability of each component will be equal to that of the pure gas. Therefore, polymers are able to separate gases in a mixture based on differences in the permeability of each gas. The ideal separation factor, $\alpha = P_1/P_2$, describes the ability of a polymer to separate two gases.

Experimental methods of determining S and D for polymers[8] fall into three general categories: (1) sorption into or out of a polymer; (2) permeation through a membrane into a closed chamber; and (3) permeation through a membrane into a flowing stream. Permeation methods have gained popularity in this and other research groups, but sorption experiments are equally valid and all necessary data may be collected in very simple experiments.

There are four basic types of sorption experiments. In integral sorption experiments, the sample is abruptly exposed to an atmosphere containing the penetrant gas and the weight gain of the polymer with time is recorded. For integral desorption experiments, the polymer sample is equilibrated at some penetrant pressure, then abruptly exposed to a penetrant-free atmosphere, usually vacuum, and the polymer weight loss is recorded until an immeasurable amount of the penetrant remains. Interval sorption (or desorption) experiments are the same as integral experiments, except that the initial (or final) penetrant concentration is greater than zero. In all of these experiments, the mass of the penetrant present in the polymer is measured as a function of time, either directly by gravimetric methods or indirectly by monitoring the change in penetrant pressure or the volume of the atmosphere surrounding the polymer. In this work, the interval desorption method was used and the penetrant mass was determined gravimetrically.

From the gravimetric data, M_t, the mass of penetrant desorbed in the interval from t_0 to t, and M_∞, the difference between the initial and final penetrant mass, can be determined. The solubility coefficient is easily determined from the relation:

$$S = M_{eq}/Vp_{eq} \qquad (5\text{-}5)$$

where M_{eq} is the mass of penetrant sorbed at the equilibrium penetrant pressure p_{eq}, and V is the volume of the polymer sample. By measuring M_{eq} for multiple values of p_{eq} at a fixed temperature, S can be determined from the slope of a plot of M_{eq}/V *versus* p_{eq}. Any deviations from linearity indicate a deviation from Henry's Law behavior.

For a plane polymer sheet the diffusion coefficient can be determined by two methods. It can be calculated from the initial slope of a plot of M_t/M_∞ *versus* $t^{1/2}$ and the relation:

$$M_t/M_\infty \approx (4/h)(D/\pi)^{1/2}t^{1/2} \qquad (5\text{-}6)$$

That is,

$$D \approx \frac{\pi(mh)^2}{16} \qquad (5\text{-}7)$$

where m is the slope of the M_t/M_∞ *versus* $t^{1/2}$ plot and h is the thickness of the polymer sheet (cm). The half-time method can be used to calculate D from $t_{1/2}$, the time at which $M_t/M_\infty = 1/2$, and the equation:

$$D \approx 0.04919/(t_{1/2}/h^2) \qquad (5\text{-}8)$$

There should be good agreement between the diffusion coefficients calculated from the initial slope and the half-time. Both calculations should be performed as a check on consistency.

5.2 Permeation Study

5.2.1 Experimental

Interval desorption experiments were performed to determine the diffusion and solubility coefficients of ethylene, propylene, and 1,3-butadiene in polyMTD at room

temperature. Two polymer films were static cast from dilute toluene solution in air using flat-bottom petri dishes. The films were placed inside a Fischer-Porter bottle and air was removed from the system by alternately evacuating and purging the vessel with argon three times. The penetrant gas was introduced at a pressure of 15 or 30 psi_a and the system was allowed to equilibrate for one hour, after which the films were quickly removed from the Fischer-Porter bottle and the change in mass as a function of time was recorded. The sample mass was measured on a Metler AJ100 digital balance.

5.2.2 Results and Discussion

Plots of M_t/M_∞ *versus* $t^{1/2}$ at 15 and 30 psi_a for ethylene, propylene, and 1,3-butadiene are shown in Figures 5-1, 5-2, and 5-3, respectively. Also shown are the fits of the initial slope as determined by linear regression of the first four to seven data points. The diffusion coefficients determined from the initial slope are summarized in Table 5.1, and those determined by the half-time method are summarized in Table 5.2.

P_{eq}	**Diffusion Coefficient** (cm^2/s)		
	Ethylene	**Propylene**	**1,3-Butadiene**
15 psi_a	1.1×10^{-10}	3.4×10^{-11}	5.3×10^{-11}
30 psi_a	6.2×10^{-11}	5.3×10^{-11}	7.4×10^{-11}

Table 5.1: Diffusion coefficients for reactant gases in polyMTD at room temperature determined from the initial slope of the M_t/M_∞ *versus* $t^{1/2}$ plots.

P_{eq}	**Diffusion Coefficients** (cm^2/s)		
	Ethylene	**Propylene**	**1,3-Butadiene**
15 psi_a	1.2×10^{-10}	3.2×10^{-11}	5.2×10^{-11}
30 psi_a	7.1×10^{-11}	5.2×10^{-11}	7.3×10^{-11}

Table 5.2: Diffusion coefficients for reactant gases in polyMTD at room temperature determined by the half-time method.

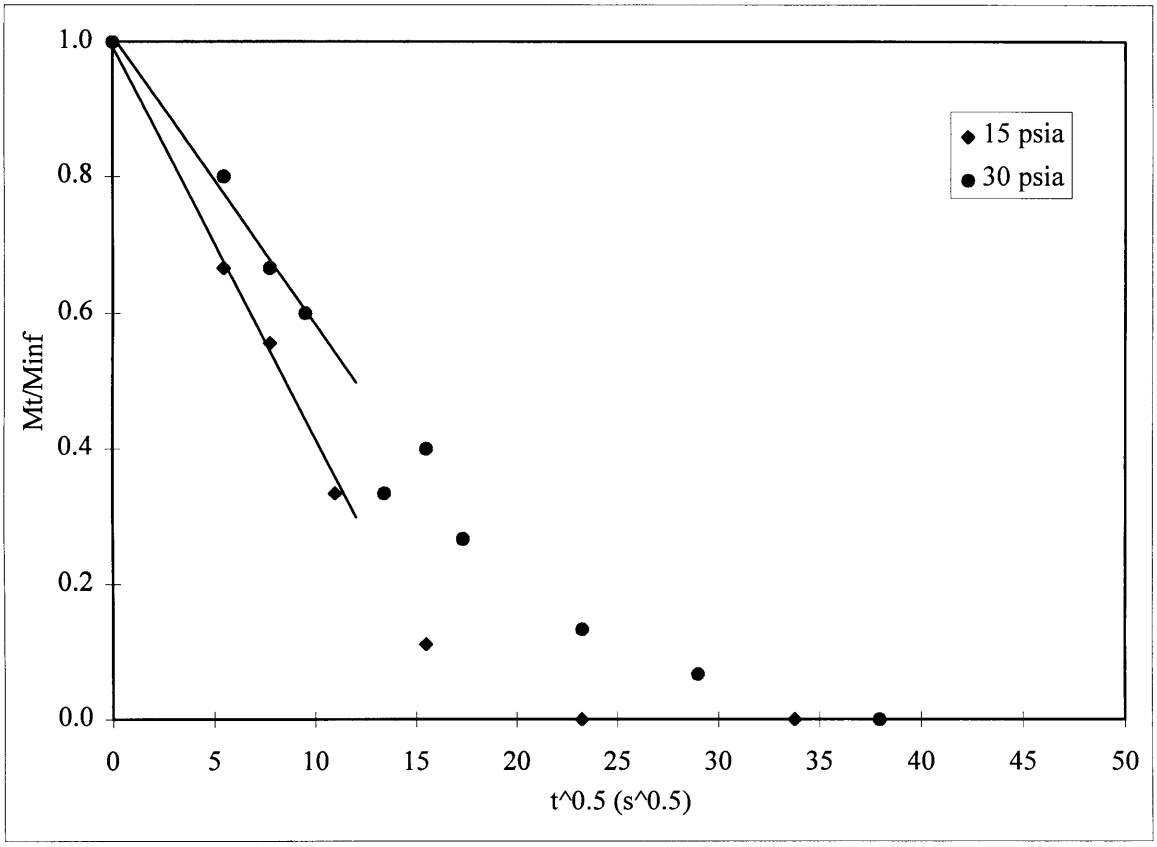

Figure 5-1: Ethylene desorption experiments: plot of M_t/M_∞ *versus* $t^{1/2}$ at 15 and 30 psi_a at room temperature. Fits of initial slope determined by linear regression are shown as solid lines.

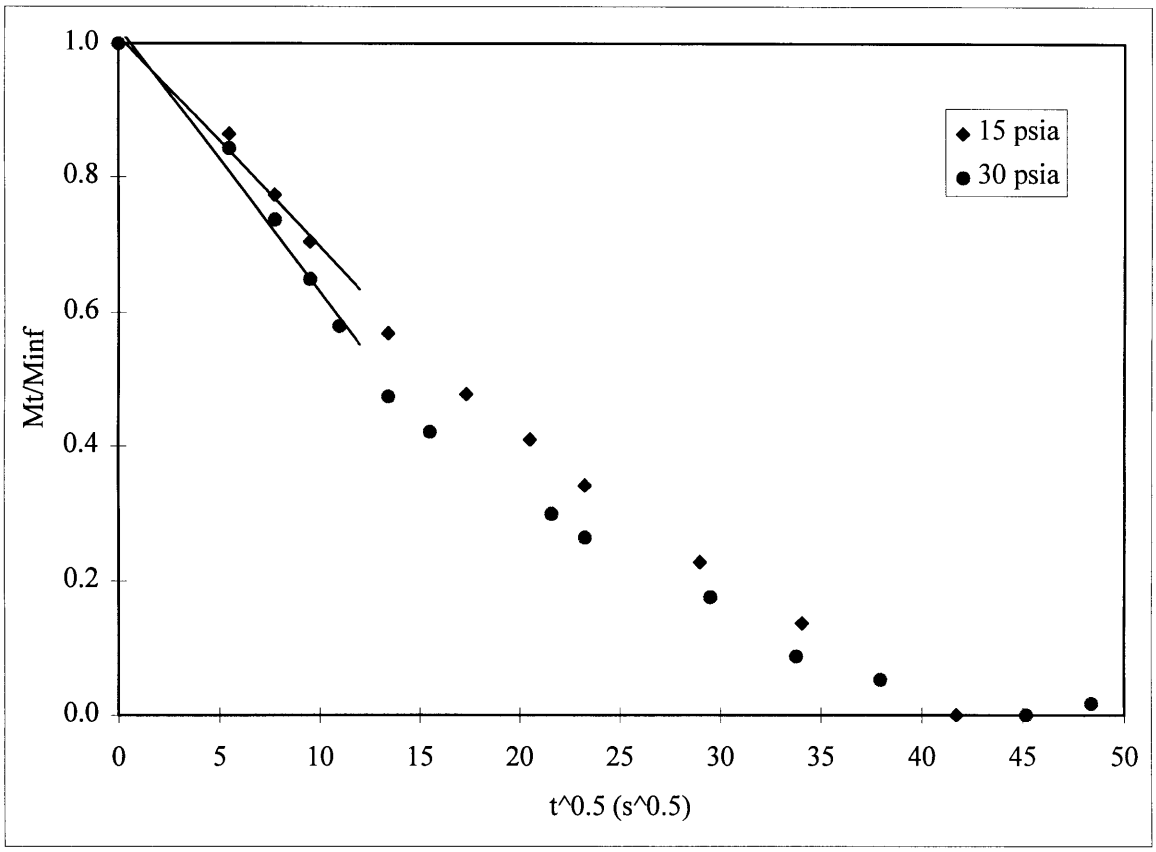

Figure 5-2: Propylene desorption experiments: plot of M_t/M_∞ *versus* $t^{1/2}$ at 15 and 30 psi_a at room temperature. Fits of initial slope determined by linear regression are shown as solid lines.

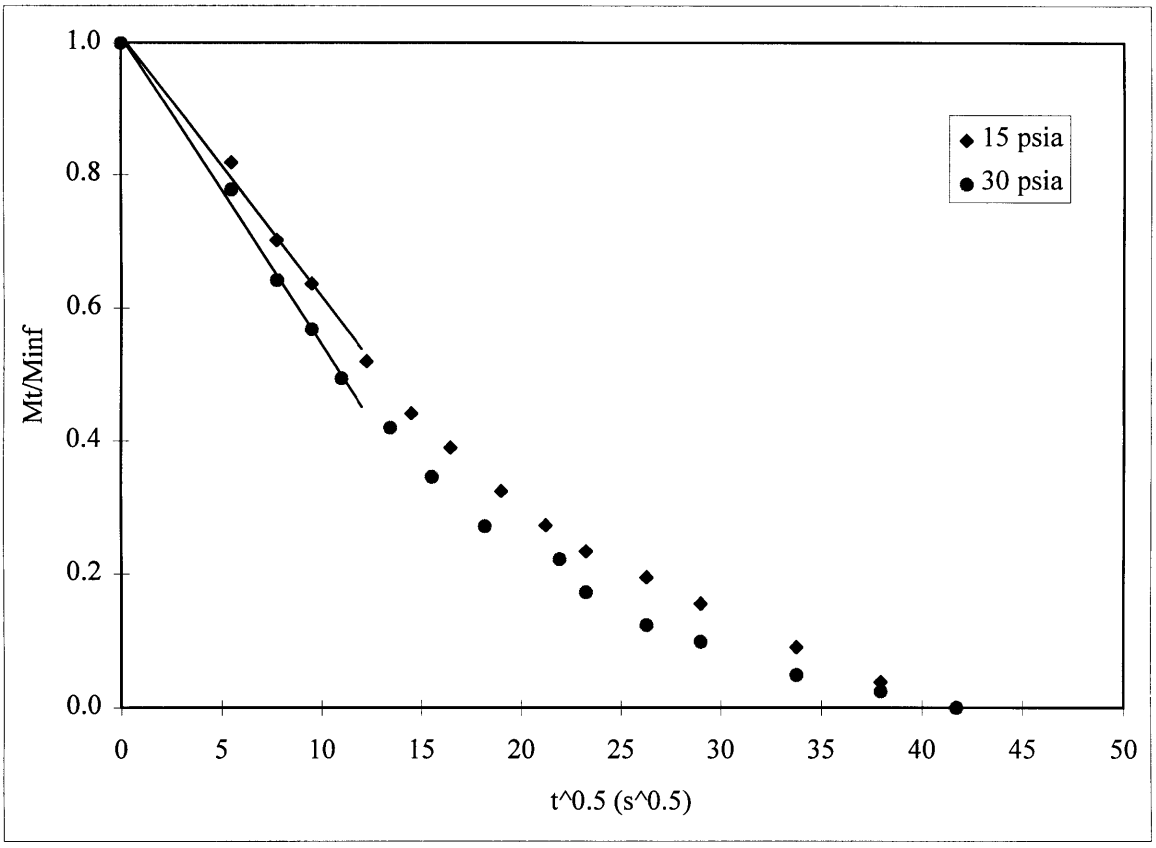

Figure 5-3: 1,3-Butadiene desorption experiments: plot of M_t/M_∞ *versus* $t^{1/2}$ at 15 and 30 psi_a at room temperature. Fits of initial slope determined by linear regression are shown as solid lines.

There is excellent agreement between the diffusion coefficients determined from the initial slope and those determined by the half-time method, except for ethylene at 30 psi_a where the values differ by 15%. There are larger differences between the diffusion coefficients determined at 15 and 30 psi_a, but the pairs of values for propylene and butadiene are of the same order of magnitude and nearly so for ethylene. Therefore, the four values of the diffusion coefficient were averaged and used to calculate the permeability of each penetrant gas. The average values are reported in Table 5.3.

Figure 5-4 is a plot of M_{eq}/V *versus* p_{eq} for the three penetrant gases. The ethylene and propylene solubility coefficients were determined from the slope of the line fit through the data by linear regression. The fits were forced through the origin because the physics of the experiment dictate that there should be no adsorbed gas in the polymer when the surrounding penetrant pressure is equal to zero. The 1,3-butadiene data set deviate from Henry's Law, which is expected because the C_4 gases were found to plasticize the polymer matrix (see Chapter 4). Therefore, the butadiene solubility coefficient was estimated from the average slope of two lines, one extending from the origin to the 15 psi_a data point, and the second from the origin to the 30 psi_a data point. The line shown in Figure 5-4 has the average slope. Table 5.3 summarizes the averaged diffusion coefficient, the solubility coefficient, and the permeability of each gas.

The data in Table 5.3 show that there is little variation among the diffusion coefficients, all three values being of the same order of magnitude. In contrast, the solubility coefficient increases by one order of magnitude from ethylene to 1,3-butadiene. Therefore, the increase in permeability with increasing molecular weight of the penetrant

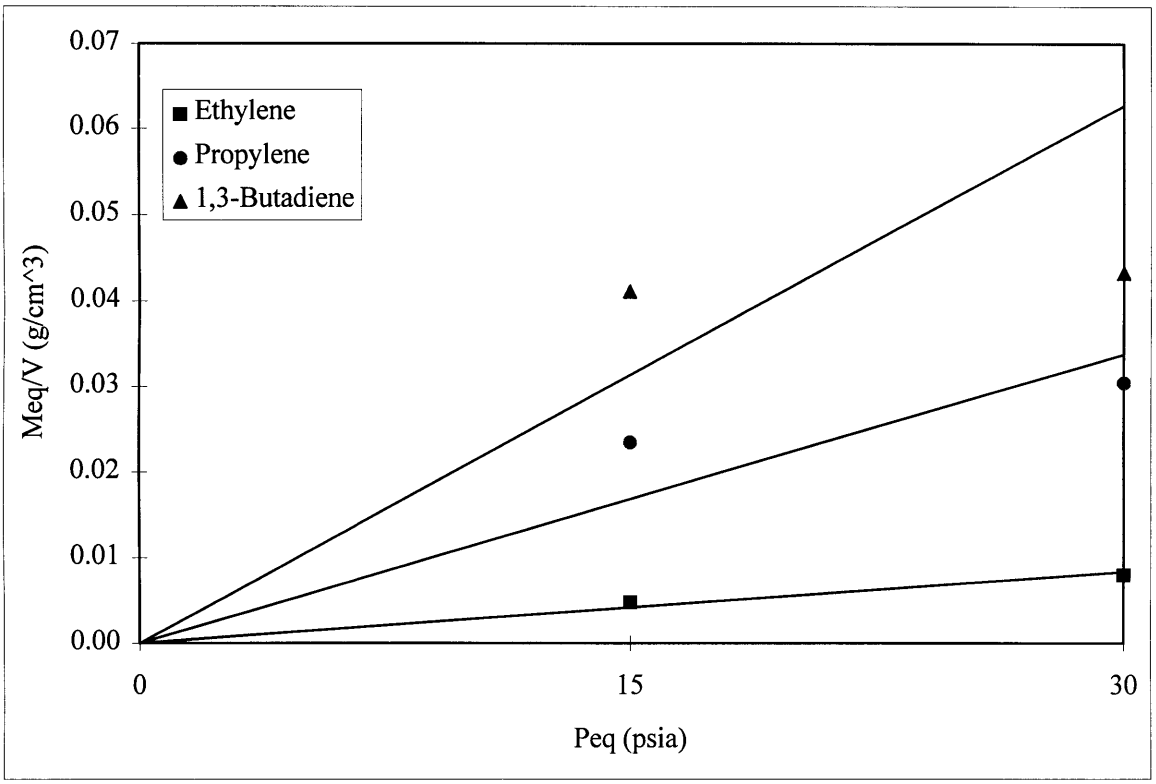

Figure 5-4: Plots of M_{eq}/V *versus* p_{eq} for ethylene, propylene, and 1,3-butadiene at room.

Penetrant Gas	**D** (cm^2/s)	**S** ($g/cm^3 psi$)	**P = D•S** ($g/cm \cdot s \cdot psi$)
Ethylene	9.1×10^{-11}	2.8×10^{-4}	2.5×10^{-14}
Propylene	4.3×10^{-11}	1.1×10^{-3}	4.8×10^{-14}
1,3-Butadiene	6.3×10^{-11}	2.1×10^{-3}	1.3×10^{-13}

Table 5.3: Diffusion coefficient, solubility coefficient, and permeability for ethylene, propylene, and 1,3-butadiene in polyMTD at room temperature. The diffusion coefficients are average values.

gas is caused by the increase in the solubility coefficient. If the hydrogenation reactions studied here are mass transfer limited, then the rate of reaction of each species in a gas mixture should be proportional to its permeability in the polymer matrix. If this is the

case, then propylene should react roughly twice as fast as ethylene when a mixture of the two gases is hydrogenated.

5.3 Ethylene and Propylene Hydrogenation Experiments

5.3.1 Hydrogenation Reactions

Ethylene and propylene hydrogenation experiments were run as batch reactions in a Fischer-Porter bottle equipped with a magnetic stirrer and a gas sampling port. The nanocomposite films (4-6 mg, 15 wt% palladium) were placed in a stainless steel sample holder and positioned roughly in the center of the reactor. The films, *ca.* 200 μm thick, were cut into one or two pieces. The reactor was alternately evacuated and purged with argon three times to remove air from the system. The reactor was then evacuated, filled with ethylene or propylene, and heated to the reaction temperature of 120°C. The system was allowed to stabilize for 20 minutes before the hydrogen gas was transferred. A hydrogen:alkene molar ratio of 2:1 was used and initial reaction pressures were typically 34 psi_g. The reactor temperature was controlled with a Cole-Parmer Digi-Sense temperature controller (model 2186-10A) and the reactor pressure was measured with a PSI-TRONIX electronic pressure gauge (model 68920-38).

5.3.2 Gas Chromatography

Gas chromatography was performed on a Hewlett-Packard HP 6890 GC equipped with a split/splitless injection port, an HP-PLOT/Al_2O_3 "S" column (50 m x 530 μm x 15 μm), and a flame ionization detector (FID). Helium was used as both the carrier gas and FID make up gas. The reactor pressure was recorded before and after sample withdrawal so that corrections could be made in calculating the catalytic activity of the polymer film.

For the ethylene hydrogenation experiments, samples (150 μL) were injected manually with a gas-tight syringe using a split ratio of 70. The column flow rate was 7.0 mL/min and the oven temperature was constant at 60°C. Samples were withdrawn from the reactor at approximately five minute intervals. For the propylene hydrogenation experiments, the oven temperature was increased to 90°C and the sampling frequency was unchanged.

5.3.3 Results and Discussion

Ethylene and propylene hydrogenation reactions were run separately using two nanocomposite catalysts. Catalyst 1 had been used previously for both ethylene and 1,3-butadiene hydrogenation experiments. Therefore, the polymer matrix of catalyst 1 had been plasticized and a considerable number of void spaces had been opened up within the polymer matrix. The clusters in catalyst 1 had a mean diameter of 35 Å (see Figure 4-2). The clusters in catalyst 2 were 19 Å in diameter (see Figure 3-6). Catalyst 2 had been used for ethylene hydrogenation experiments, but it had only been used for one 1,3-butadiene hydrogenation run, so the polymer matrix contained few macroscopic voids. The maximum activity of catalyst 1 for each hydrogenation run is given in Table 5.4. Data for catalyst 2 are given in Table 5.5.

The maximum activity of catalyst 1 for both ethylene and propylene hydrogenation is higher than that of catalyst 2, in spite of the fact that catalyst 2 has smaller clusters and presumably a greater total palladium surface area. This observation is explained by the difference in the degree of C_4 exposure. Catalyst 1 had had extensive exposure to C_4's, so its mass transfer resistance was reduced resulting in higher activity

Catalyst 1

	Maximum Activity (mol/mol Pd • s)	
Run	**Ethylene**	**Propylene**
1	4.5×10^{-2}	2.2×10^{-2}
2	6.5×10^{-2}	2.1×10^{-2}
3	7.0×10^{-2}	2.2×10^{-2}
4	6.4×10^{-2}	1.9×10^{-2}
5	3.8×10^{-2}	1.9×10^{-2}
6	3.3×10^{-2}	
7	3.1×10^{-2}	
Average	**4.9×10^{-2}**	**2.1×10^{-2}**
Standard Deviation	1.5×10^{-2}	1×10^{-3}

Table 5.4: Maximum activity of catalyst 1 for hydrogenation of ethylene or propylene at 120°C, P_{H2} = 30 psi_a, and P_{alkene} = 15 psi_a.

Catalyst 2

	Maximum Activity (mol/mol Pd • s)	
Run	**Ethylene**	**Propylene**
1	7.8×10^{-3}	9.2×10^{-3}
2	5.9×10^{-3}	7.0×10^{-3}
3	6.7×10^{-3}	9.3×10^{-3}
4	7.5×10^{-3}	8.9×10^{-3}
5	9.3×10^{-3}	7.2×10^{-3}
6	9.1×10^{-3}	7.9×10^{-3}
7	8.7×10^{-3}	6.3×10^{-3}
8		6.6×10^{-3}
Average	**7.9×10^{-3}**	**7.8×10^{-3}**
Standard Deviation	1.2×10^{-3}	1.1×10^{-3}

Table 5.5: Maximum activity of catalyst 2 for hydrogenation of ethylene or propylene at 120°C, P_{H2} = 30 psi_a and, P_{alkene} = 15 psi_a

values. Similar increases in activity were observed for ethylene hydrogenation before and after exposure to C_4's (see Section 3.3.5).

Ethylene is hydrogenated at about twice the rate of propylene on catalyst 1, but the average maximum rates are equal on catalyst 2. Based on the results of the permeation study, and assuming that mass transfer limitations dominate, the catalysts are expected to be roughly twice as active for propylene hydrogenation as they are for ethylene. The fact that this hypothesis is not born out experimentally may be because the polymer segments surrounding the catalytically active sites create steric crowding, making it more difficult for the propylene molecules to adsorb on the palladium surface. Or it may be that the difference in permeability of the gases is too small to manifest itself in these experiments. However, it may also be that the differences in activity for ethylene and propylene hydrogenation may be too small to draw definitive conclusions.

5.4 Ethylene/Propylene Mixture Hydrogenation Experiments

5.4.1 Hydrogenation Reactions

Hydrogenation of ethylene/propylene mixtures was carried out in a manner similar to hydrogenation of single gases. After the evacuation/purge cycles were completed ethylene, then propylene were transferred to the reactor. The reactor was heated to 120°C before the hydrogen gas was introduced to the reactor. A hydrogen:ethylene:propylene ratio of 4:1:1 was used, and initial pressures were approximately 34 psi_g.

5.4.2 Gas Chromatography

For the ethylene/propylene hydrogenation experiments, samples (150 μL) were injected manually with a gas-tight syringe using a split ratio of 70. The column flow rate

was 7.0 mL/min and the oven temperature was constant at 70°C. Gas samples were withdrawn from the reactor at approximately seven minute intervals.

5.4.3 Results and Discussion

Mixtures of ethylene and propylene were hydrogenated using catalyst 1 and 2. The maximum activity for hydrogenation of each gas in the mixture is reported in Table 5.6 for catalyst 1, and Table 5.7 for catalyst 2. The hydrogenation rates are again almost twice as fast on catalyst 1 as on catalyst 2, due to the lengthy exposure of catalyst 1 to C_4 gases. Based on the permeability values calculated for ethylene and propylene, and the assumption that the hydrogenation reactions are mass transfer limited, the propylene hydrogenation rate is expected to be roughly twice that of ethylene. However, ethylene is hydrogenated *ca.* 40% faster than propylene in both cases.

There is a consistent trend throughout these experiments for the ethylene hydrogenation rate to exceed that of propylene, contrary to predictions based on the relative permeability of the gases. Although the differences in the rates are not large, the trend points towards the conclusion that some other phenomenon, such as the adsorption kinetics of the reactants onto the palladium surface, plays an important role in determining the rate of reaction.

Comparing these results to more traditional shape selective catalysts, the variation in activity with reactant size is not as great as it is for zeolite or functionalized clay catalysts. If the objective is to hydrogenate a single species in a gas mixture, it is not as effective to use differences in the permeability of gases in a polymer as the basis for

selectivity as it is to use an extremely fine pore structure able to distinguish among molecules based on their size.

Catalyst 1

	Maximum Activity (mol/mol Pd•s)		Activity Ratio
Run	**Ethylene**	**Propylene**	
1	7.5×10^{-3}	5.5×10^{-3}	1.4
2	7.8×10^{-3}	5.6×10^{-3}	1.4
3	7.1×10^{-3}	6.3×10^{-3}	1.1
4	1.2×10^{-2}	9.2×10^{-3}	1.3
5	1.5×10^{-2}	1.1×10^{-2}	1.4
6	1.4×10^{-2}	1.0×10^{-2}	1.4
Average	**1.1×10^{-2}**	**7.9×10^{-3}**	**1.4**
Std. Dev.	0.3×10^{-2}	2.2×10^{-3}	

Table 5.6: Maximum activity of catalyst 1 for hydrogenation of ethylene and propylene in a mixture at 120°C, $P_{H2} = 30$ psi_a, and $P_{ethylene} = P_{propylene} = 7.5$ psi_a. The activity ratio is equal to the maximum ethylene hydrogenation activity divided by the maximum propylene hydrogenation activity.

Catalyst 2

	Maximum Activity (mol/mol Pd•s)		Activity Ratio
Run	**Ethylene**	**Propylene**	
1	8.2×10^{-3}	8.8×10^{-3}	0.93
2	5.9×10^{-3}	4.2×10^{-3}	1.4
3	9.8×10^{-3}	6.9×10^{-3}	1.4
4	4.9×10^{-3}	3.1×10^{-3}	1.6
5	4.2×10^{-3}	2.7×10^{-3}	1.6
6	5.1×10^{-3}	2.3×10^{-3}	2.2
7	6.4×10^{-3}	4.1×10^{-3}	1.6
Average	**6.4×10^{-3}**	**4.6×10^{-3}**	**1.4**
Std. Dev.	1.8×10^{-3}	2.2×10^{-3}	

Table 5.7: Maximum activity of catalyst 2 for hydrogenation of ethylene and propylene in a mixture at 120°C, $P_{H2} = 30$ psi_a, and $P_{ethylene} = P_{propylene} = 7.5$ psi_a. The activity ratio is equal to the maximum ethylene hydrogenation activity divided by the maximum propylene hydrogenation activity.

5.5 Summary

A study of the permeability of ethylene, propylene, and 1,3-butadiene in polyMTD at room temperature was carried out. This study revealed that while the diffusion coefficients of the gases are similar and of the same order of magnitude, the solubility coefficient increases by an order of magnitude from ethylene to 1,3-butadiene. Therefore, the permeability increases by nearly an order of magnitude from ethylene to 1,3-butadiene as a result of the large increase in the solubility coefficient. Based on the ratio of the ethylene and propylene permeability, it was hypothesized that the nanocomposites should be about twice as active for propylene hydrogenation as for ethylene and that this should result in the selective hydrogenation of propylene in a mixture of the two gases.

Ethylene and propylene reactions were carried out separately and in a mixture on two catalysts. Mass transfer resistance in catalyst 1 had been reduced by exposure to C_4's, but catalyst 2 had smaller clusters and thus a greater total palladium surface area. For all reactions, the activity was higher for catalyst 1 than catalyst 2, demonstrating the effect of decreased mass transfer resistance on reaction rates. Contrary to the hypothesis, ethylene was hydrogenated *ca.* 40% faster than propylene in a mixture of the two gases, and the ethylene activity was equal to or greater than the propylene activity when the gases were reacted separately. The difference in the ethylene and propylene permeability may not have been great enough to manifest itself in these experiments, or it may be that some other phenomenon, such as the kinetics of adsorption of the reactant molecules on the palladium surface, plays an important role in determining the rate of reaction.

5.6 References

(1) Satterfield, C. N. *Heterogeneous Catalysis in Industrial Practice*; Second Edition; McGraw-Hill, Inc.: New York, 1991, pp. 226-247.

(2) Corbin, D. R.; Abrams, L.; Bonifaz, C. *J. Catal.* **1989**, *115*, 420.

(3) Yamaguchi, I.; Joh, T.; Takahashi, S. *J. Chem. Soc., Chem. Commun.* **1986**, *18*, 1412.

(4) Shimazu, S.; Hirano, T.; Uematsu, T. *Appl. Catal.* **1987**, *34*, 255.

(5) Choudary, B. M.; Mukkanti, K.; Subba Rao, Y. V. *J. Mol. Catal.* **1988**, *48*, 151.

(6) Kofinas, P., Doctoral Thesis, Massachusetts Institute of Technology, Department of Materials Science and Engineering **1994**.

(7) Rein, D. H., Doctoral Thesis, Massachusetts Institute of Technology, Department of Chemical Engineering **1991**.

(8) Felder, R. M.; Huvard, G. S. in *Methods of Experimental Physics*; R. A. Fava, Editor; Academic Press: New York, 1980, vol. 16, ch. 17.

6. Summary and Directions for Future Investigations

6.1 Summary

This project built on previous work done in the Cohen and Schrock groups on methods to synthesize metal nanoclusters within bulk, microphase-separated diblock copolymers. The organometallic monomer $Pd(Cp^N)PA$ was synthesized and the product structure was verified by NMR analysis. Diblock copolymers containing 50 wt% of the organometallic block were synthesized by ring opening metathesis polymerization. GPC analysis showed that the polymers had a narrow molecular weight distribution, with a typical polydispersity of 1.1. When polymer films were formed by static casting, the polymer microphase separated, resulting in a non-equilibrium cylindrical morphology with a d-spacing of *ca.* 200 Å. Clusters were synthesized within the films by exposing them to hydrogen at 100°C for 2-3 days. TEM analysis showed that the clusters were roughly spherical, had a narrow size distribution, and were located predominantly within the original organometallic domains. The clusters were generally 14-35 Å in diameter. SAXS analysis indicated that in samples with smaller clusters, the organometallic repeat units may have been reduced to a lesser extent.

Gas phase experiments demonstrated that the palladium nanocluster/diblock copolymer composite materials were active catalysts for hydrogenation of ethylene, propylene, and 1,3-butadiene, despite the fact that the clusters are completely embedded within a non-porous polymer matrix. Although comparisons among the activity data sets are complicated by the plasticizing effect of C_4 gases and the slowly increasing size of the clusters with repeated use, the activity of the nanocomposites for hydrogenation generally

increased in the order: propylene < ethylene < 1,3-butadiene. The nanocomposite also showed good selectivity for butenes over *n*-butane in the hydrogenation of 1,3-butadiene and the selectivity for 1-butene in particular could be improved by lowering the reaction temperature and/or the hydrogen partial pressure. As mentioned earlier, the C_4 gas mixture was a plasticizer for the polymer matrix, causing 15-60 μm diameter voids to be opened up within the matrix. These void spaces reduced mass transfer resistance within the films, increasing the activity of the films for ethylene and propylene hydrogenation.

Interval desorption experiments were conducted on a polyMTD sample at room temperature to study the permeability of each reactant gas in the polymer matrix. These experiments revealed that while the diffusion coefficients of ethylene, propylene, and 1,3-butadiene in polyMTD are similar, the solubility coefficient increases by one order of magnitude with increasing penetrant molecular weight. Therefore, the permeability (i.e. the product of the diffusion and solubility coefficients) increases by nearly one order of magnitude from ethylene to 1,3-butadiene. Assuming that mass transfer through the polymer matrix is the rate limiting step in the hydrogenation reactions, the activity of the nanocomposites should increase with increasing reactant permeability. This should also apply to mixtures; that is, the reactant with the highest permeability in a mixture should react the fastest. Based on these assumptions, it was expected that propylene would be hydrogenated at about twice the rate of ethylene, whether the gases are hydrogenated separately or in a mixture.

Ethylene and propylene hydrogenation experiments were carried out separately and in a mixture using two different nanocomposite samples. In separate experiments,

ethylene reacted at the same rate or faster than propylene; and in mixtures, ethylene consistently reacted about 40% faster than propylene. These results point to the conclusion that some other phenomenon, such as the adsorption/desorption kinetics on the palladium cluster surface, is important in determining the rate limiting step.

6.2 Directions for Future Investigations

Partial hydrogenation of alkynes and dienes, and dehydrogenation of alkanes to produce alkenes are important industrial reactions. Table 6.1 illustrates the value-added nature of alkene feed stocks by comparing their uses to those of the corresponding alkanes.[1] Ethylene is the major feed stock for polyethylene; it is also the source of a

Hydrocarbon	Uses
Methane	fuel gas
Ethane	fuel gas
Propane	fuel gas, liquefied petroleum gas
n-Butane	motor gasoline
Ethylene	fuel gas, petrochemicals, polymers
Propylene	fuel gas, petrochemicals, polymers, polymer gasoline
1-Butene	synthetic rubber, chemicals
2-Butene	alkylate polymer gasoline, motor gasoline

Table 6.1: Industrial uses of light hydrocarbon feed stocks.[1]

number of commodity chemicals, such as ethylene oxide, ethanol, ethyl benzene, and vinyl acetate. Propylene is also used for polyolefins and petrochemicals including isopropyl alcohol, cumene, acrylonitrile, and propylene oxide. Finally, *n*-butenes are converted to *sec*-butyl alcohol, then methyl ethyl ketone, and butadiene is used in polymers and is a copolymer with styrene and acrylonitrile.

Because of the commercial value of ethylene, propylene, and butenes, the following sections will focus on partial hydrogenation of alkynes and dienes, and the dehydrogenation of alkanes. The selectivity of Pd cluster-containing nanocomposites for partial hydrogenation of 1,3-butadiene has been demonstrated. The nanocomposites are also active for hydrogenation of ethylene and propylene. The activity of supported palladium catalyst for the reverse reaction is firmly established and it can be reasonably assumed that the nanocomposites will also be active for dehydrogenation reactions.

6.2.1 Dehydrogenation Reactions and Membrane Reactors

Many commodity chemicals, including ethylene, propylene, butenes, and styrene, are made by thermal or catalytic cracking of low molecular weight hydrocarbons.[2] Dehydrogenation reactions are equilibrium limited and steam is usually injected with the hydrocarbon feed to decrease the alkane partial pressure, improving the thermodynamics and increasing the theoretical maximum yield. The reactions are endothermic, so processes must be operated at high temperatures, typically 750-950°C, to achieve reasonable conversions. However, high operating temperatures result in high energy costs, coking of the catalyst, and loss of catalytic activity and selectivity. Therefore, new reactor configurations must be considered if higher yields and lower energy costs are to be achieved.

Membrane reactors have been applied to the dehydrogenation of alkanes.[3-12] A membrane reactor is similar in principle to a heat exchanger, except that the tubes are composed of a semipermeable or permselective membrane. Dense palladium membranes are semipermeable; they are permeable to hydrogen, but impermeable to hydrocarbons.

Polymers are permselective membranes, and their separation capability is based on differences in permeability among various gases. Use of a semipermeable or permselective membrane enables selective removal of one or more low molecular weight products from a reaction mixture. Therefore, by a simple application of LeChatelier's principle, a membrane reactor can be used to shift the equilibrium of a dehydrogenation reaction toward the desired product by selective removal of hydrogen. This means that the reaction temperature can be lowered, reducing energy costs, and product selectivities are often improved because removal of hydrogen cuts off certain byproduct reaction pathways. Further, the cost and complexity of the dehydrogenation process can be reduced by combining reaction and separation into a single unit operation.

Membrane reactors may be designed in any of a number of geometries, but the shell-and-tube reactor, depicted schematically in Figure 6-1, is the most common. In the shell-and-tube membrane reactor, the feed stream may flow on the shell or tube side, but the shell side is more common because it usually results in better activity and selectivity. A sweep gas is used on the tube side to remove hydrogen from the system and increase conversion. The hatched region in Figure 6-1 represents the semipermeable or permselective membrane.

Dense palladium and palladium alloy membranes have been incorporated into membrane reactors and used to dehydrogenate ethane, cyclohexane, and isopropanol.[3] The membranes act as both the catalyst and a semipermeable membrane. These membranes are attractive because they have perfect selectivity for hydrogen (hydrogen is actually dissolved in the membrane), making 100% conversion to alkenes possible.

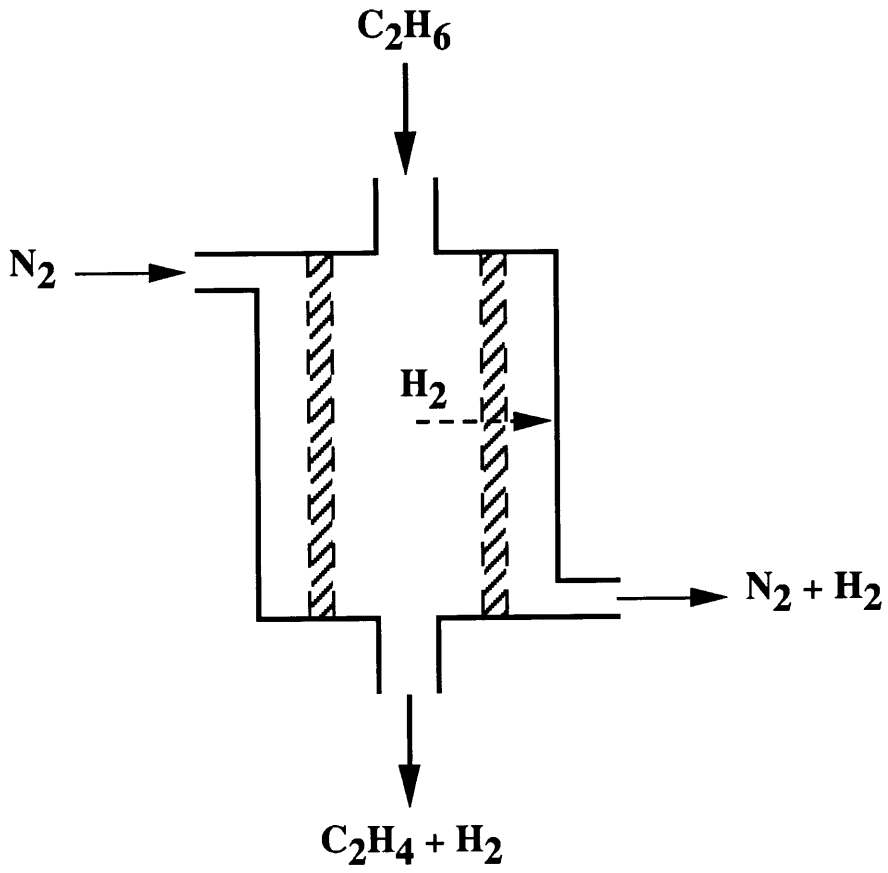

Figure 6-1: Schematic diagram of a membrane dehydrogenation reactor. The hatched region represents the semipermeable or permselective membrane.

However, palladium and palladium alloy membranes suffer from low flux, high cost, and susceptibility to sintering, embrittlement, metal fatigue, sulfur poisoning, and coking.[4,5]

More recently, inorganic membranes have been studied for use in membrane dehydrogenation reactors. These membranes have the advantage of good chemical resistance, high temperature stability, well-controlled pore size distribution, and favorable heat transfer characteristics. Common types of inorganic membrane include porous Vycor™ glass and porous γ-Al_2O_3 tubes with pore diameters of $\approx$ 40 Å. Because the pores are so small, gas transport is by Knudsen diffusion and permselectivity is based on differences in molecular weight. Therefore, inorganic membranes are useful for dehydrogenation reactions because separation of hydrogen from higher molecular weight hydrocarbons is the objective.

Both experimental and modeling studies of ethane,[6] propane,[3,4,7] butane,[8] isobutane,[9,10] and ethyl benzene[11,12] dehydrogenation using membrane reactors have been conducted. In one study,[6] a shell-and-tube membrane reactor constructed from a composite membrane of porous Vycor™ glass coated with a dense Pd/Ag semi-permeable membrane and packed with a dehydrogenation catalyst was applied to ethane dehydrogenation. Reactions were run at 114°C and 130 kPa. Conversions up to 2.57% in a single pass were reported. This was a significant improvement over the 0.87% conversion predicted from thermodynamic calculations assuming no removal of hydrogen. The conversion increased with increasing residence time and increasing sweep gas flow rate, but operating at these conditions can lead to product loss to the shell side when permselective, rather than semipermeable, membranes are used.

Polymer-based nanocomposite catalysts could be incorporated into a membrane dehydrogenation reactor, acting either as the catalyst, or as the catalyst and the permselective membrane. However, temperature limitations and mass transfer resistance are likely to remain factors in limiting the range of application of these materials.

6.2.2 Partial Hydrogenation Reactions

Alkene process streams produced by catalytic cracking of low molecular weight hydrocarbons contain small amounts of alkynes and dienes as impurities.[13] These multiply-unsaturated species must be removed to make the process streams suitable for motor fuel or petrochemical feed stocks. For example, a typical C_3 process stream contains roughly 90% propylene, 5% propane, and 5% methyl acetylene and propadiene. To prepare a high purity polyolefin feed, the methyl acetylene and propadiene must be removed while minimizing saturation and oligomerization reactions. The feed streams are purified by partial hydrogenation. A number of different catalysts have been used, including Ni or Zn on Al_2O_3 or SiO_2; Cd, Ca, Ba, St, or Mg on Cr_2O_3; Cu on Al_2O_3, MgO, or SiO_2; metallic Ni; Pd, Pt or a Pd/Pt alloy on glass; and Pd, Rh, or Ir on SiO_2. Of the group VIII elements, palladium is the most active and selective catalyst for partial hydrogenation of alkynes and dienes, and its performance can be enhanced by addition of a small amount of a promoter such as Cr or Ag.

Partial hydrogenation is also used to selectively hydrogenate benzene,[14] cyclopentadiene,[15] isoprene, and butadiene to the corresponding alkene. Partial hydrogenations can be run in the gas or liquid phase, or as mixed phase reactions. High catalyst selectivity is more important than high activity, so reactions are often carried out

in the liquid phase to enhance selectivity. However, this approach requires separation of the supported catalyst from solvent, products, and reactants. Selectivity may also be improved by lowering the reaction temperature or by operating at low hydrogen partial pressures, but reducing P_{H2} too far will result in unacceptably low conversions.

A particularly interesting study of partial hydrogenation investigated the use of catalytic membranes for the gas phase selective hydrogenation of dienes at 40°C and atmospheric pressure.[15] The catalytic membranes were prepared by deposition of Pd-polymer complexes from aqueous solution onto the inside wall of microporous hollow fiber (MPHF) membranes. The complexes were reduced by passing an ethanol/water solution of hydrazine through the membranes. The MPHF membranes were made of cellulose acetate, polysulfone, or polyacrylonitrile and consisted of a thin, dense outer layer supported by a microporous "sponge" layer. These materials made effective permselective membranes, especially after the polymer-stabilized catalyst had been deposited. The membranes were incorporated into a membrane reactor and gas phase partial hydrogenation reactions were carried out with a hydrocarbon/nitrogen mixture flowing on the tube side, and a hydrogen/nitrogen mixture flowing on the shell side. The catalytic membrane reactor was effective for partial hydrogenation of cyclopentadiene, isoprene, and butadiene. The catalyst activity increased as the shell side H_2/N_2 flow rate or ratio increased, but at the expense of selectivity. For comparison, a second set of experiments was conducted where hydrogen was premixed with the hydrocarbon on the tube side of the reactor. Selectivities were not as good as the previous case, where hydrogen entered the tube-side gradually by permeating the membrane walls. These

experiments demonstrated that slowly metering hydrogen along the length of the reactor improves selectivity by keeping the hydrogen partial pressure low and the hydrocarbon partial pressure high throughout the reactor. The properties of the catalytic membrane were found to depend on both the particular polymer used for the membrane and the polymer stabilizing the catalyst.

Partial hydrogenation is a promising application for polymer-stabilized nanocluster materials because high operating temperatures are neither required nor desired and selectivity is more important than activity, so the mass transfer limitations imposed by the polymer matrix are not as important and may even be an advantage. Furthermore, ROMP diblock copolymers soluble in water or organic solvents can be synthesized and it should be easy to deposit them within MPHF membranes.

6.2.3 Bimetallic and Alloy Clusters

Using alloys or bimetallic clusters could improve the catalytic performance of the nanocomposites in three different ways.[16] First, alloying is an established method of improving the activity or selectivity of a catalyst. The alloy nanoclusters will have a different electronic structure than either of the pure metal clusters, possibly bringing about advantageous changes. Second, similar to alloying, adding a small amount of a second metal atom, called a promoter, can sometimes dramatically change the catalytic properties of metallic clusters. Third, bimetallic clusters can be synthesized where the catalytically active metal is present as the minority component, but located preferentially on the cluster surface. This is advantageous when the catalytically active metal is

expensive (e.g. platinum or palladium) and can be concentrated on the surface of a less expensive metal cluster (e.g. nickel).

6.2.4 Polymer Matrices

Polymer-based nanocomposite materials could be made more suitable as catalysts by improving the polymer properties. Clusters could be incorporated into high T_g, or high temperature stable polymers, extending the practical range of operating conditions of the materials. Clusters stabilized in a polyMTD matrix could also be used at higher temperatures than have been used in this work. Reactions were run well below the T_g of polyMTD to minimize agglomeration of the clusters, which was assumed to be more rapid in a rubbery matrix than in a glassy one. However, this assumption should be challenged because no noticeable increase in cluster size was observed when a nanocomposite sample was stored in a vacuum oven for three days at $\approx 210°C$, slightly above the T_g of polyMTD (see Figures 6-2 and 6-3).

The catalytic activity of the nanocomposites could also be increased by improving mass transport within the polymer matrix. This could be done by "foaming" the films by exposing them to a plasticizer, or by selectively decomposing one of the blocks in a microphase-separated diblock copolymer creating pores on the order of 100 Å in diameter. A third method would be to deposit the polymer onto a porous support material such as porous glass, alumina, or silica, or onto the microporous support layer of a MPHF membrane, or asymmetric pervaporation membrane. The polymer matrix would no longer be required to act as a physical support, so very thin layers could be used, minimizing the mass transfer resistance caused by the polymer matrix.

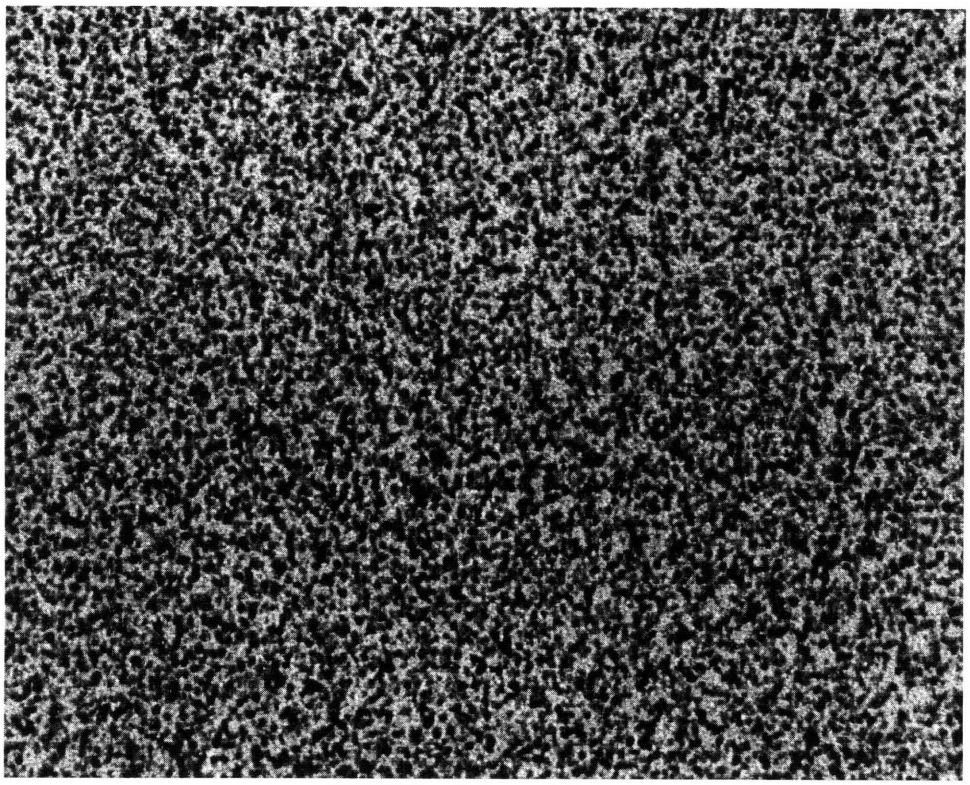

Figure 6-2: Nanocomposite sample before annealing. This sample was not used for hydrogenation reactions. (bar = 1000 Å)

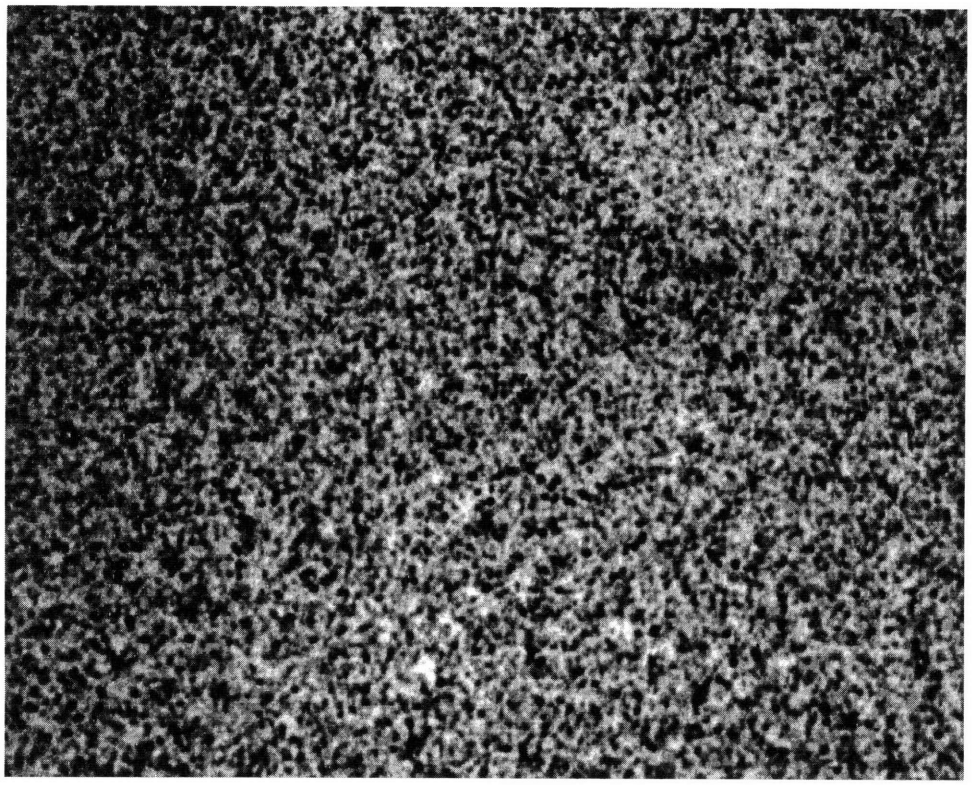

Figure 6-3: Nanocomposite sample after annealing at ≈ 210°C for three days. This sample was not used for hydrogenation reactions. (bar = 1000 Å)

6.3 References

(1) *Kirk-Othmer Encyclopedia of Chemical Technology*; Fourth Edition; Executive Editor: J. I. Kroschwitz; Editor: M. Howe-Grant; John Wiley& Sons: New York, NY, 1996, Vol. 18, pp. 453-454, 460-468; Vol. 9, pp. 883-915; Vol. 4, 701-735.

(2) *Kirk-Othmer Encyclopedia of Chemical Technology*; Third Edition; Executive Editor: M. Grayson; Assoc. Editor: D. Eckroth; John Wiley& Sons: New York, NY, 1983, Vol. 21, pp. 770-801.

(3) Hseih, H. P. *Catal. Rev. - Sci. Eng.* **1991**, *33*, 1.

(4) Ziaka, Z. D.; Minet, R. G.; Tsotsis, T. T. *J. Mem. Sci.* **1993**, *77*, 221.

(5) Ziaka, Z. D.; Minet, R. G.; Tsotsis, T. T. *AIChE Journal* **1993**, *39*, 526.

(6) Gobina, E.; Hughes, R. *J. Mem. Sci.* **1994**, *90*, 11.

(7) Badra, C. *Sep. Sci. Technol.* **1994**, *29*, 275.

(8) Gokhale, Y. V.; Noble, R. D.; Falaner, J. L. *J. Mem. Sci.* **1993**, *77*, 197.

(9) Ioannides, T.; Gavalas, G. R. *J. Mem. Sci.* **1993**, *77*, 207.

(10) Matsuda, T.; Koike, I.; Kubo, N.; Kikuchi, E. *Appl. Catal. A: Gen.* **1993**, *96*, 3.

(11) Tiscareno-Lechuga, F.; Hill Jr., C. G. *Appl. Catal. A: Gen.* **1993**, *96*, 33.

(12) Becker, Y. L; Dixon, A. G.; Moser, W. R.; Ma, Y. H. *J. Mem. Sci.* **1993**, *77*, 233.

(13) Fajardo, J. C.; Cabanes, A. L.; Godinez, C.; Villora, G. *Chem. Eng. Comm.* **1996**, *140*, 21.

(14) Milone, C.; Neri, G.; Donato, A.; Musolino, M. G.; Mercadante, L. *J. Catal.* **1996**, *59*, 253.

(15) Gao, H.; Xu, Y.; Liao, S.; Liu, R.; Liu, J.; Li, D.; Yu, D.; Zhao, Y.; Fan, Y. *J. Mem. Sci.* **1995**, *106*, 213.

(16) Ponec, V.; Bond, G. C. *Catalysis by Metal and Alloys*; Elsevier: Amsterdam, The Netherlands, 1995.

Appendix: Kinetics and Mechanism of Alkene Hydrogenation Reactions

(1) Takasu, Y.; Sakuma, T.; Matsuda, Y. *Chem. Lett.* **1985**, *8*, 1179. Ethylene hydrogenation was studied over 13 Å diameter palladium clusters deposited on a graphite plate. The reaction rate was 2×10^{17} molecules/cm^{2}s at 20°C and $P_{H2} = P_{C2H4} = 0.67$ Torr.

(2) Zhvanetskii, I. M.; Berenblym, A. S.; Shub, F. S.; Avetisov, A. K. *Kinet. and Catal.* **1989**, *30*, 739. The activity of Pd/Al_2O_3 catalysts for ethylene hydrogenation was studied as a function of the depth of impregnation of the support. Reactions were run at 318 or 373K, ethylene:hydrogen molar ratios of 3 to 200, and a hydrogen concentration of 0.2-6 x 10^{-6} mol/cm^3.

(3) Gates, B. C.; Katzer, J. R.; Schuit, G. C. A. *Chemistry of Catalytic Processes*; McGraw-Hill: New York, NY, 1979, Ch 3. The mechanism of ethylene hydrogenation over metal catalysts is discussed. In general, adsorption strength on metals increases in the order: alkanes < alkenes < alkynes. For hydrogenation reactions over metal catalysts, the reaction rate is usually first order in the hydrogen partial pressure and zero or negative order in the hydrocarbon partial pressure.

(4) Ponec, V.; Bond, G. C. *Catalysis by Metals and Alloys*; Elsevier: Amsterdam, The Netherlands, 1995. Alkene isomerization mechanisms are discussed (p. 482). The kinetics and mechanism of ethylene hydrogenation (pp. 486-488) and 1,3-butadiene (pp. 500-504) are also discussed.

(5) Sekitani, T.; Takaoka, T.; Fujisawa, M.; Nishijima, M. *J. Phys. Chem.* **1992**, *96*, 8462. Ethylene adsorption on the Pd(110) surface was studied.

(6) Cremer, P.S.; Somorjai, G. A. *J. Chem. Soc. Faraday Trans.* **1995**, *91*, 3671. Extensive kinetic data are given and mechanisms are discussed for ethylene hydrogenation on platinum.

(7) Cartright, R. D.; Goddard, S. A.; Rekoske, J. E.; Dumesic, J. A. *J. Catal.* **1991**, *127*, 342. The kinetics of ethylene hydrogenation over platinum were studied.

(8) Fahmi, A.; Vansanten, R. A. *J. Phys. Chem.* **1996**, *100*, 5676. The adsorption energy of ethylene on small palladium clusters was measured. E_{ads} was -23 kcal/mol for π bonding and -51 kcal/mol for di-σ bonding.

(9) Murzin, D. Yu.; Touroude, R.; Naito, S. *React. Kinet. Catal. Lett.* **1995**, *55*, 199. Propylene was hydrogenated over a Pd/SiO_2 catalyst at 338K and $P_{C3H6} = 25$ Torr. The reaction rate varied from 1.3×10^3 s^{-1} to 6.8×10^3 s^{-1} as P_{H2} was increased from 50 to 400 Torr.